University of Memphis
University of Memphis Digital Commons

Electronic Theses and Dissertations

7-23-2013

Structural, Magnetic and Mssbauer Studies of Dy2Fe17-xZrx (0 x 1) and Dy2Fe16Ga1-xZrx (0 x 1) and Gd2Fe16Ga0.5TM0.5 (TM = Cr, Mn, Co, Ni, Cu, Zn) Compounds.

Jiba Nath Dahal

Follow this and additional works at: https://digitalcommons.memphis.edu/etd

Recommended Citation
Dahal, Jiba Nath, "Structural, Magnetic and Mssbauer Studies of Dy2Fe17-xZrx (0 x 1) and Dy2Fe16Ga1-xZrx (0 x 1) and Gd2Fe16Ga0.5TM0.5 (TM = Cr, Mn, Co, Ni, Cu, Zn) Compounds." (2013). *Electronic Theses and Dissertations*. 777.
https://digitalcommons.memphis.edu/etd/777

This Thesis is brought to you for free and open access by University of Memphis Digital Commons. It has been accepted for inclusion in Electronic Theses and Dissertations by an authorized administrator of University of Memphis Digital Commons. For more information, please contact khggerty@memphis.edu.

STRUCTURAL, MAGNETIC AND MÖSSBAUER STUDIES OF $Dy_2Fe_{17-X}Zr_X$, $Dy_2Fe_{16}Ga_{1-x}Zr_x$ AND $Gd_2Fe_{16}Ga_{0.5}TM_{0.5}$ (TM = Cr, Mn, Co, Ni, Cu, Zn) COMPOUNDS

by

Jiba Nath Dahal

A Thesis

Submitted in Partial Fulfillment of the

Requirements for the Degree of

Master of Science

Major. Materials Physics

The University of Memphis

August 2013

TO MY PARENTS

ACKNOWLEGEMENT

I would like to express the deepest gratitude to my adviser Prof. Sanjay R. Mishra for his guidance and continual support in the planning and development of my research. I would also like to express my appreciation to my committee members, Dr. M. Shah Jahan and Dr. Donald R. Franceschetti for their time and effort to make my research successful. My sincere gratefulness goes to the Department of Physics for providing me an opportunity to pursue Master's degree with full financial support. I am thankful to Dr. Syed Ali Sikanther for his assistance on XRD powder refinements.

I express my appreciation to my friends and all the supportive ones who directly or indirectly helped me to make my thesis successful.

I am grateful to my family whose love and support made me successful to accomplish whatever I have so far. Finally but not least, my deep love to my wife Gita Adhikari and my son Sujit Dahal for supporting me in every step of my career.

ABSTRACT

Dahal,Jiba Nath. MS. The University of Memphis. August, 2013. Structural, Magnetic and Mössbauer Studies of $Dy_2Fe_{17-x}Zr_x$ ($0 \leq x \leq 1$) and $Dy_2Fe_{16}Ga_{1-x}Zr_x$ ($0 \leq x \leq 1$) and $Gd_2Fe_{16}Ga_{0.5}TM_{0.5}$ (TM = Cr, Mn, Co, Ni, Cu, Zn) Compounds. Major Professor. Sanjay R. Mishra.

The main drawbacks of rare earth intermetallic magnets are their low Curie temperature (T_c) and magnetic anisotropies. Many efforts have been made to improve these properties of R_2Fe_{17} permanent magnets by doping metals and non-metals atom for Fe or inserting interstitials atoms in R_2Fe_{17} lattice. In the present work, the effect of substitution of non-magnetic atom, Zr for Fe in $Dy_2Fe_{17-x}Zr_x$ and $Dy_2Fe_{16}Ga_{1-x}Zr_x$ and magnetic atoms in $Gd_2Fe_{16}Ga_{0.5}TM_{0.5}$ (TM = Cr, Mn, Co, Ni, Cu, Zn) are studied. The structural and magnetic properties of these compounds have been studied via x-ray diffraction, vibrating sample magnetometer (VSM) and ^{57}Fe Mössbauer Spectroscopy. An increase in unit cell volume with the increase in Zr content is observed in $Dy_2Fe_{17-x}Zr_x$ and $Dy_2Fe_{16}Ga_{1-x}Zr_x$ but no systematic variation in the unit cell volume is observed with transition metal doping. The Curie temperature (Tc) of $Dy_2Fe_{17-x}Zr_x$ and $Dy_2Fe_{16}Ga_{1-x}Zr_x$ reaches a maximum value of 510K at $x = 0.75$ and 505.1 K at $x = 0.5$ Zr substitution respectively. These observed values of Tc in $Dy_2Fe_{16.25}Zr_{0.75}$ and $Dy_2Fe_{16}Ga_{0.5}Zr_{0.5}$ are 102 K and 97 K higher than their Dy_2Fe_{17} (Tc = 408 K) . This improvement in Tc is attributed to improved Fe-Fe exchange interaction due to unit cell volume expansion. The achieved Curie temperatures of transition metal doped intermetallic are also better than Gd_2Fe_{17} and $Gd_2Fe_{16}Ga_1$. The magnetization value of $Dy_2Fe_{17-x}Zr_x$ and $Dy_2Fe_{16}Ga_{1-x}Zr_x$ decreased at the rate of 10.99 emu/gm and 9.244 emu/gm per Zr atom respectively. The difference in magnetization values between Zr and Ga-Zr doped samples may be attributed to the variation in d-electron density and magnetovolume effect. The room temperature

Mössbauer analysis showed decrease in average hyperfine field and increase in isomer shift with Zr doping for $Dy_2Fe_{17-x}Zr_x$ and $Dy_2Fe_{16}Ga_{1-x}Zr_x$. But the variation in average hyperfine field in $Gd_2Fe_{16}Ga_{0.5}TM_{0.5}$ was observed to depend on the magnetic nature of TM element and the unit cell volume. However isomer shift showed continuous increase with the increase increase in atomic number of TM atoms.

TABLE OF CONTENTS

LIST OF TABLES

LIST OF FIGURES

CHAPTER 1

INTRODUCTION

1.1 Magnetism

Magnet is a material that produces magnetic field and consequently attracts other magnetic substances within the field. More than 2000 years ago, Chinese navigators were the first to use the magnetic materials as compass [1]. The definition of magnet was still incomplete when quantum mechanics explained orbital and spin motion of electrons to define magnetism. After that, many more studies have been made to improve the quality of magnet. In an industrial revolution of 19^{th} century, the improvement on magnets subsequently led to the discovery of the Faraday's law. With continuous advancement on magnets, there has been considerable progress on the exploration of man made permanent magnets with better magnetic properties.

1.2 Permanent Magnet

Materials that can be magnetized and are strongly attracted to the magnets are called the ferromagnetic materials or ferrimagnetic materials. The ferromagnetic materials which can be permanently magnetized and can create own persistent magnetic fields are called permanent magnets. The ferromagnetic materials can be classified into two sub categories. soft ferromagnetic and hard ferromagnetic materials. The soft ferromagnetic materials are characterized by a lower value of coercivity (Hc) <10 Oe and larger value of saturation magnetization (Ms) >100 emu/gm. Because of the low value of Hc, these soft ferromagnetic materials can be magnetized and demagnetized easily as their domain wall can easily migrate. On the other hand, the hard ferromagnetic materials which are commonly known as permanent magnets have higher value of coercivity

(>3500 Oe) and also desired to have high value of saturation magnetization. $SmCo_5$, $Nd_2Fe_{14}B$, Al-Ni-Co are widely used hard ferromagnetic materials.

Permanent magnet should possess two different properties. Firstly, they should retain the magnetization when the external magnetizing field is removed. Secondly, they should have demagnetizing force due to a reverse magnetic field. Remenant magnetization (M_r) and coercivity (Hc) are the main parameters to express these properties. $(BH)_{max}$ is called the energy product which measures the storage and usable magnetic flux density and is roughly proportional to the rectangular area under second quadrant of the hysteresis loop. The quality of hard magnetic materials is the measure of energy product $(BH)_{max}$ [1]. The earliest application of permanent magnet was the needle of a magnetic compass, while these permanent magnets are extensively used in various fields these days. They are used to make the electro-mechanical machine and devices like electric motors, electro-mechanical actuators, measuring instruments, electric current control devices etc. They are also useful for the acoustic transducers like sound generators, sound receivers, audio frequency transducers etc. Microwave/MM-wave devices and electron ion beam control devices are made by using the permanent magnets. For instance, the use of permanent magnets in power tubes, waveguide devices, particle accelerators, mass spectrometers etc. has considerable importance. They are highly used in the hospitals mainly for NMR imaging devices, surgical clamps, mechanical prostheses etc. [2]. The reduction of size of the instruments with better performance requires continuous focus on the permanent magnets. The comparisons of soft and hard magnetic materials are better understood as shown in **Fig. 1.1**. Sometimes, magnet with high Hc has disadvantages because they are difficult to magnetize. So, the intermediate

materials have great importance. For this, most of the works have been done to make the combined forms of magnet by using hard and soft magnetic materials.

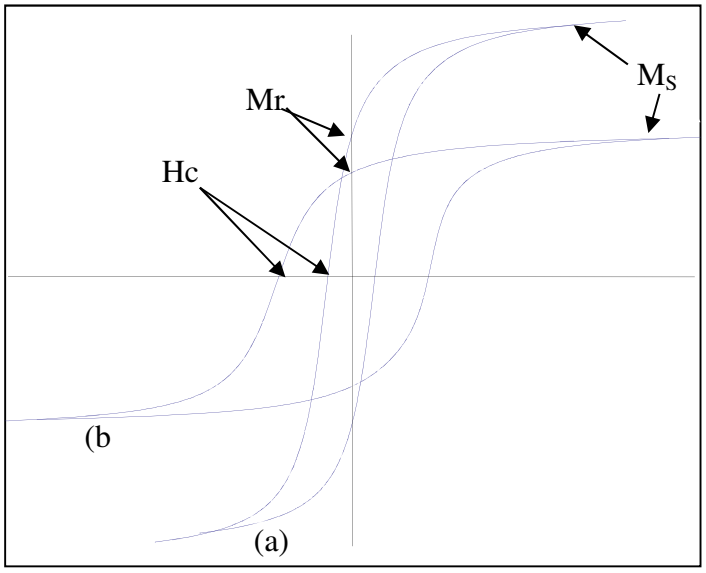

Fig. 1.1. Hysteresis loops (a) soft magnetic materials (b) hard magnetic materials.

1.3 Types of permanent magnets

The earliest form of magnet was the loadstone (also called “armed”) where soft irons were attached to concentrate the flux. Later, high carbon steel magnets obtained by quenching were used as compass needles for centuries. According to the Magnetic Materials Processing Association (MMPA), the permanent magnets are classified into three different groups.

1.3.1 Ceramic magnet

Ceramic magnets are largely made up of iron oxide and are commonly called ferrites. The general formula for such type of magnet is $MFe_{12}O_{19}$ (M denotes for Ba, Sr, Pb) [3]. These types of magnets have high coercive force, resistance to corrosion and high heat tolerance. The energy product of these magnets is ~3.5 MGOe (Mega Gauss Oersted) [3]. They are relatively cheap and commonly available as compared to the other types of permanent magnets. So, these types of ceramic magnets are mostly used nowadays. The drawbacks of ceramic magnets are they have low energy product or strength, low mechanical strength and the presence of ferrite powder on the surface of the materials which can rub off and damage its surface.

1.3.2 Alnico magnets

The magnets which are made up of an alloy of aluminum (Al), Nickel (Ni), and cobalt (Co) with small amount of other elements like silicon (Si), niobium (Nb), zirconium (Zr) etc. added to enhance the properties of the magnets are called Alnico magnets. The development of alnico began in 1931 A.D. when T. Mishima in Japan discovered that an alloy of iron, nickel, and aluminum had a coercivity of 400 Oe, double that of the best steel magnet of the time [4]. These types of magnets have good temperature stability, good resistance to corrosion but are easily demagnetized by shock. Moreover, they have higher energy products $(BH)_{max}$ up to 5.5 MGOe [3]. Still they have drawbacks like higher cost, low coercive force and low energy product. Mostly these are useful for light weight electric motors, generators, electro-mechanical actuators etc. [2].

1.3.3 Rare Earth Transition metals Magnets

The rare earth transition metals magnets are formed when 3d-transition metals (TM) are alloyed with 4f-transition rare-earth elements (RE) like Sm, Nd, Dy, Gd, Pr, Ce etc. [2]. These intermetallic compounds have high Curie temperature above the room temperature. Further addition of B, C, Si, Ti, Ga etc. with these binary intermetallic compounds makes the rare earth magnets more strong. R-TM intermetallic were discovered in 1966 when K. J. Strnat and G. Hoffer of the U.S. Air Force Materials Laboratory reported the YCo_5 has an anisotropy constant of 5.5×10^7 ergs/cm^3 [5]. So they are the newest and still growing family of hard magnetic alloys. Samarium-cobalt and neodymium-iron-boron magnets are the well-known magnets and widely used permanent magnetic materials [6]. Neodymium-iron-boron (Nd-Fe-B) magnets are the most advanced commercialized permanent magnets available nowadays. They have the highest energy products $(BH)_{max}$ approaching 52 MGOe and is mechanically stronger than Samarium-Cobalt ($SmCo_5$) magnets with energy product ~20 MGOe [3].

Fig. 1.2 shows the development and reduction in size of different magnets with the same amount of energy.

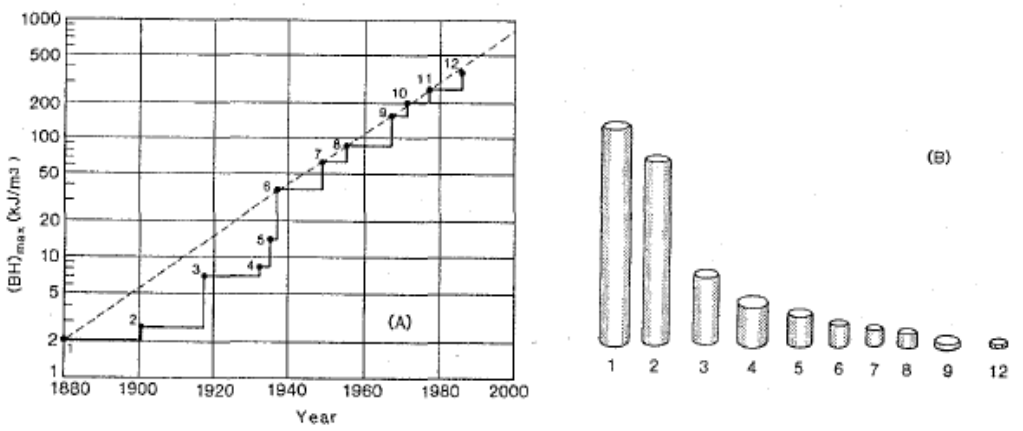

Fig. 1.2. History of $(BH)_{max}$ since 1880.

Description of Fig. (A). (1) Carbon steel, (2) tungsten steel, (3) cobalt steel, (4) MK steel, (5) "Ticonal II", (6) "Ticonal G", (7) Ticonal GG", (8) Ticonal XX", (9) $SmCo_5$, (10) $(SmPr)Co_5$, (11) $SmCo_7$, (12) NdFeB. (B). Keeping $B \times \phi$ and $H \times L$ constant (B= magnetic induction, H = Magnetic field strength, ϕ = cross section of the magnet and L = length of the magnet) , the volume of the magnet decreases with increasing (BH)max. The number in (B corresponds to the number in (A) [Xiao Qunfeng Thesis work ISBN. 90-5776-098-3]

1.4 Hysteresis loop

All magnetic materials are made up of magnetic domains. A magnetic domain is a region with uniform magnetization and the collection of such magnetic domain aligned in same direction causes net magnetization of the magnets. Thus magnetic domains structure is responsible for the magnetic behavior of the ferromagnetic materials like Fe, Ni, Co etc. and their alloys and ferrites. Ferromagnetic material will not return back to zero magnetization once they are magnetized in one direction. In ordered to make zero magnetization, we must apply the field in the opposite direction. The magnetization of the ferromagnetic materials always lags behind the applied field which produces the

hysteresis loop. When an external magnetic field is applied to ferromagnetic materials then the atomic dipoles will align in the same direction. If this external magnetic field is removed, then part of alignment will be retained and the materials is said to be magnetized. The lack of retraceability of the magnetization curve is the property called hysteresis which is due to the magnetic domains in the material and is very much useful for the magnetic memory devices like tape recording and storage of data on computer disks.

When a magnetic field **H** is applied to ferromagnetic materials, it develops the flux density **B** due to the spin orientation of magnetic domains. The relation between induced flux density **B** and applied field **H** is given by using the equation,

$$\mathbf{B} = \mu_0 (\mathbf{H} + \mathbf{M}) = \mu_0 \mathbf{H} + \mathbf{J} \qquad \text{(SI)} \qquad \text{.....(1)}$$

where **M** is the magnetization, **J** is the polarization and μ_0 is the permeability of free space equal to $4\pi \times 10^{-7}$(Tm/A). The loop or graph between induced **B** (or **M**) and applied **H,** as shown below in **Fig. 1.3**, called hysteresis loop. The maximum value of magnetization where all the domains of the magnet are parallel to each other is called saturation magnetization (Ms) and the value of magnetization when the applied field is zero is called remanent magnetization (Mr). The negative magnetic field applied on the magnet to make zero magnetization is called coercivity (Hc).

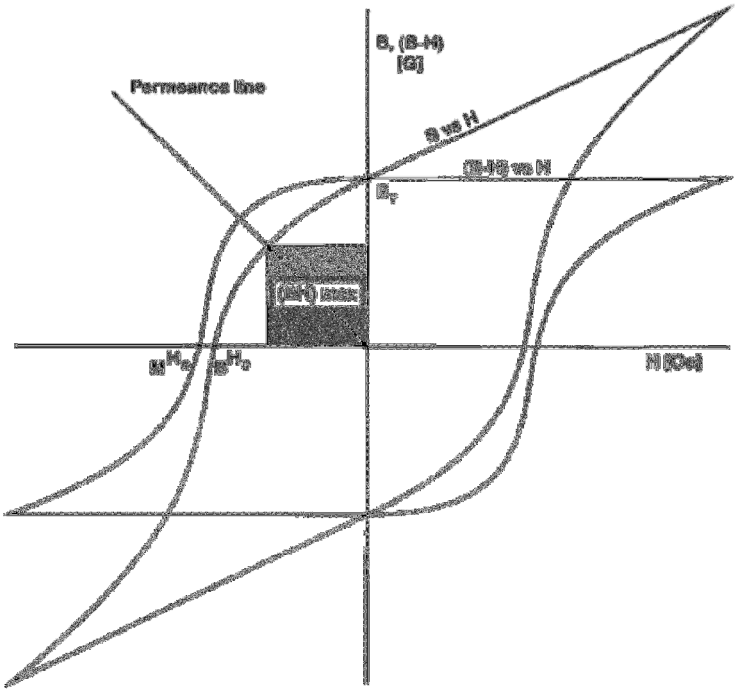

Fig. 1.3. Hysteresis loop of magnetic materials [[1].

Magnetic materials have two different types of properties (a) Intrinsic (b) Extrinsic magnetic properties.

1.4.1 Intrinsic magnetic properties

Saturation magnetization (M_s) and magneto crystalline anisotropy constant (k_I) are primary magnetic properties of the magnet and they are related to the magnetic structure. Magnetocrystalline anisotropy comes in to play when magnetic moment in a single crystal tends to move from the easy to the hard direction.

1.4.2 Extrinsic magnetic properties

Remanence (Mr), Coercivity and maximum energy product $(BH)_{max}$ that arises from the microstructure are called the extrinsic magnetic properties. It depends on the history of the sample that includes anything depending upon the grain size.

1.5 Trend in permanent magnet improvement

The loadstone is the first permanent magnet known in ancient time before 600 B.C. It was also called magnetite (Fe_3O_4). It received its classical name *magnes* because it was found in Magnesia and is said due to its abnormal properties and its attractive powers. The first artificial permanent magnets were designed by "touching" iron needles in a loadstone. In literature, several studies are found regarding the development of artificial permanent magnets. Later in the 17^{th} century, the loadstone was made square ends and iron plates were kept in contact to increase the attractive force on iron. In 1675 A.D., Boyle observed the demagnetization of magnet by heating and proved that the magnetism was a matter of the dis-position or internal constitution of the iron, without any apparent change in the metal. Servingion Savery was the first man to make strong permanent magnets. Later, Gowin Knight (1713-1772) made powerful magnet of steel bar each 15.0x1.0x0.5 inch size and Christie rearranged it and changed its shape into horseshoe-pattern magnets which was used by Faraday in his famous experiment "rotation copper disk" in 1831. Around 1873, Jules C. Jamin (**Fig. 1.4**) claimed that he made the most powerful magnet in the world [7].

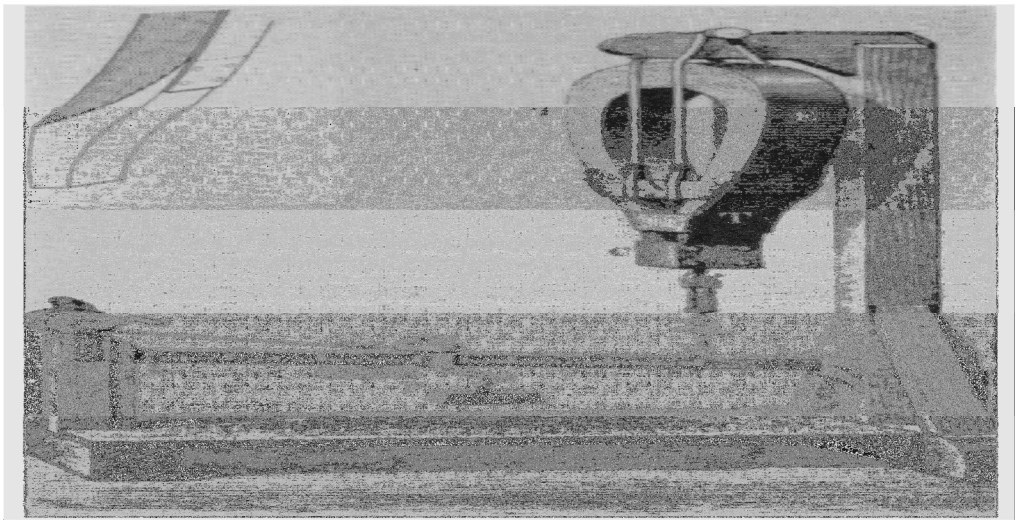

Fig. 1.4. Jamin's great permanent magnet [7].
(*Note*. The method of fitting the soft iron pole pieces is shown in the inset)

Modern history of permanent magnets began after 1900 when the chromium addition to loadstone increased the energy density by 0.3 MGOe. In 1917, Kotaro Honda was able to find the energy product 1 MGOe and coercive force 250 Oe by using 35% Co. Later in 1931, introduction of Alnico magnet made revolutionary change with the increase of energy product up to 9.5 MGOe and coercivity ~2 KOe. Thereafter, the permanent magnets are commercially available [2]. With the use of Alnico magnets, it was possible to replace electromagnets with the permanent magnets and their uses are widespread on motors, generators, loudspeakers etc. [7]. The achieved coercivity is still low because it comprises from shape anisotropy. Shape anisotropy is the preferential alignment of atomic moment in a given direction due to the shape of the magnetic particle. Hexagonal ferrite is the first group of ferrite whose coercive force is from magnetocrystalline anisotropy rather than the shape anisotropy and for $SrAl_4Fe_8O_{19}$ it is reported that the coercivity ~18KOe still low saturation magnetization (Ms), remanent magnetization (Mr) and low $(BH)_{max}$ [8].

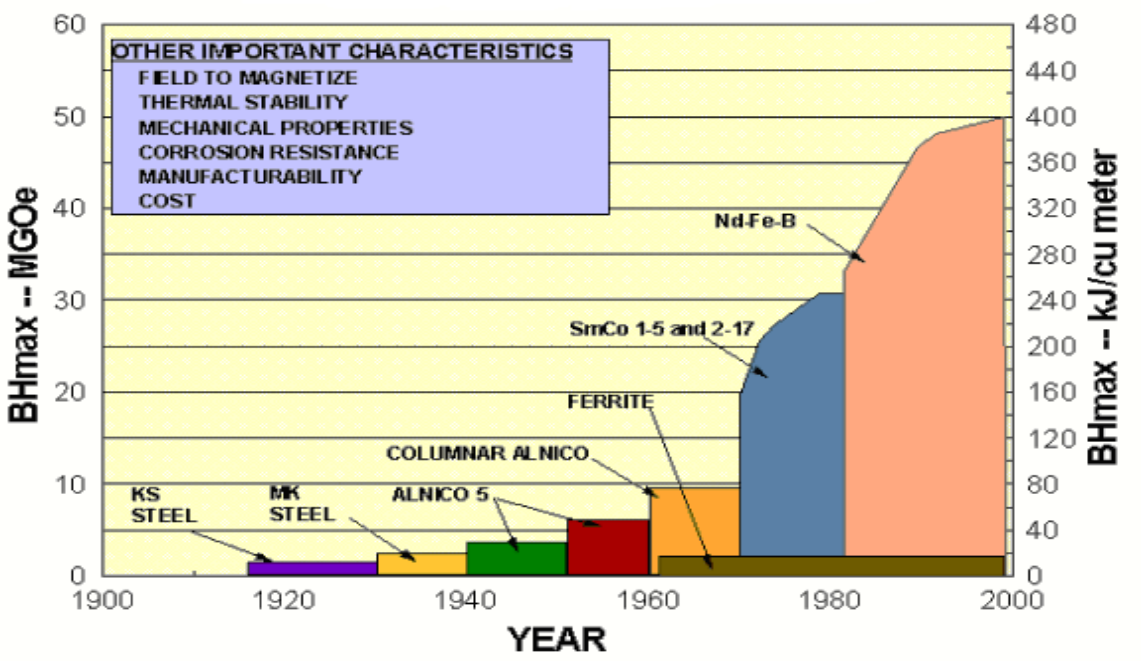

Fig. 1.5. Development of permanent magnet in the 1900's (© Arnold magnetic Technologies).

Low cost and huge suppies of raw material are two major advantages of ferrite. They can be easily produced and their process is adopted for high volume as well as moderately high service temperature. They are very useful in electric motors, DC motors, battery operation in automobile etc. In order to improve all these limitations of permanent magnets, a new class of permanent magnet materials called ferromagnetic intermetallic compounds of rare earth-cobalt alloys (Sm-Co Base) have been introduced since 1970 [2]. Since 1983, the Rare Earth-Iron alloys (RE-Fe-B base) made the drastic development of permanent magnets. In these types of compounds 3d-transition iron or cobalt metals are made alloyed with rare-earth (RE) to form rare-earth permanent magnet (REPM). Since the transition metals provide high magnetization and rare earth elements provide high uniaxial crystal anisotropy, these magnets have very good magnetic properties as compared to the magnets formed during early 1930. It is also found that the R_2Fe_{17}

permanent magnet can dissolve different elements to make the permanent magnet stronger. **Fig. 1.5** and **Fig. 1.6** clearly explain the improvement on $(BH)_{max}$ and coercivity of the permanent magnet till 2000.

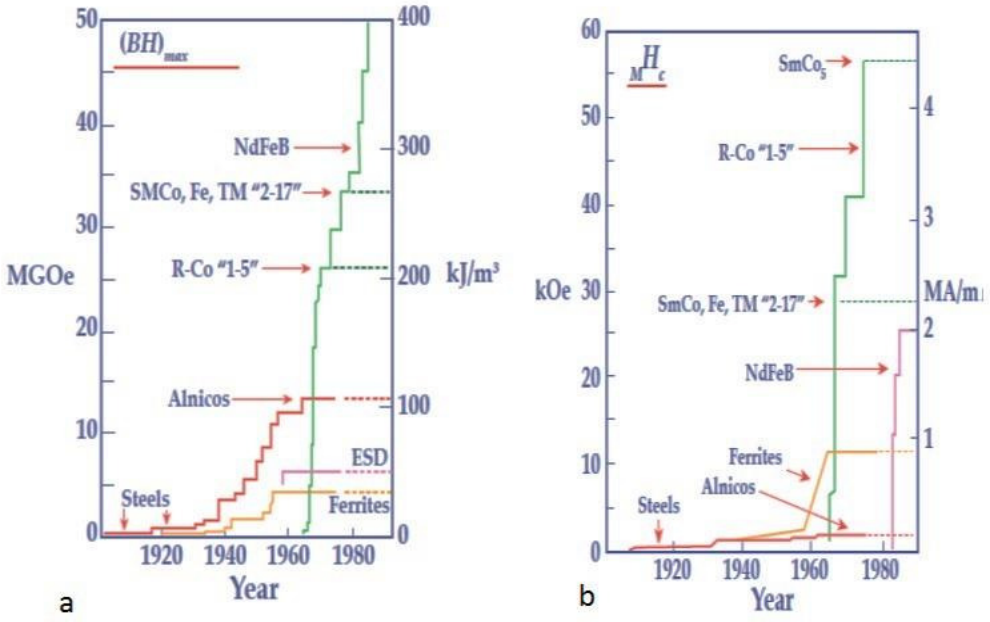

Fig. 1.6 . The development of permanent magnets in the 20th Century using as a measure the laboratory record values of a) energy product b) Coercivity [2].

1.6 Rare-earth based permanent magnet

The elements with atomic number 57-70 along with Yttrium (Y) in the periodic table are called rare earth elements. The rare earth (RE) elements have their own important properties. They are so called because it is uncommon to find them in commercially viable concentrations. They lie in two categories, soft RE and hard RE, with varying level of uses and demand. Among the hard rare earth elements, Nd, Eu, Tb, Dy and Y are very precious because their existence in the earth is on the verge of collapse. **Fig. 1.7** explains the relative abundance of rare-earth elements with the comparison of other elements found in nature.

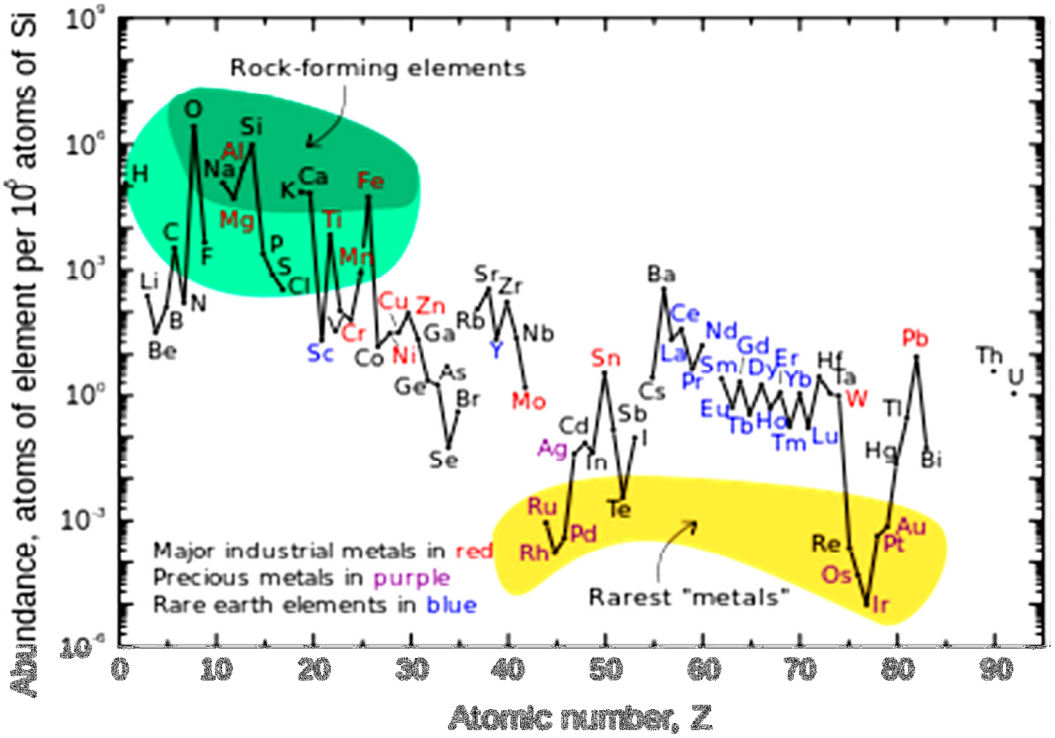

Fig. 1.7. Relative abundance of elements worldwide. [8]

Dysprosium (Dy) and Gadolinium (Gd)

Dysprosium (Dy) and Gadolinium (Gd) are important because of their good physical properties. They are soft and easy to break. Dy and its compounds are highly susceptible to magnetization, and they are mostly used in data storage applications. They are equally applicable to use in laser materials and commercial lighting. They are also useful for nuclear reactors because of their high thermal neutron absorption cross section. It can also be used in Nd-Fe-B magnet to increase the coercivity of the hybrid motor vehicle and dosimeter for measuring ionizing radiation. The increasing demand of Dy has made it more expensive as compared to the others. **Fig. 1.8** explains the comparative prices of Dy, Nd and Sm. It is found that China is the largest producer of the permanent magnet in the world. About 64% of the production of permanent magnet is produced in

China. Compared to ferrite and alnico magnets, the rare earth based permanent magnets are sold in Japan after 1995 by the development of Nd-Fe-B magnet.

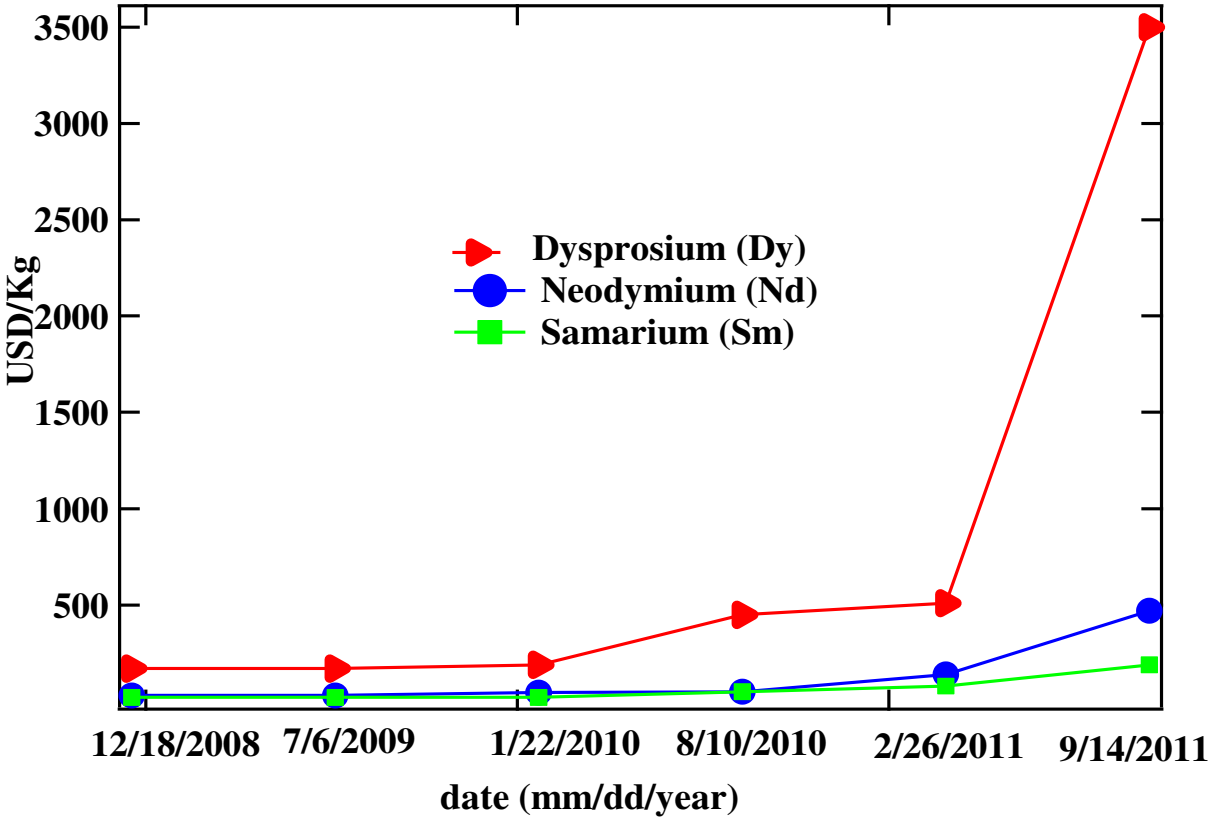

Fig. 1.8 . Price history of Dy, Sm and Nd since 2008 to 2011. [9]

1.7 Crystal structure of R_2Fe_{17} type intermetallic compound

Iron-rich rare-earth (R) intermetallic compounds commonly denoted by R_2Fe_{17} are very important permanent magnets because of their potential applications in the field of magnet. Though these compounds have low Curie temperature and magnetic anisotropy they possess the highest saturation magnetization. The intermetallic with light rare earth elements crystallize in rhombohedral Th_2Zn_{17} structure (space group $R\bar{3}$ m) and heavy rare earths are crystallize in hexagonal Th_2Ni_{17} structure (space group $P6_3/mmc$) with 3

molecules in the unit cell in each case. In general, R_2Fe_{17} compounds are derived from the $CaCu_5$ type structure by the ordered substitution of one third of rare-earth atoms by a pair (dumbbell) of Fe atoms [10]. The general structure is $3RFe_5$-R+2Fe = R_2Fe_{17} [11]. **Fig. 1.9** and **Fig. 1.10** show the hexagonal and rhombohedral structure of R_2Fe_{17} compounds. The number of formula units on the hexagonal and rhombohedral structure are two and three, respectively. The double layers are stacking on hexagonal structure as in **Fig. 1.9** and three layers are stacking on the rhombohedral structure as in **Fig. 1.10**. Rhombohedral structure has one R site (6*c*) and four Fe sites (6*c*, 9*d*, 18*f*, 18*h*) whereas, hexagonal structure has two R sites (2b, 2d) and four Fe sites (4*f*, 6*g*, 12*j*, 12*k*) [12].

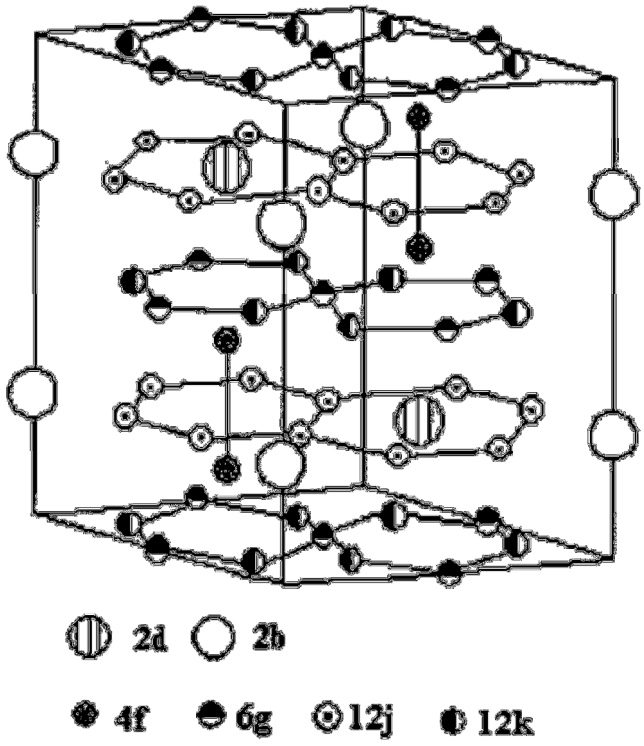

Fig. 1.9. Hexagonal Th_2Ni_{17} structure

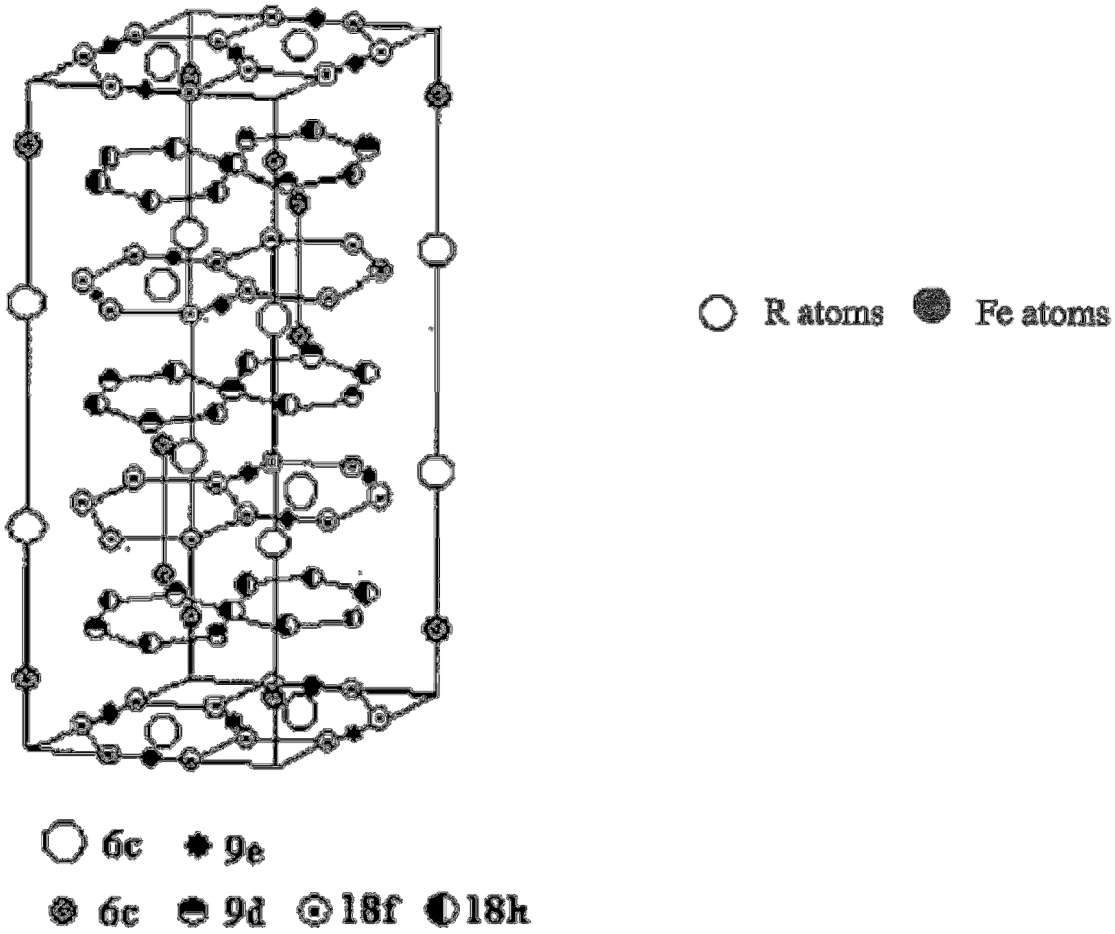

Fig. 1.10. Rhombohedral Th_2Zn_{17} structure.

CHAPTER 2

LITERATURE REVIEW

Intermetallic compounds based on rare-earth elements (R) and 3d-transition elements (T) are very important from the fundamental as well as technological point of view. They possess outstanding magnetic properties because of their high saturation magnetization (Ms). $SmCo_5$ permanent magnets have excellent magnetic properties, but because of the slow commercialization, they cannot fulfill the demand of the permanent magnets in the world. In contrast of $SmCo_5$, R_2Fe_{17} compounds were adopted in late 1970's and the values of $(BH)_{max}$ and Hc were found to be about 26 MGOe and 15 kOe, respectively [3]. In spite of these properties, they have very low Curie temperature (~473 K for Gd_2Fe_{17} and ~300 K for Dy_2Fe_{17}) and magnetic anisotropies [13]. The comparative details about the study of Curie temperature for R_2Fe_{17} intermetallic compound are shown in the Fig. 2.1.

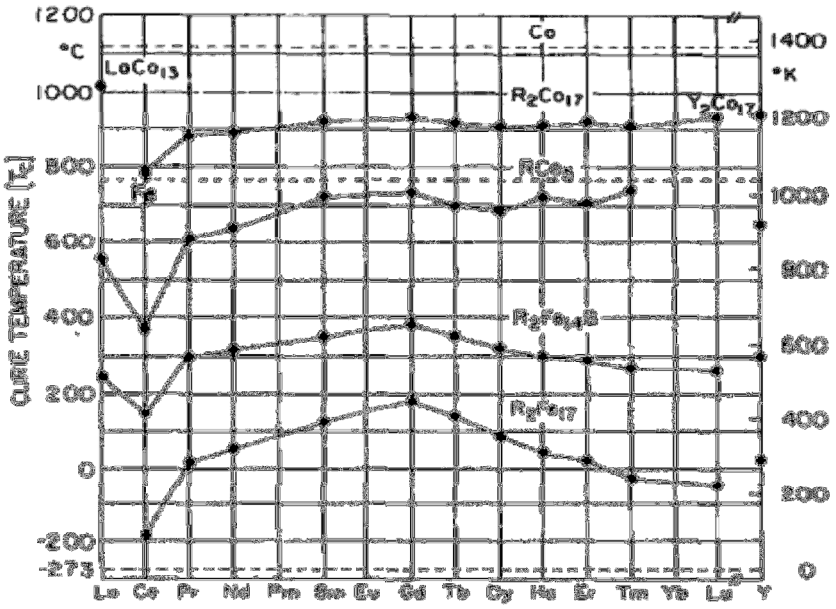

Fig. 2.1. Curie temperature for different series of R-TM intermetallic compound [13].

It is found from Fig. 2.1 that Gd_2Fe_{17} intermetallic compound has the highest Curie temperature while Dy_2Fe_{17} intermetallic compound has Curie temperature lower than Gd_2Fe_{17} but it is higher than other R-TM intermetallic. So, they are in better focus for the improvement in the Curie temperature. In R_2Fe_{17} intermetallic compounds, the R sublattice anisotropy originates mainly from the crystalline electric fields on the 4*f* orbital [10]. R sublattice anisotropy is smaller than the Fe sublattice anisotropy; as a result, the resulting anisotropy is planner. Thus, Curie temperature enhancement in R_2Fe_{17} intermetallic can be obtained by the following two major approaches.

1) Substitution of Fe atoms by magnetic atoms such as (Co, Ni, Cr, Mn, Ni), non-magnetic atoms (Al, Si, Ga) and refractory atoms (Ti, V, Mo, Nb, W, Zr)
2) Interstitial substitution of non-metals such as C, N and H in R_2Fe_{17} lattice.

The substitution of non-magnetic atoms at Fe sites have been reported to increase ferromagnetic coupling which in turn increases the Curie temperature [Li *et al* (1993), Wang and Dunlap *et al* (1993), Yelon *et al* (1993), Suresh *et al* (1996)] and magneto-crystalline anisotropy [Baogen Shen *et al* (1995) and Cheng *et al* (1995)]. Some of the significant improvements in Curie temperature of R_2Fe_{17} with substitution of non-magnetic atom such as Ga on the basis of previous word are listed in **Table 2.1**.

Table 2.1. Tc of R_2Fe_{17} compounds and $R_2Fe_{17-x}Ga_x$.

R_2Fe_{17} compounds	**T_c K)**	**$R_2Fe_{17-x}Ga_x$ compounds**	**T_c (K)**
Ce_2Fe_{17}	238	$Ce_2Fe_{15}Ga_2$	406
Gd_2Fe_{17}	429	$Gd_2Fe_{16}Ga_1$	560
		$Gd_2Fe_{14}Ga_3$	601
Dy_2Fe_{17}	370	$Dy_2Fe_{16}Ga_1$	462
Nd_2Fe_{17}	330	$Nd_2Fe_{16}Ga_1$	440
Er_2Fe_{17}	305	$Er_2Fe_{16}Ga_1$	415
Tm_2Fe_{17}	288	$Tm_2Fe_{16}Ga_1$	410
Ho_2Fe_{17}	330	$Ho_2Fe_{14}Ga_3$	560
Sm_2Fe_{17}	398	$SM_2Fe_{16}Ga_1$	485

Jun-xian Zhang *et al* [14] reported that introducing carbon into $R_2Fe_{17-x}Ga_xC$ can increase the Curie temperature because of the Fe-Fe exchange coupling with increased Ga content. Introducing nitrogen on interstitial sites of $R_2Fe_{17}N_x$ can also increase the Curie temperature due to volume expansion because of the increase in the distance of iron atoms and change the other magnetic properties of R_2Fe_{17} compounds [15, 16]. It is found that nitrogen and carbon materials are not stable at their sintering temperatures ~800 ^oC. **Table 2.2** shows the Curie temperature enhancement of R-TM intermetallic with carbon and nitrogen on them. [17].

Table 2.2 . Curie temperature of $R_2Fe_{17}C_1$ and $R_2Fe_{17}N_1$ compounds.

$R_2Fe_{17}C_1$	Tc (K)	$R_2Fe_{17}N_1$	Tc (K)
$Ce_2Fe_{17}C_1$	297	$Ce_2Fe_{17}N_1$	700
$Pr_2Fe_{17}C_1$	370	$Pr_2Fe_{17}N_1$	720
$Nd_2Fe_{17}C_1$	449	$Nd_2Fe_{17}N_1$	740
$Sm_2Fe_{17}C_1$	552	$Sm_2Fe_{17}N_1$	750
$Gd_2Fe_{17}C_1$	582	$Gd_2Fe_{17}N_1$	740
$Tb_2Fe_{17}C_1$	537	$Tb_2Fe_{17}N_1$	730
$Dy_2Fe_{17}C_1$	515	$Dy_2Fe_{17}N_1$	720
$Ho_2Fe_{17}C_1$	504	$Ho_2Fe_{17}N_1$	710
$Er_2Fe_{17}C_1$	488	$Er_2Fe_{17}N_1$	690
$Tm_2Fe_{17}C_1$	498	$Tm_2Fe_{17}N_1$	690
$Yb_2Fe_{17}C_1$	477	$Yb_2Fe_{17}N_1$	675
$Lu_2Fe_{17}C_1$	490	$Lu_2Fe_{17}N_1$	675
$Y_2Fe_{17}C_1$	502	$Ye_2Fe_{17}N_1$	690

It is also reported that Pr_2Fe_{17}, Nd_2Fe_{17} and Gd_2Fe_{17} with their hydrides can also cause significant change in the Curie temperature and magnetic anisotropy properties [18, 19, 20, 21]. It is found that the improvements in the magnetic properties are arising from the decrease of negative exchange-interaction because of the change in shape of unit cell volume caused by the addition or substitution of material. Betancourt *et al* (2003) [22] reported that Zr and Nb doped for Fe show moderate improvement in magnetic properties. It is reported that with the substitution of Cr, Nb, Ti, Zr on $Pr_8Fe_{84}M_2B_6$ (M= Cr, Nb, Ti, Zr), the hard magnetic properties are enhanced and the coercivity on $Pr_8Fe_{84}Nb_2B_6$ magnets reaches 6.5 kOe with maximum energy product of 9 MGOe [23, 24]. The curie temperatures of Ce_2Fe_{17} [25], Gd_2Fe_{17} [26], Dy_2Fe_{17} [27], Pr_2Fe_{17} [18], Nd_2Fe_{17} [28], Er_2Fe_{17} [29], Tm_2Fe_{17} [30], Lu_2Fe_{17} [31, 32] , Ho_2Fe_{17} [33], Sm_2Fe_{17} [34]

are improved by the addition of smaller elements like Si, Cr, Mn and bigger elements like Ga. H. Luo *et al* (1997) also reported that the Curie temperatures of Nb, Zr, V, Cr doped R_2Fe_{17} compounds can be increased by the addition of carbide in them [35].

Rational

Many researches have focused on improving magnetic properties of R_2Fe_{17} compound as it offers high magnetization value due to the presence of 17 Fe atoms. However R_2Fe_{17} compound have low Tc and low magnetic anisotropy. The substitution effect of Al, Ga and Si on magnetic properties of $R_2Fe_{17-x}M_x$ (M=Al, Ga, Si) is well documented in the literature [36, 37, 38] . The substitution of Al and Ga for Fe brings lattice expansion while substitution of Si for Fe brings lattice contraction [36, 37, 38]. In spite of the observed variation on unit cell volume, the enhancement in the Tc was observed and it was found that the observed Tc is independent to the substituted elements [36, 37, 38]. Among Al, Si and Ga, Ga substituted compounds show high Tc (For example $Sm_2Fe_{16}Ga$ ~485 K [39], $Dy_2Fe_{16}Ga$ ~462 K [27]. Furthermore, additional enhancement in Tc for Ga substituted R_2Fe_{17} compounds is obtained by introducing carbon in $R_2Fe_{17}C_x$ [40]. This improvement in Tc is overshadowed by a concomitant deterioration in saturation magnetization. Furthermore, this improvement in Tc is achieved at high value of doping exceeding $x > 5$ in $R_2Fe_{17-x}M_x$ (M = Al, Ga, Si) [36, 37, 38]. The high level of doping for Fe brings in magnetic dilution effect. The metalloid doped compounds such as $R_2Fe_{17}N_x$ have high Tc but are difficult to process at high temperature due to dissociation of compounds. In view of above discussion,

1. It is desired to have high Tc compounds with high Ms value.

2. It is desired to have stable metallic compounds which can withstand high temperature processing steps.

Keeping the two facts listed above and from the literature review data, we purpose to study following two sets of substituted R_2Fe_{17} intermetallic compounds, with primary focus of Tc enhancement.

i) Substitution of non-magnetic Zr atom for Fe in $Dy_2Fe_{17-x}Zr_x$. Zr atom having atomic radius 2.06 Å which is bigger than Fe atom having atomic radius 1.56 Å and thus it is expected to increase unit cell volume which in turn enhance Tc.

ii) a) Substitution of of Ga with non-magnetic atom Zr in $Dy_2Fe_{16}Ga_{1-x}Zr_x$ to understand the role of Ga in Tc enhancement.

b) Substitution of Ga with magnetic atoms such as Cr, Mn, Co, Ni, Cu, Zn in $Gd_2Fe_{16}Ga_{0.5}TM_{0.5}$ to understand the role of TM metal in Tc enhancement.

The literature describing the substitution of transition metals like Cr, Mn, Co, Ni, Cu, Zn etc. on R_2Fe_{17} compounds are scarce.

The R_2Fe_{17} compounds with Gd and Dy are chosen because of the following reason.

- They have high magnetocrystalline anisotropy which is good for large coercivity (Hc).
- They have high Bohr magnetron number (Gd = 8 μ_B, and Dy = 10.63 μ_B) [41].
- Heavier rare earth elements have smaller atomic sizes and higher solubility in α-Fe.

- From the experiment on $Nd_2Fe_{14}B$, it was found that the magnetic anisotropy of $Dy_2Fe_{14}B$ greater than $Nd_2Fe_{14}B$. Thus magnetic properties can be enhanced by using Dy instead of Nd [42].

Similarly, the reasons for choosing Zr dopant on Dy_2Fe_{17} and $Dy_2Fe_{16}Ga_{1-x}Zr_x$ and transition metal (TM) on Gd_2Fe_{17} compounds are as follows.

- Some transition elements such as Cr, and Mn etc. have shown improved solubility and Curie temperature Tc [35, 43].
- The saturation magnetization and Curie temperature and Fe hyperfine fields are remarkably affected by Zr substitution [22, 35].

CHAPTER 3

EXPERIMENTAL

First, synthesis and characterization of $Dy_2Fe_{17-x}Zr_x$ and $Dy_2Fe_{16}Ga_{1-x}Zr_x$ were carried out and their structural and magnetic properties were compared. Secondly, the effect of doping of transition metal (TM) in $Gd_2Fe_{16}Ga_{0.5}TM_{0.5}$ (TM = Cr, Mn, Co, Ni, Cu, Zn) were carried out, and its structural and magnetic properties were studied.

3.1 Objectives

1. To synthesis non-magnetic atom doped $Dy_2Fe_{17-x}Zr_x$ and $Dy_2Fe_{16}Ga_{1-x}Zr_x$ intermetallic alloys.
2. To synthesis magnetic atom doped $Gd_2Fe_{16}Ga_{0.5}TM_{0.5}$ (TM = Cr, Mn, Co, Ni, Cu, Zn)
3. To develop understanding on the role of non-magnetic and magnetic in governing the magnetic properties and Tc of alloys.

   In order to meet the above objectives the following samples were synthesized.

   a) $Dy_2Fe_{17-x}Zr_x$ (x = 0.00, 0.25, 0.50, 0.75, 1.00)

   b) $Dy_2Fe_{16}Ga_{1-x}Zr_x$ (x = 0.00, 0.25, 0.50, 0.75, 1.00)

   c) $Gd_2Fe_{16}Ga_{0.5}TM_{0.5}$ (TM = Cr, Mn, Co, Ni, Cu, Zn)

3.2 Synthesis

The samples $Dy_2Fe_{17-x}Zr_x$ and $Dy_2Fe_{16}Ga_{1-x}Zr_x$ (x = 0.00, 0.25, 0.50, 0.75, 1.00) and $Gd_2Fe_{16}Ga_{0.5}TM_{0.5}$ (TM = Cr, Mn, Co, Ni, Cu, Zn) were prepared via arc melting in a high purity argon atmosphere. The elements used were ~99.9% purity and bought from Sigma Aldrich. Extra 5% Dy and Gd were added to compensate for the evaporation loss during melting. In order to make the good homogeneous alloy, the ingots were re-melted

for 3-4 times. Thus prepared alloy was then made into fine powder. The structural and phase properties of powdered alloy were studied using x-ray powder diffraction (XRD) with Cu Kα radiation using x-ray diffractometer. The powder samples were pressed into hydraulic press at 7000 Psi. The magnetic properties were studied using vibrating sample magnetometer (VSM) in the field 1.2 T. The room temperature saturation magnetization was obtained from fitting the experimental data of M vs. H curves. The values of the Curie temperature were derived from the temperature dependence of magnetization M (emu/gm) vs. temperature. ^{57}Fe Mössbauer spectra were collected at room temperature (RT) with a 25 mCi ^{57}Co Rh source with line width 0.25mm/sec. The spectrometer was calibrated at RT with α-Fe foil.

3.3 Sample Characterization

3.3.1 X-ray diffraction (XRD)

X-ray diffraction is the technique to determine the atomic and molecular structure of a crystal. It is well developed and reliable technique to perform the analysis of structures and phases. In the present study, x-ray diffractometer with Cu-Kα radiation (wavelength, λ=1.54056 Å) was used for the determination of crystal structure and phase of the samples. The powder samples were placed on a zero background (Si) sample holder. Diffraction patterns were collected from 20^{o}-70^{o} with a scan speed of 0.02 degree/step and acquisition time of ~ 0.048sec. The XRD patterns of the samples were matched with ICCD data.

Lattice parameters '*a*' and '*c*' were calculated using the equation

$$d_{(hkl)} = \left(\frac{4(h^2 + hk + k^2)}{3a^2} + \frac{l^2}{c^2} \right)^{-\frac{1}{2}} \quad \ldots\ldots\ldots\ldots\ldots\ldots\ldots\ldots\ldots\ldots \quad (2)$$

where ‘h’, ‘k’ and ‘l’ are the miller indices of a plane. The lattice parameters were also extracted from the Rietveld refinement technique [44].

3.3.2 Vibrating Sample Magnetometer (VSM)

The saturation magnetization moment (Ms) and remenance (Mr) of the intermetallic were measured by using the vibrating sample magnetometer (VSM) in a maximum 12 kOe magnetic field. Furthermore, the Curie temperature measurement at 5000 Oe was performed.

3.3.3 Mössbauer Spectroscopy

Mössbauer spectroscopy is the advance technology based on the quantum mechanical “Mössbauer effect” and provides unique measurements of electronic, magnetic and structural properties within materials [45]. It is also useful for quantitative phase analyses or determination of concentration of resonant elements in different phases even for the amorphous solids. It needs the recoil-free, resonant absorption and emission of gamma rays. Mössbauer spectra give quantitative information on “hyperfine interaction,” where electron around a nucleus perturbs the energies of nuclear states. Hyperfine interaction causes very small perturbation of 10^{-9} to 10^{-7} eV in the energies range of Mössbauer gamma rays [46]. **Fig. 3.1** shows the emission of gamma rays and decay of ^{57}Fe from its parent ^{57}Co. Only around 10% of the excited ^{57}Fe nuclei emit a 14.4 keV gamma rays through the magnetic dipole transition from the metastable I =3/2 state to the I = 1/2 ground state (I is the nuclear spin)

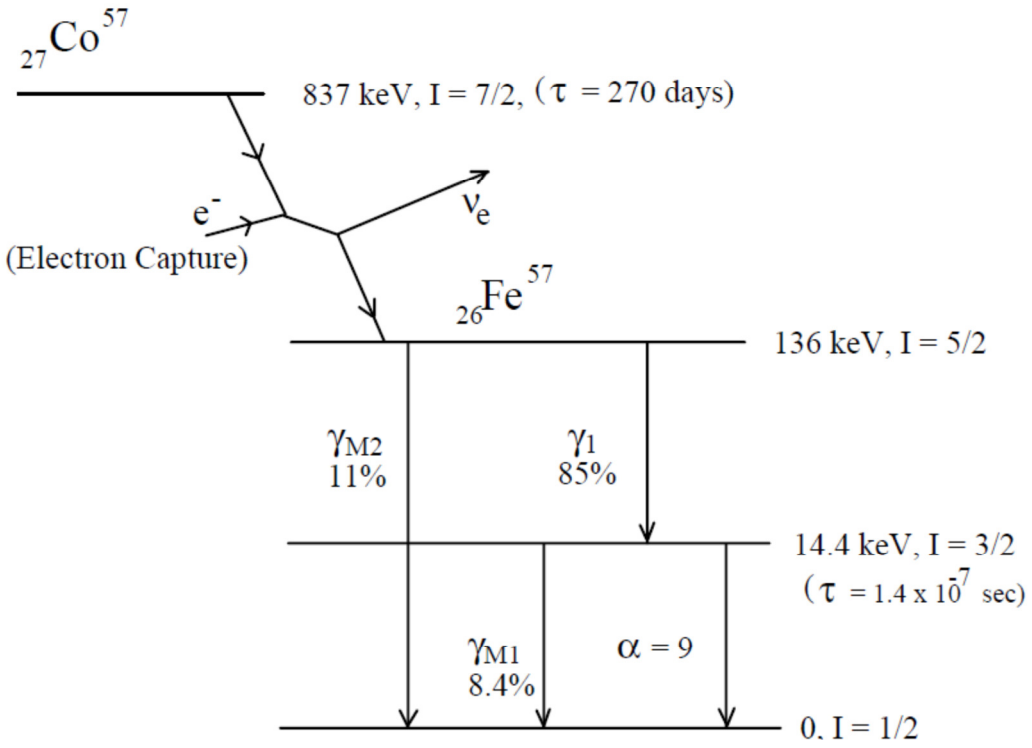

Fig. 3.1. Energy level scheme of ^{57}Co. Mössbauer spectroscopy involves the 14.4 keV transition and intensities are given in % of decays.

The schematic diagram to collect the Mössbauer spectra for the intermetallic is shown in **Fig. 3.2**. The spectra were plotted with WMOSS software after calibrated the spectrometer by α-Fe. The hyperfine field (B_{hf}), isomer shift (δ or IS), and quadrupole splitting (Δ or QS) and percentage of area occupied by the different sites were extracted from the fit.

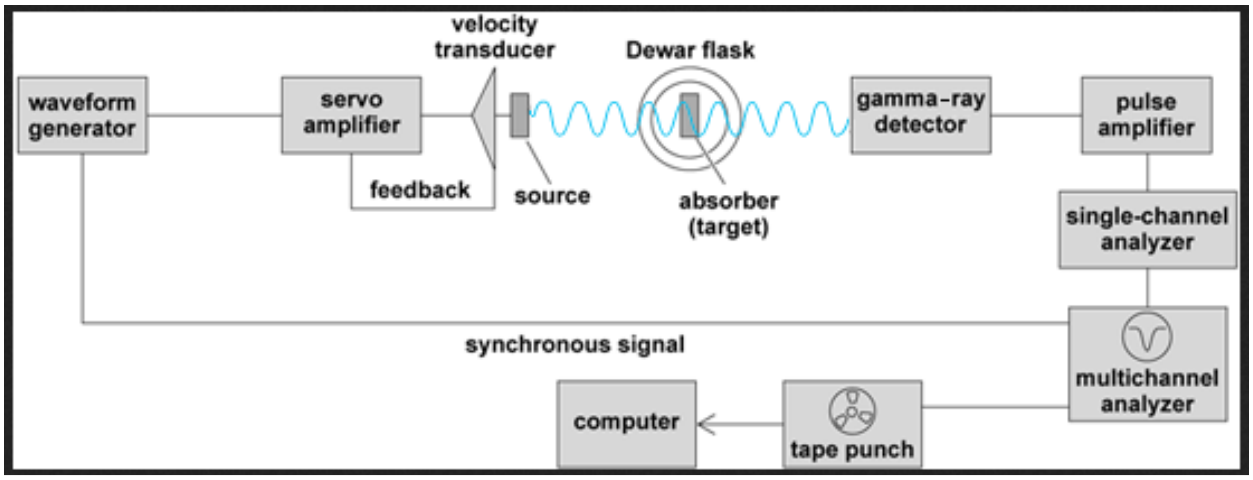

Fig. 3.2. Schematic diagram of Mössbauer spectrometer [45].

Hyperfine interaction happens because of the interaction between Mössbauer nucleus and its surrounding environment and brings the change in the energy levels basically by three main interactions. the isomer shift, the electric quadrupole splitting, and the hyperfine magnetic field. The recoil-free fraction (*f*) is also another factor that plays the important role in Mössbauer spectrometry.

- **Isomer shift (δ)**

Isomer shift is the shift in energy caused by the transition of electron in s-electron. It is the direct measure of electron density at the nucleus. Isomer shift (IS) arises due to alterations in the electrostatic response between the non-zero probability *s*- orbital electrons and the non-zero volume nucleus orbiting around it. The whole spectrum is shifted towards –ve direction or towards +ve direction depending upon the value of isomer shift. It was found that the 3d electrons are responsible to partly screen the nuclear charge from the 4s electrons so the increasing number of 3d electrons reduces the s-electron density at ^{57}Fe nucleus causing more positive shift [46].

- **Electric quadrupole splitting**

The symmetry of the nucleus depends on its spin which differs for the ground and excited states of the nucleus. In the electric field gradient there will be different alignments of the electric quadrupole moment of the nucleus for different interaction energies. Thus it is the measure of non-spherical nuclear charge distribution which is caused by the nuclei state having an angular momentum quantum number I > 1/2. In the case of an isotope with a I = 3/2 excited state, such as ^{57}Fe or ^{119}Sn, the 3/2 to 1/2 transition is split into two substates $m_I = \pm 1/2$ and $m_I = \pm 3/2$ causing two specific peaks in a spectrum called 'doublet'. Thus the Quadrupole splitting is measured as the separation between these two peaks which gives the nature of electric field at the nucleus. **Fig. 3.3** explains more about quadrupole splitting.

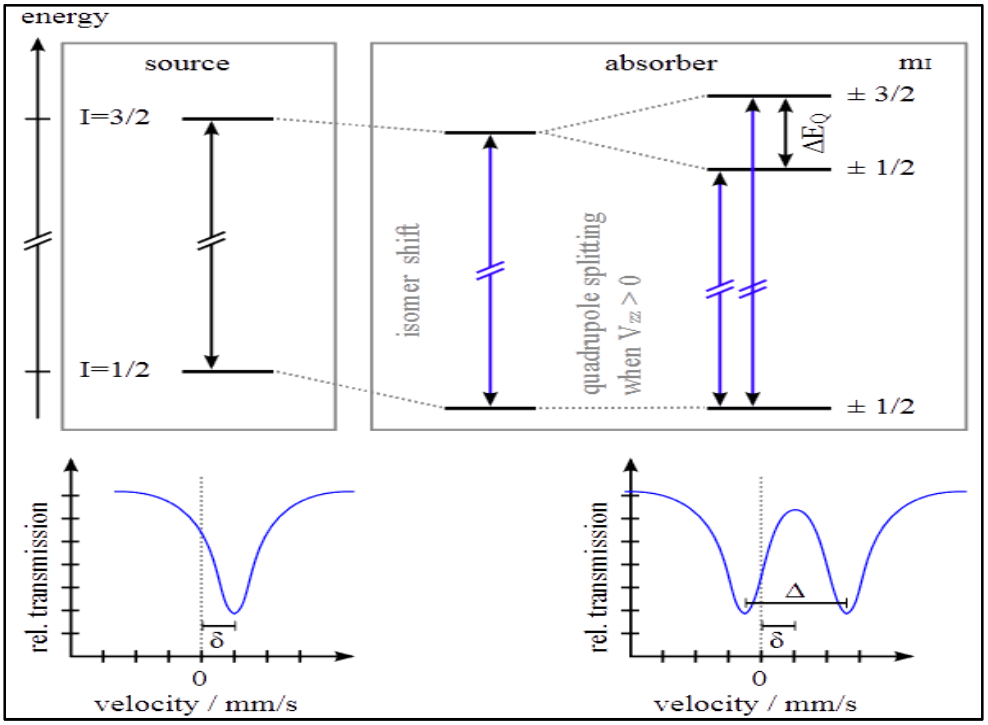

Fig. 3.3. Isomer shift and quadrupole splitting of the nuclear energy levels and corresponding Mössbauer spectra.

- **Hyperfine magnetic field splitting**

The spin can be oriented with different projection along a magnetic field, and hence the energies of nuclear transitions are therefore different and should be modified when the nucleus is in magnetic field. They are sometimes called "nuclear Zeeman effect." Thus the hyperfine magnetic fields causes the degeneracies of the spin states of the nucleus arises because of the different transitions in the Mössbauer spectrum as shown in **Fig. 3.4**. There are only six transition from I = ±1/2 to I = ±3/2 subjected to the selection rule and causes sextet spectrum which is very close to the magnetic field experienced by the nucleus below Curie temperature (Tc) called hyperfine field (B_{hf})

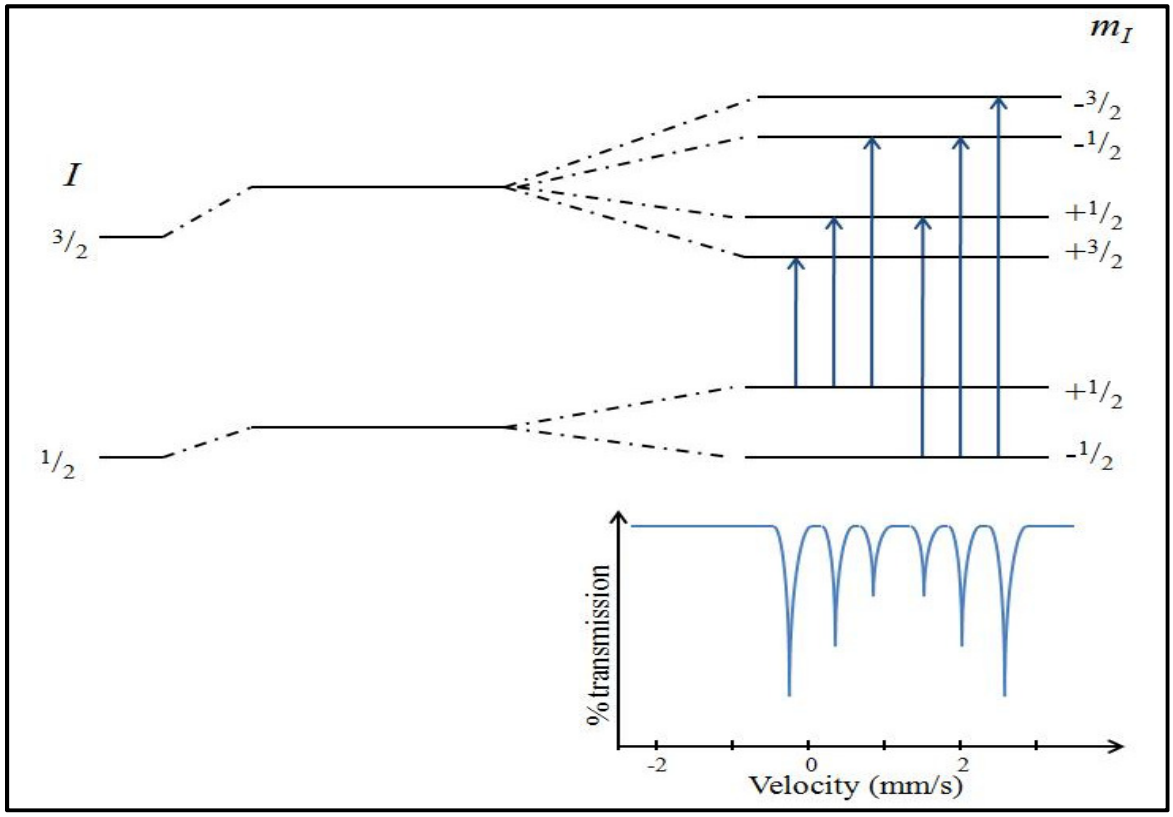

Fig. 3.4. Magnetic splitting of the nuclear energy levels and the corresponding Mössbauer spectrum.

.

CHAPTER 4

RESULT AND DISCUSSION

4.1 Structural analysis of $Dy_2Fe_{17-x}Zr_x$

The structural properties of $Dy_2Fe_{17-x}Zr_x$ (x = 0.00, 0.25, 0.50, 0.75, 1.00) were investigated using powder x-ray diffraction experiment using Cu-Kα radiation. **Fig. 4.1** shows that the XRD pattern of $Dy_2Fe_{17-x}Zr_x$ intermetallic as a function of Zr content. The XRD result shows that the samples have Th_2Ni_{17} structure (hexagonal, space group, $P6_3/mmc$).

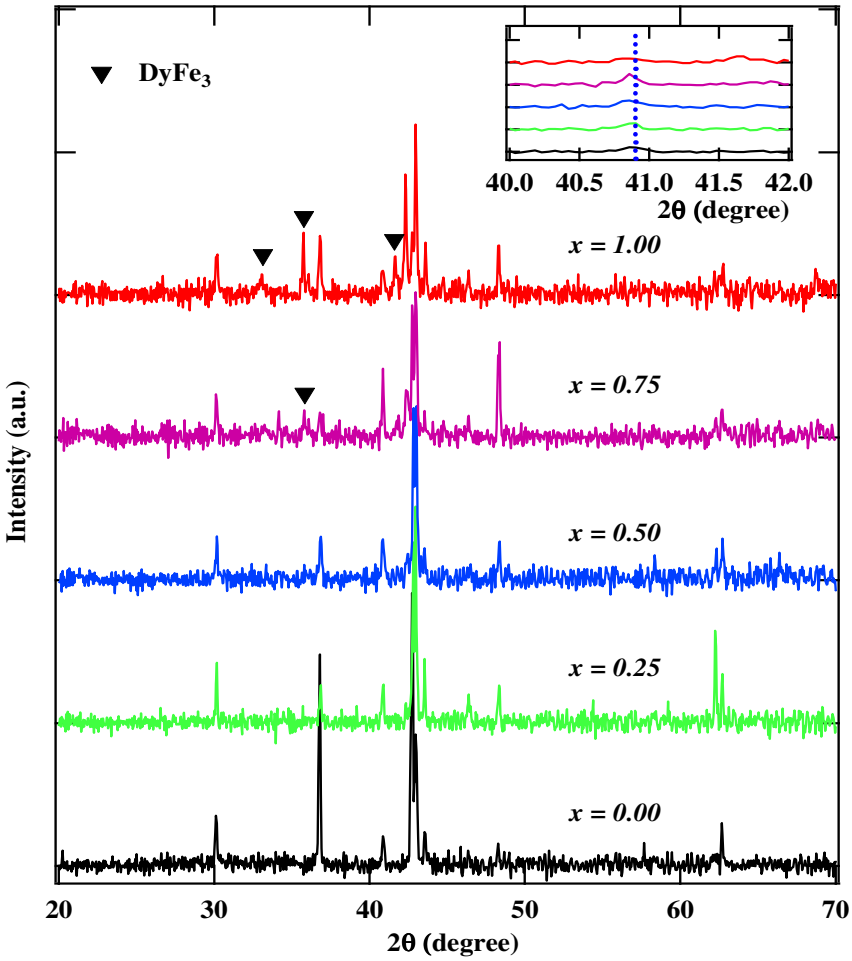

Fig. 4.1. x-ray diffraction patterns of $Dy_2Fe_{17-x}Zr_x$ compounds.

The XRD patterns also show that the peaks shift towards lower diffraction angles indicating the unit cell volume expansion upon Zr substitution. The samples are in single phase up to x = 0.5. At higher concentrations of Zr (x > 0.5) the XRD patterns show the presence of secondary paramagnetic phase of $DyFe_3$ [47, 48, 49].

The XRD data was analyzed using Rietveld refinement. Rietveld refinement is a technique to refine crystal structure and perform quantitative phase analysis. It was discovered by Rietveld in 1969 A.D. It is based on the least square fitting between step-scan data of measured diffraction pattern and simulated x-ray diffraction pattern. One can obtain lattice parameter, scale factor, peak profile, particle size etc. using Rietveld analysis [44]. The Rietveld refinement of raw data was performed using Th_2Ni_{17} structure with four in-equivalent 4*f*, 6*g*, 12*j* and 12*k* Fe sites, and two 2*b* and 2*d* sites for Dy by Rietveld refinement by assuming ionic radii fo Zr, Fe, Dy as 0.84(3) Å, 0.55(3) Å and 1.03(3) Å respectively. The fitted data are shown in Fig.4.2.a. – Fig. 4.2.e.

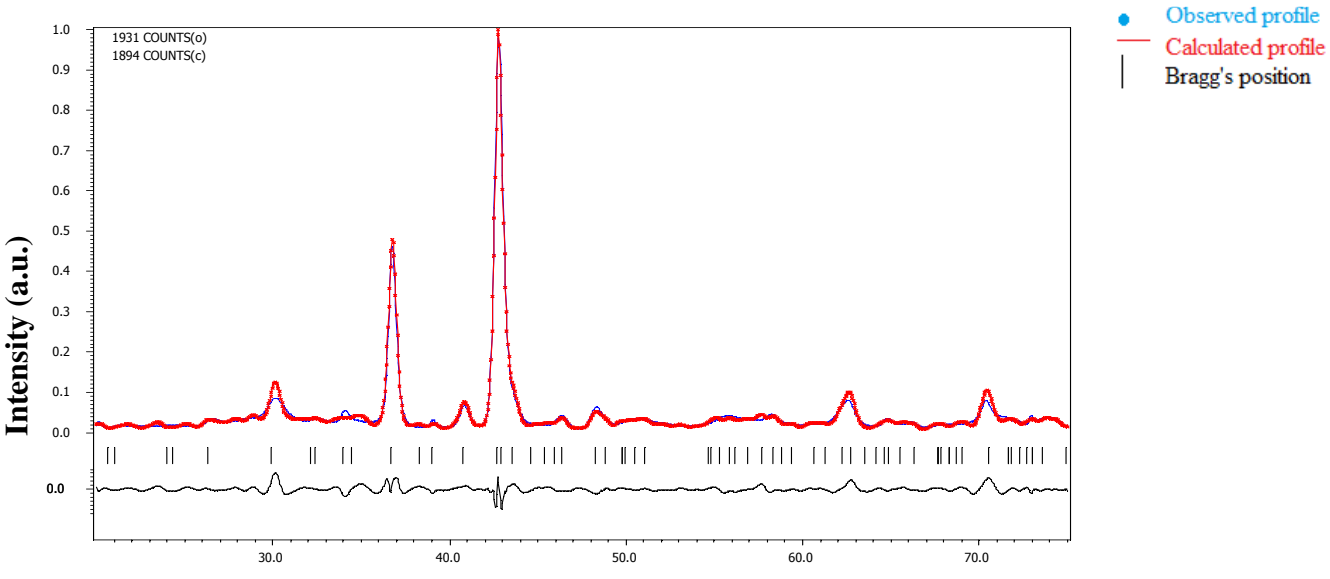

Fig. 4.2 a. Rietveld refinement profile for Dy_2Fe_{17}.

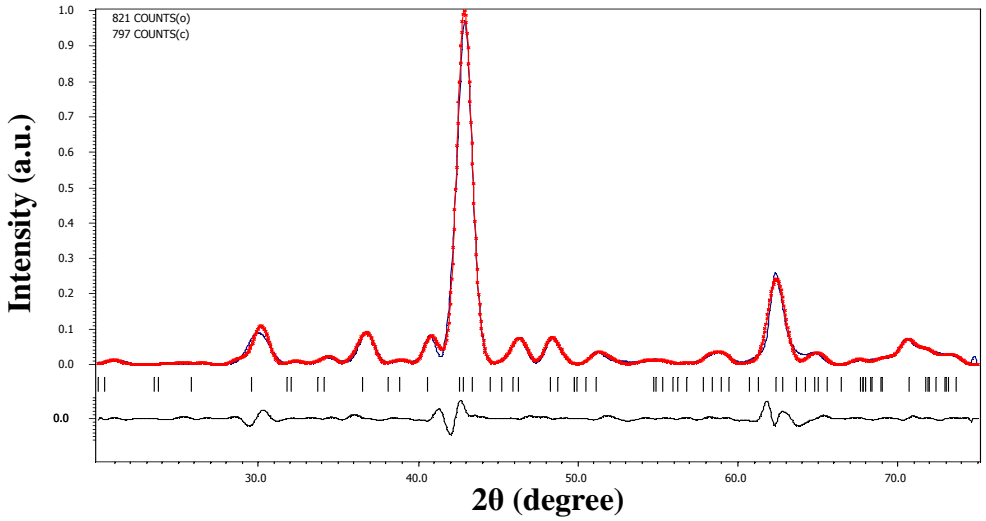

Fig. 4.2 b. Rietveld refinement profile for $Dy_2Fe_{16.75}Zr_{0.25}$.

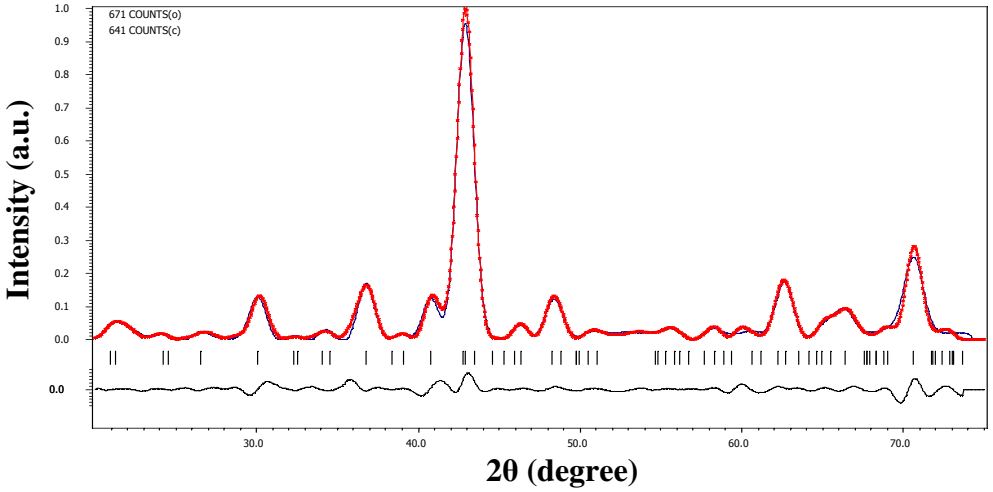

Fig. 4.2 c. Rietveld refinement profile for $Dy_2Fe_{16.5}Zr_{0.5}$.

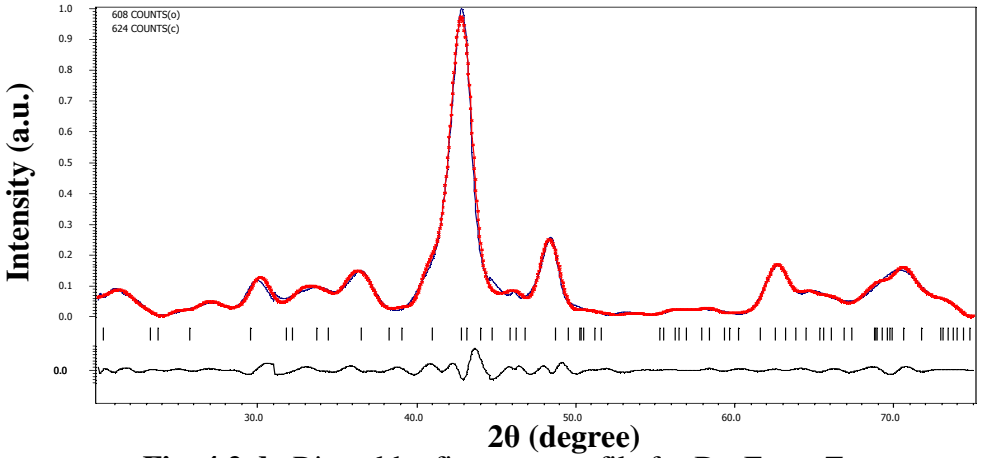

Fig. 4.2 d. Rietveld refinement profile for $Dy_2Fe_{16.25}Zr_{0.75}$.

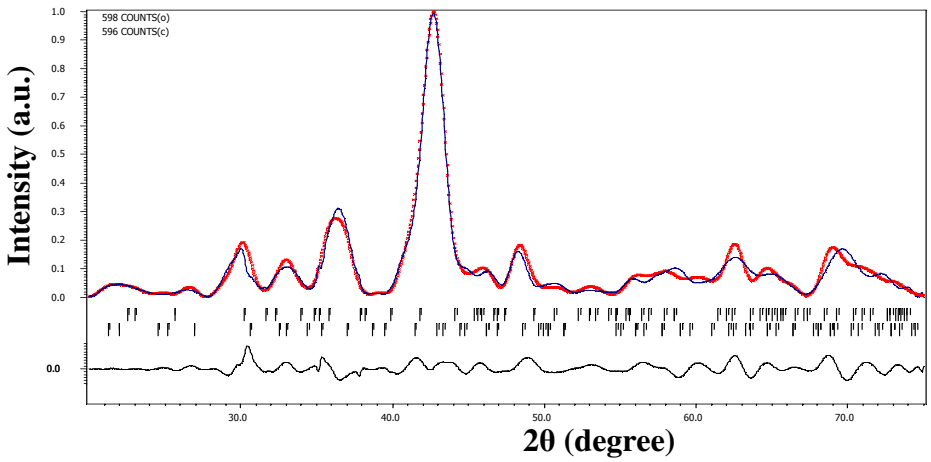

Fig. 4.2 .e . Rietveld refinement profile for $Dy_2Fe_{16}Zr_1$.

Lattice parameters of $Dy_2Fe_{17-x}Zr_x$

In substituted R_2Fe_{17} compounds, the lattice parameters '*a*' and '*c*' and the unit cell volume (V) vary differently for different substituents for Fe. The trend of lattice parameters and unit cell volume expansion in the previous studies Ce_2Fe_{17-}xGax [37], $Tb_2Fe_{17-x}Ga_x$ [50], and $Dy_2Fe_{17-x}Ga_x$ [27] shows that the unit cell volume expands with the Ga substitution. Similar unit cell volume expansion have been observed in other non-magnetic atom doped compounds such as $Nd_2Fe_{17-x}Al_x$ [25], R_2Fe_{17-x} $(A, T)_x$ {A= Al, Si, Ga; T= Transition metal} [10]. The lattice parameters '*a*'and '*c*' along with unit cell volume of $Dy_2Fe_{17-x}Zr_x$ derived from Rietveld refinement are plotted as a function of Zr content are shown in **Fig 4.3** and lattice parameters values are listed in **Table 4.1**. From **Fig. 4.3**, it is observed that the lattice parameters '*a*' increases at the rate of 0.0716 Å/Zr-atom and '*c*' increases at the rate of 0.0436 Å/Zr-atoms. The corresponding increase in the unit cell volume is 8.2084 $Å^3$/Zr-atoms. The increase in the unit cell volume is expected because atomic radius of Zr (2.06 Å) is greater than the atomic radius of Fe (1.56 Å).

Table 4.1. Lattice parameters and unit cell volume of $Dy_2Fe_{17-x}Zr_x$ obtained from Rietveld refinements of XRD data.

			$Dy_2Fe_{17-x}Zr_x$				
x	**a (Å)**	**c (Å)**	**V (Å^3)**	**R_{obs}(%)**	***w*R_{obs}(%)**	**R_p(%)**	***w*R_p(%)**
0.00	8.45541(11)	8.29036(4)	513.303(18)	4.17	5.95	10.65	14.49
0.25	8.46147(19)	8.29361(13)	515.456(21)	3.13	4.16	12.32	15.43
0.50	8.46963(16)	8.30442(12)	516.913(16)	4.16	4.33	11.91	17.21
0.75	8.4749(14)	8.30836(11)	517.725(21)	4.52	5.11	9.32	10.12
1.00	8.53823(17)	8.33743(19)	522.429(13)	5.01	6.99	9.96	10.21

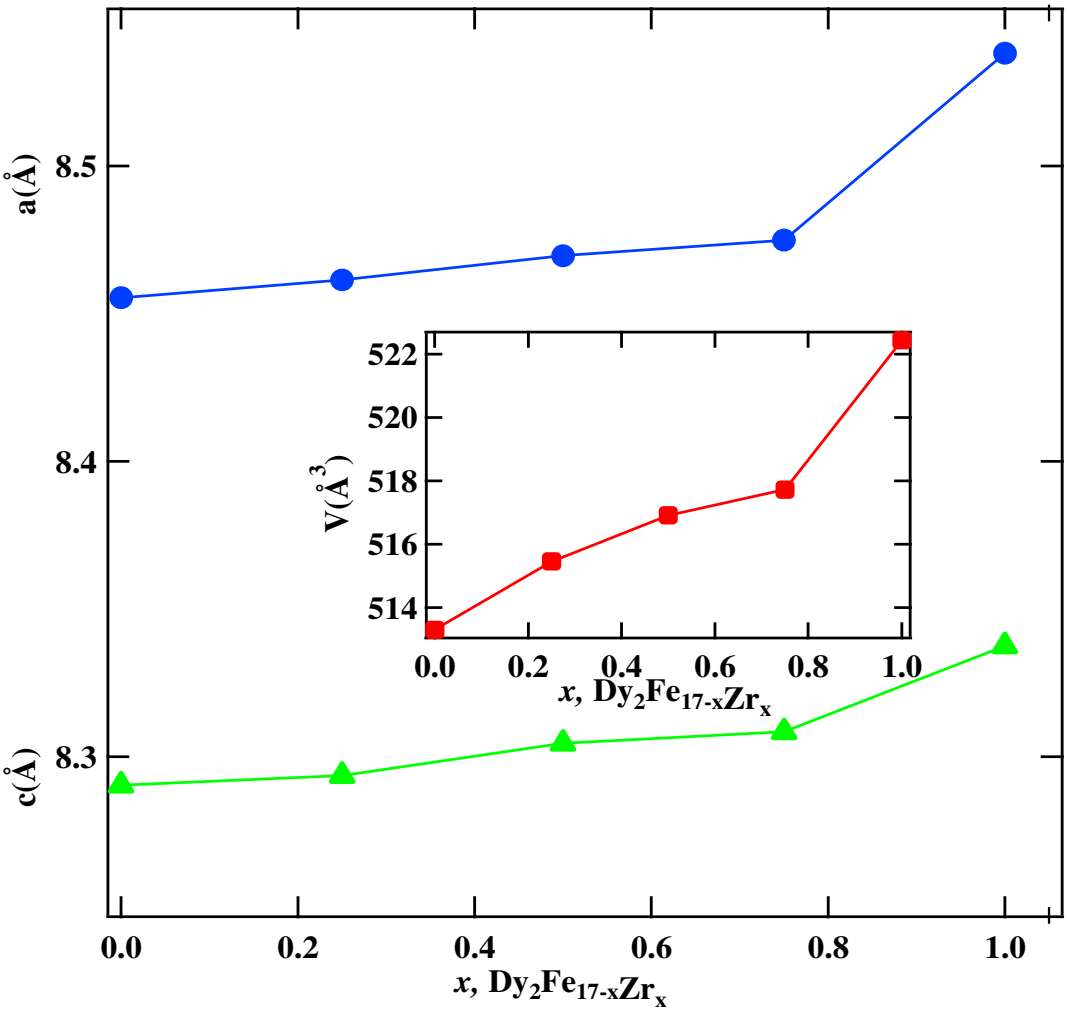

Fig. 4.3 . Lattice parameters *a* and *c* with unit cell volume of $Dy_2Fe_{17-x}Zr_x$ as a function of Zr content.

Site occupancy of $Dy_2Fe_{17-x}Zr_x$

From the XRD pattern it is found that $Dy_2Fe_{17-x}Zr_x$ compounds are hexagonal in structure. The hexagonal compounds possess four 4*f*, 6*g*, 12*j* and 12*k* Fe sites. Previous studies on a wide variety of rare-earth-transition metal intermetallic have shown that the preferred occupancy of the transition metal is independent of the rare earth sites. It is observed from Rietveld refinement of the powder sample for $Dy_2Fe_{17-x}Zr_x$ that Zr occupies the transition metal sites namely 4*f*, 6*g*, 12*j* and 12*k*. The percentage site occupancy of Zr is plotted in **Fig. 4.4** and is listed in **Table 4.2**. From **Fig. 4.4** it is noticed that Zr preferentially occupy 12*j* and 12*k* Fe sites. It is observed that the site occupancy increases with the increase in Zr content. The pattern of replacement of iron by zirconium is similar to that observed with Ga substitution such as, $Tb_2Fe_{17-x}Ga_x$ [51] and $R_2Fe_{17-x}(A,T)_x$ (A= Al, Si, Ga; T = transition metal) [10]. This substitution pattern is observed to be different than Al and Si substitution where Al preferentially occupy 18*f* and 18*h* sites in Th_2Zn_{17} structure in $R_2Fe_{17-x}Al_xC$ and $Nd_2Fe_{17-x-z}Al_xSi_z$ [52, 50]

Table 4.2. The site occupancy table for $Dy_2Fe_{17-x}Zr_x$

	Site occupancy for $Dy_2Fe_{17-x}Zr_x$ (%)							
x	**Fe(4*f*)**	**Fe(6*g*)**	**Fe(12*j*)**	**Fe(12*k*)**	**Zr(4*f*)**	**Zr(6*g*)**	**Zr(12*j*)**	**Zr(12*k*)**
0.00	16.9(59)	24.3(6)	49.5(95)	50.9(31)				
0.25	16.5(2)	24.1(7)	52.0(1)	48.0(4)	0.04(3)	0.52(6)	0.74(1)	0.68(13)
0.50	15.7(1)	24.3(4)	48.5(12)	47.5(7)	0.47(14)	1.32(15)	1.41(3)	2.11(17)
0.75	15.9(2)	23.9(5)	47.7(1)	47.1(17)	0.73(8)	1.40(3)	2.20(6)	2.20(15)
1.00	15.6(4)	22.6(4)	31.5(1)	47.0(3)	0.98(7)	2.61(6)	3.14(3)	2.84(11)

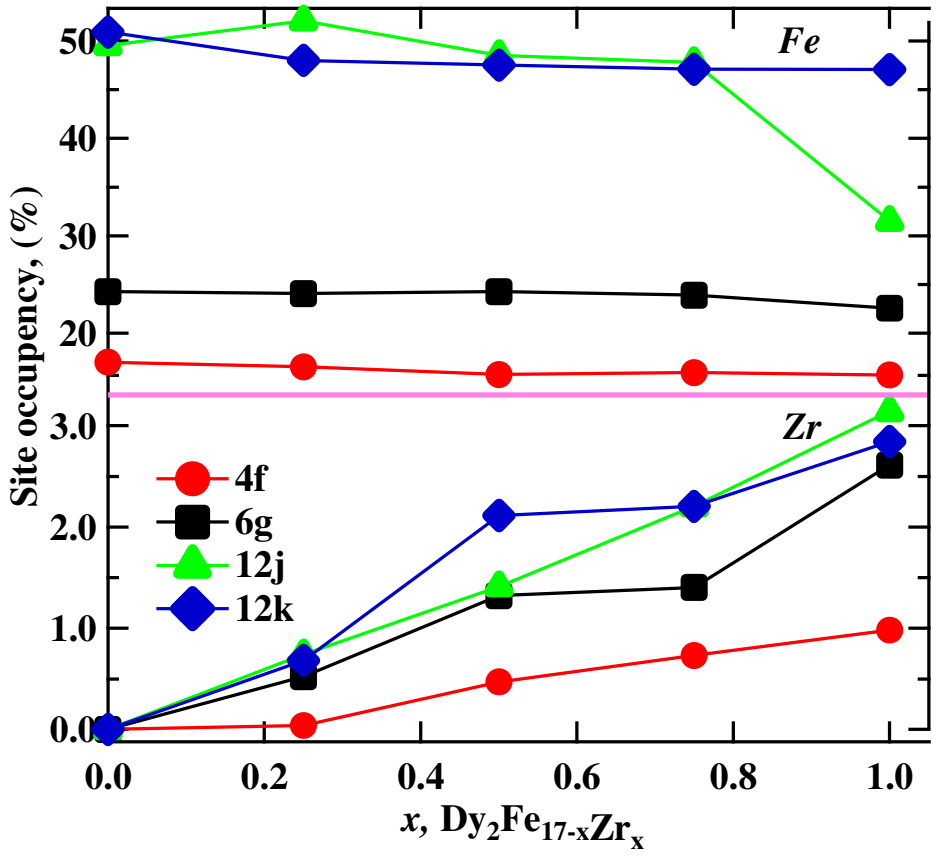

Fig. 4.4 . The percentage occupancy of Fe and Zr at iron sites in $Dy_2Fe_{17-x}Zr_x$ as a function of Zr content.

Bond length of $Dy_2Fe_{17-x}Zr_x$

It is usually believed that the exchange interaction between Fe pairs are negative with Fe-Fe interatomic distances less than 2.45 Å, and positive with interatomic distances greater than 2.45 Å. The bond lengths between Fe-Fe sites as a function of Zr substitution in $Dy_2Fe_{17-x}Zr_x$ are tabulated in **Table 4.**3. It is seen from **Fig. 4.5** that there is an overall increase in Fe-Fe bond length with Zr substitution. However, maximum change in Fe-Fe bond length is observed to occur for 6*g*-12*j*, 6*g*-12*k* and 12*j*-12*j* sites. This change in bond length will affect the strength of Fe-Fe exchange interaction.

Table 4.3. Bond length for $Dy_2Fe_{17-x}Zr_x$

	Bond length for $Dy_2Fe_{17-x}Zr_x$(Å)				
x	***4f*-4*f***	***6g*-12*j***	***6g*-12*k***	***12j*-12*j***	***12k*-12*k***
0.00	2.406	2.418	2.443	2.425	2.440
0.25	2.407	2.495	2.630	2.552	2.449
0.50	2.412	2.542	2.669	2.560	2.458
0.75	2.427	2.801	2.693	2.572	2.464
1.00	2.439	2.851	2.772	2.592	2.488

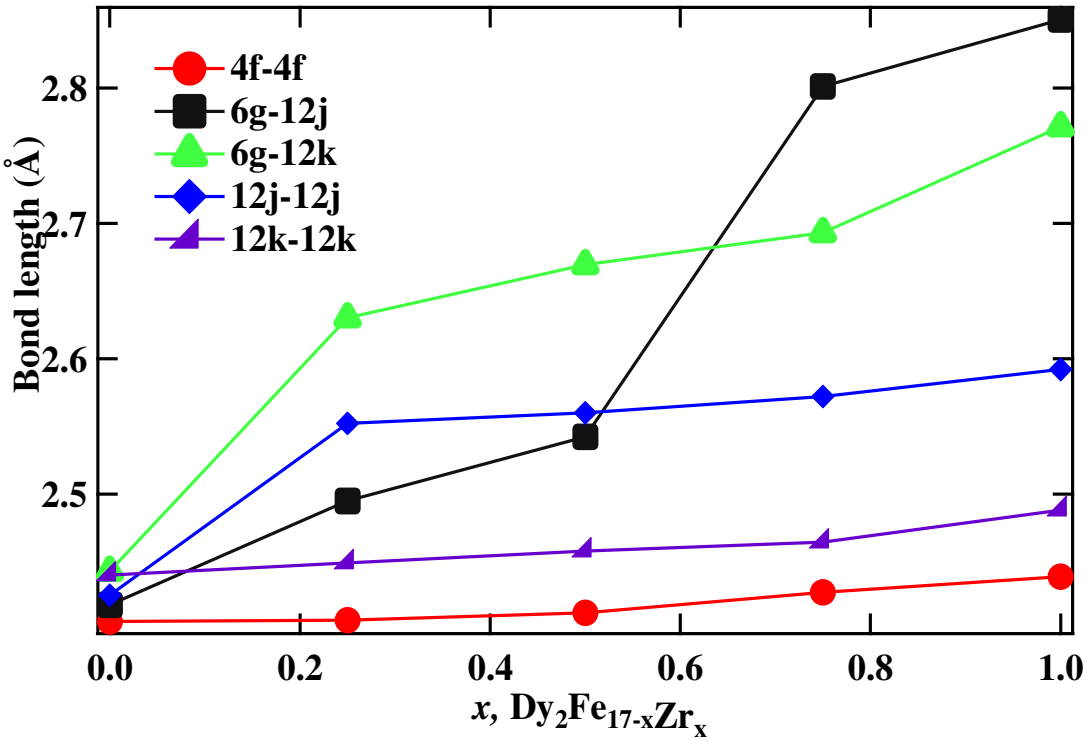

Fig. 4.5. Dependence of bond lengths on *x* of $Dy_2Fe_{17-x}Zr_x$.

4.2 Structural analysis of $Dy_2Fe_{16}Ga_{1-x}Zr_x$

The structural properties of the $Dy_2Fe_{16}Ga_{1-x}Zr_x$ (x = 0.00, 0.25, 0.50, 0.75, 1.00) samples are carried out using the XRD with Cu-Kα radiation. The XRD patterns of

$Dy_2Fe_{16}Ga_{1-x}Zr_x$ are shown in **Fig. 4.6**.The XRD patterns show that the samples are in the hexagonal Th_2Ni_{17} structure with the space group $P6_3/mmc$.

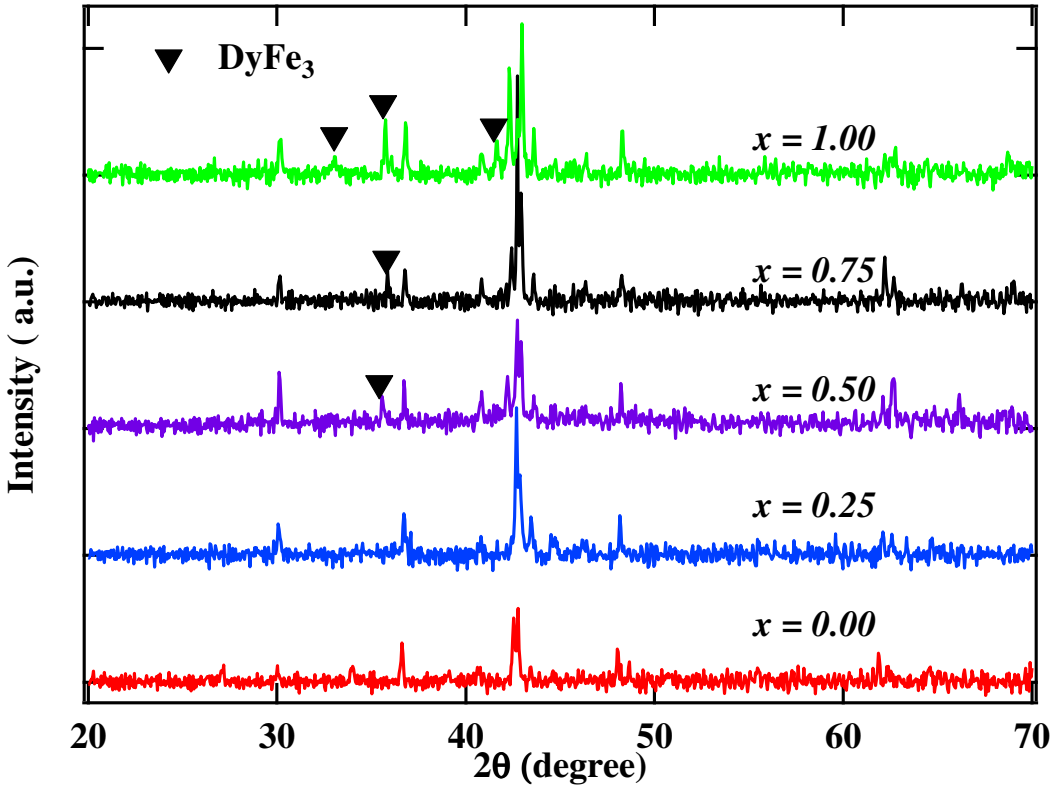

Fig. 4.6 . X-ray diffraction patterns of $Dy_2Fe_{16}Ga_{1-x}Zr_x$ compounds.

The XRD pattern show that the samples are in the single phase up to 0.25. At $x >$ 0.25 emergence of a paramagnetic $DyFe_3$ phase was observed. The XRD data were fitted using Rietveld analysis considering Th_2Ni_{17} structure with four in-equivalent 4*f*, 6*g*, 12*j* and 12*k* sites. The ionic radii for Zr, Fe, Dy and Ga are 0.84(3) Å, 0.55(3) Å and 1.03(3) Å and 0.62(3) Å respectively considered for the Rietveld refinement. The fitted data is shown in the **Fig. 4.7a** - **Fig. 4.7 e**.

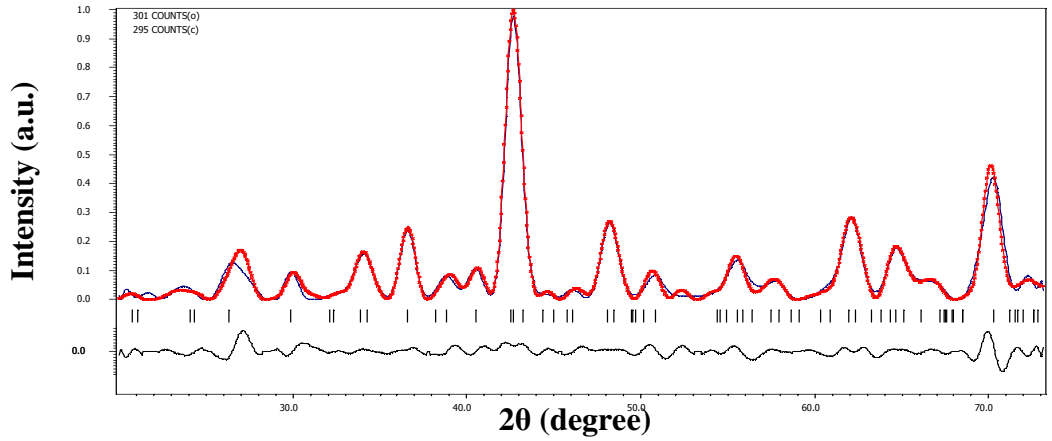

Fig. 4.7 a. Rietveld refinement profile for $Dy_2Fe_{16}Ga_1$.

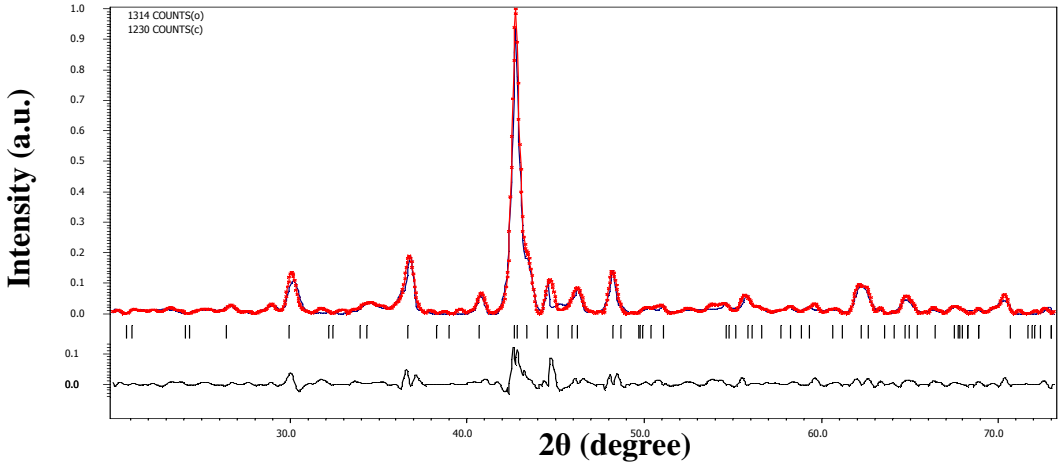

Fig. 4.7 b . Rietveld refinement profile for $Dy_2Fe_{16}Ga_{0.75Zr0.25}$.

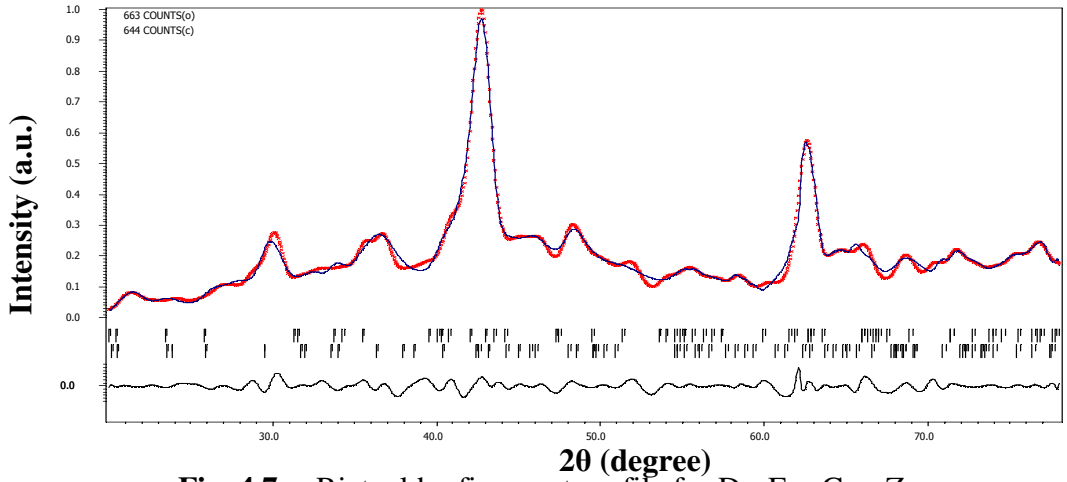

Fig. 4.7 c. Rietveld refinement profile for $Dy_2Fe_{16}Ga_{0.5}Zr_{0.5}$.

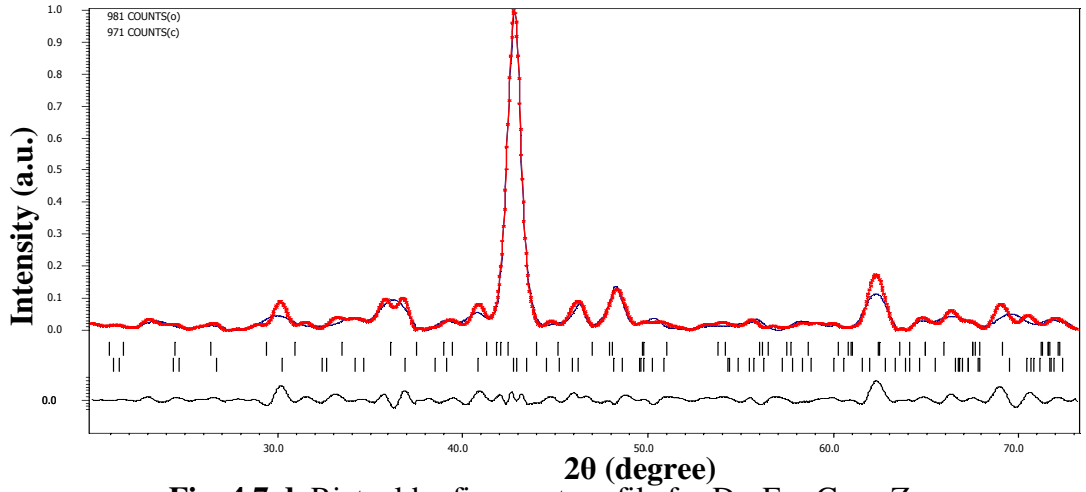

Fig. 4.7 d. Rietveld refinement profile for $Dy_2Fe_{16}Ga_{0.25}Zr_{0.75}$.

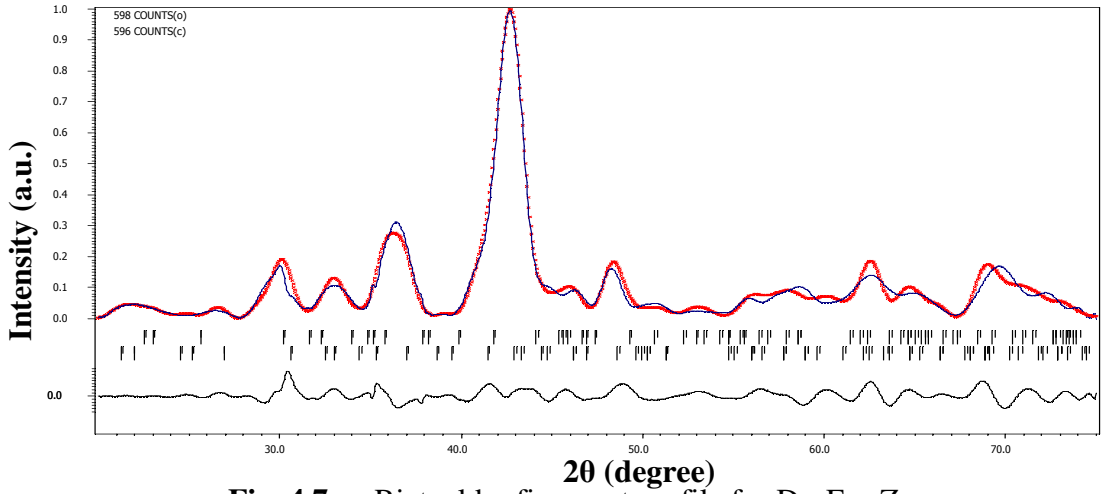

Fig. 4.7 e . Rietveld refinement profile for $Dy_2Fe_{16}Zr_1$.

Lattice parameters of $Dy_2Fe_{16}Ga_{1-x}Zr_x$

The lattice parameters '*a* 'and '*c*' along with unit cell volume of $Dy_2Fe_{16}Ga_{1-x}Zr_x$ as a function of Zr content is plotted in **Fig. 4.8** and tabulated in **Table 4.4**. The lattice parameters '*a*', '*c*' and unit cell volume of $Dy_2Fe_{16}Ga_{1-x}Zr_x$ were obtained from the Rietveld refinement. From **Fig. 4.8**, it is observed that the lattice parameters '*a*' increases at the rate of 0.0796 Å/Zr atom and '*c*' increases at the rate of 0.0522 Å/Zr. The corresponding increase in the unit cell volume is 8.826 $Å^3$/Zr atoms which is closed to the

literature $Nd_2Fe_{17-x-y}Ti_xAl_y$ and $Nd_2Fe_{17-x-z}Al_xSi_z$ [53, 50]. The increase in the unit cell volume is expected as the Zr atom radius (2.06 Å) is greater than the atomic radius of Ga (1.36Å). The observed value of unit cell expansion in $Dy_2Fe_{16}Ga_{1-x}Zr_x$ is higher than that observed for $Dy_2Fe_{17-x}Zr_x$.

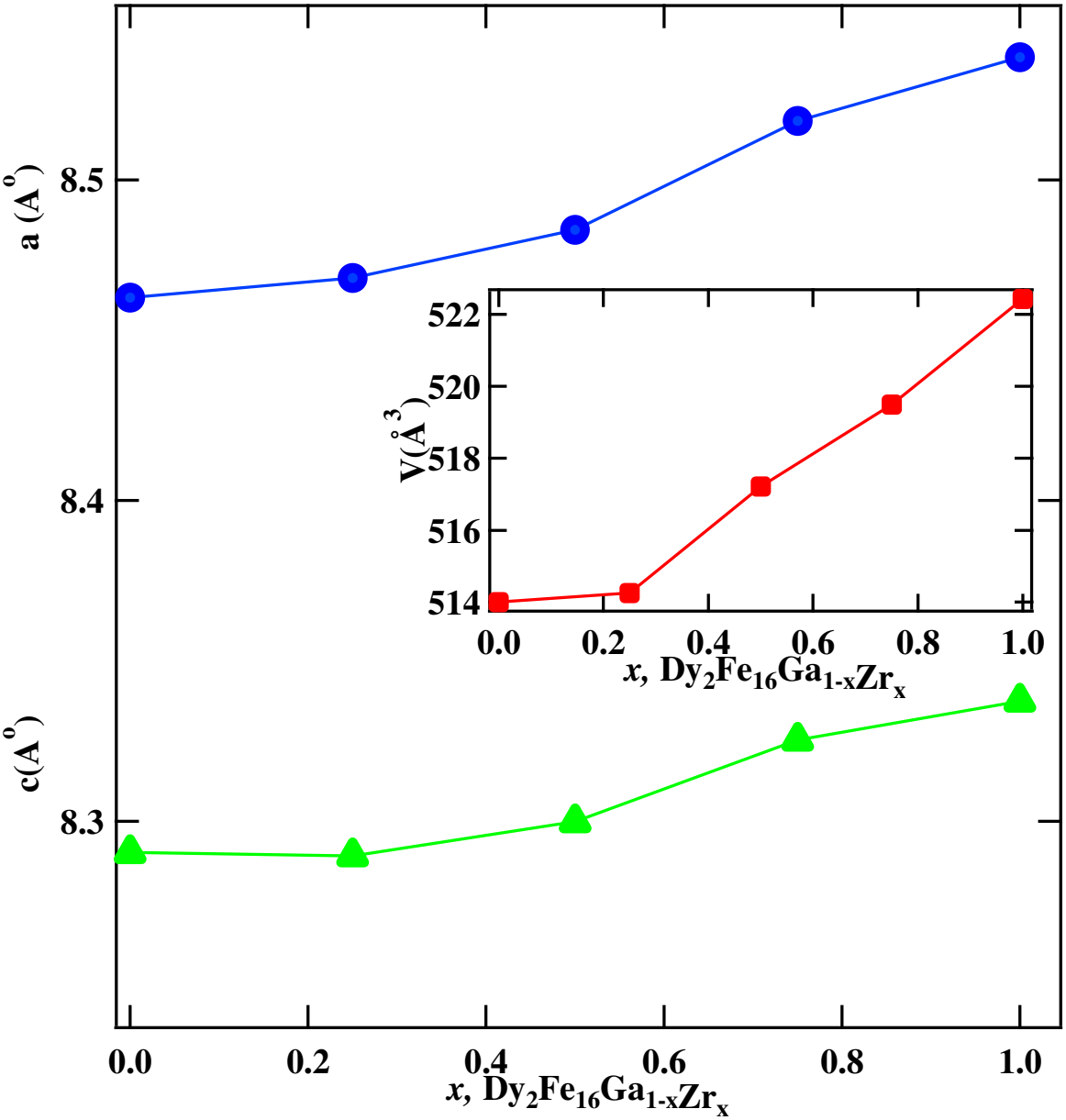

Fig. 4.8. Lattice parameters and unit cell volume of $Dy_2Fe_{16}Ga_{1-x}Zr_x$ alloy.

Table 4.4. Lattice parameters and unit cell volume of $Dy_2Fe_{16}Ga_{1-x}Zr_x$ obtained from Rietveld refinements of XRD data.

	$Dy_2Fe_{16}Ga_{1-x}Zr_x$						
x	***a* (Å)**	***c* (Å)**	**V (Å^3)**	**R_{obs} (%)**	**wR_{obs} (%)**	**R_p (%)**	**wR_p (%)**
0.00	8.46324(3)	8.29025(3)	514.013(26)	5.97	6.17	10.21	12.13
0.25	8.46943(15)	8.28922(7)	514.265(28)	5.65	6.97	13.64	16.98
0.50	8.48437(12)	8.29985(5)	517.221(23)	4.52	5.11	9.32	10.12
0.75	8.51833(7)	8.32536(7)	519.498(13)	5.21	6.12	12.21	11.21
1.00	8.53823(17)	8.33743(19)	522.429(13)	5.01	6.99	9.96	10.21

Site occupancy of $Dy_2Fe_{16}Ga_{1-x}Zr_x$

The site occupancy of Zr and Ga for $Dy_2Fe_{16}Ga_{1-x}Zr_x$ is plotted in **Fig. 4.9** and listed in **Table 4.5**. As reported in the literature, Ga mostly occupies 12*j* and 12*k* sites [10, 43]. Rietveld analysis shows that Zr preferentially replaces Ga from 12*j* and 12*k* sites and shows minimum affinity for 4*f* and 6*g* sites. The rise in Zr occupancy and decrease in the Ga occupancy at 12*j* and 12*k* site shows that Zr is replacing Ga.

Table 4.5. The site occupancy table for $Dy_2Fe_{16}Ga_{1-x}Zr_x$

	Site occupancy for $Dy_2Fe_{16}Ga_{1-x}Zr_x$ (%)							
x	**Ga(4*f*)**	**Ga(6*g*)**	**Ga(12*j*)**	**Ga(12*k*)**	**Zr(4*f*)**	**Zr(6*g*)**	**Zr(12*j*)**	**Zr(12*k*)**
0.00	0.86(21)	1.36(15)	3.57(16)	3.14(23)	0.00	0.00	0.00	0.00
0.25	0.88(43)	1.13(43)	2.13(12)	2.16(11)	0.27(12)	0.38(14)	0.71(36)	0.72(41)
0.50	0.49(31)	0.73(42)	1.47(13)	1.47(32)	0.49(41)	0.73(32)	1.43(32)	1.45(11)
0.75	0.14(22)	0.37(62)	0.74(16)	0.73(31)	0.62(21)	1.51(21)	1.85(22)	1.92(13)
1.00	0.00	0.00	0.00	0.00	0.98(7)	2.61(6)	3.14(3)	2.84(11)

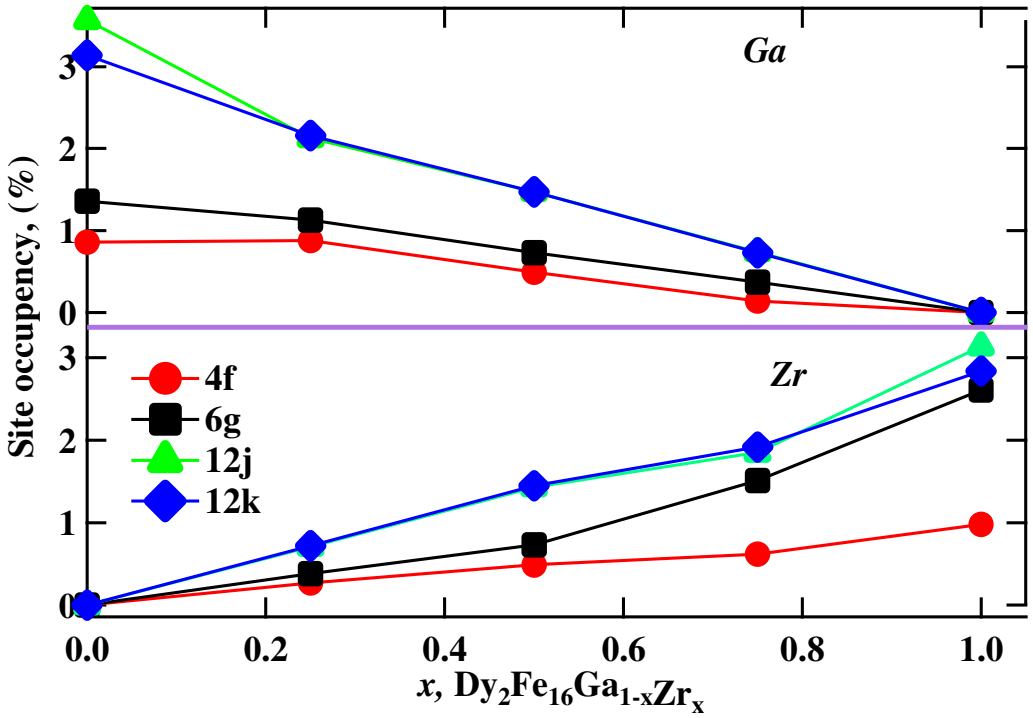

Fig. 4.9. The percentage occupancy of Fe and Zr at Ga sites in $Dy_2Fe_{16}Ga_{1-x}Zr_x$ as a function of Zr content.

Bond length of $Dy_2Fe_{16}Ga_{1-x}Zr_x$

The bond lengths between Fe-Fe sites as a function of Zr substitution in $Dy_2Fe_{16}Ga_{1-x}Zr_x$ are shown in **Fig. 4.10** and numerical values are listed in **Table 4.6**. It is seen from **Fig. 4.10** that sites distances increases with Zr substation. This increase in the bond length between the Fe-Fe atoms is coming from the unit cell expansion.

Table 4.6 . The Fe-Fe bond length for $Dy_2Fe_{16}Ga_{1-x}Zr_x$

	Bond length for $Dy_2Fe_{16}Ga_{1-x}Zr_x$(Å)				
x	***4f*-*4f***	***6g*-12*j***	***6g*-12*k***	***12j*-12*j***	***12k*-12*k***
0.00	2.418	2.433	2.455	2.442	2.447
0.25	2.423	2.443	2.469	2.443	2.447
0.50	2.435	2.462	2.479	2.488	2.474
0.75	2.437	2.466	2.483	2.499	2.478
1.00	2.439	2.85	2.771	2.592	2.488

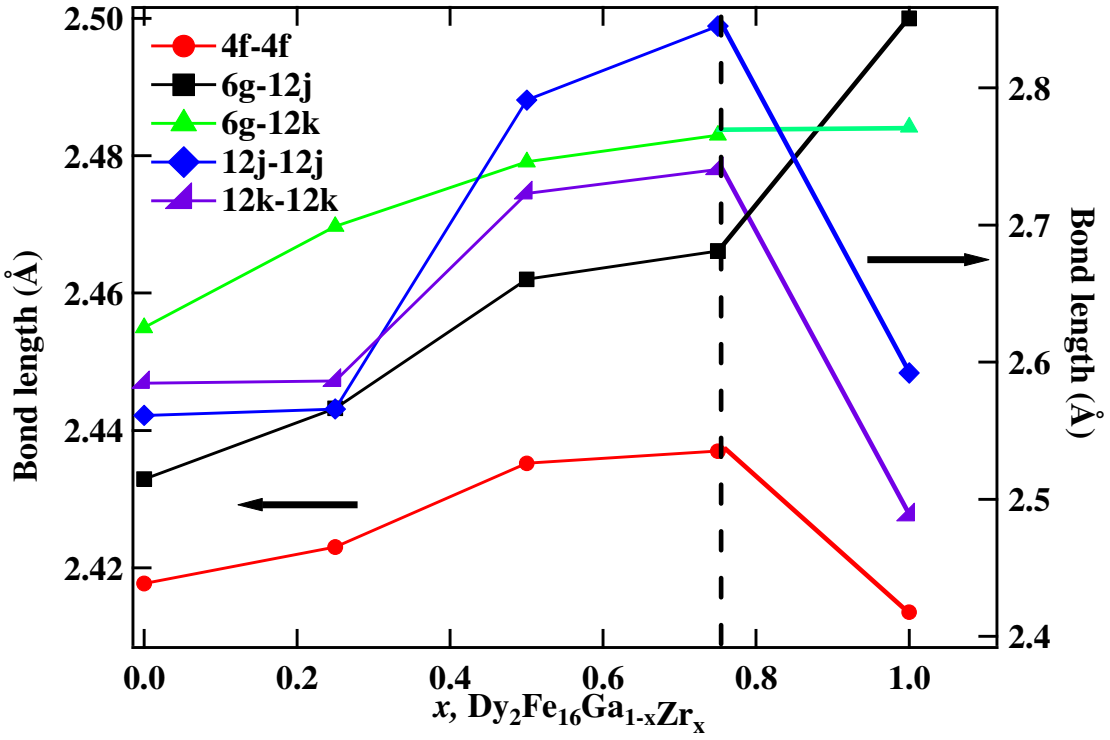

Fig. 4.10. Dependence of bond lengths on x of $Dy_2Fe_{16}Ga_{1-x}Zr_x$.

4.3 Magnetic properties of $Dy_2Fe_{17-x}Zr_x$ and $Dy_2Fe_{16}Ga_{1--x}Zr_x$

The room temperature magnetic properties obtained from M vs. H measurement for $Dy_2Fe_{17-x}Zr_x$ and $Dy_2Fe_{16}Ga_{1-x}Zr_x$ are plotted in **Fig. 4.11** and **Fig. 4.12** respectively. The room temperature magnetic parameters are listed in **Table 4.7**. The M vs. H plot show that the saturation magnetization (Ms) decreases with increase in the Zr substitution in both $Dy_2Fe_{17-x}Zr_x$ and $Dy_2Fe_{16}Ga_{1-x}Zr_x$. The decrease in saturation magnetization on $Dy_2Fe_{17-x}Zr_x$ with increase in Zr content is attributed to the substitution of non-magnetic Zr atom for Fe atom. This decrease in the saturation magnetization is the result of dilution effect, *i.e.* replacing Fe atom (2.2 μ_B) with non-magnetic Zr atom. The net magnetization of R_2Fe_{17} compound results from magnetic R atoms and Fe atoms. Replacing Fe atoms with non-magnetic atoms obviously reduces the net magnetic moments per unit cell. Similar reduction in Ms has been reported earlier for $Dy_2Fe_{17-x}Ga_x$ [27], $Ce_2Fe_{17-x}Ga_x$

[37], $Sm_2Fe_{17-x}Ga_x$ [34], $Sm_2Fe_{17-x}Cr_x$ [54], $R_2Fe_{17-x}Al_xC$ [52] compounds. From **Fig. 4.13** it is observed that the saturation magnetization of $Dy_2Fe_{17-x}Zr_x$ is observed to decrease linearly at the rate of 10.99 emu/gm per Zr atom.

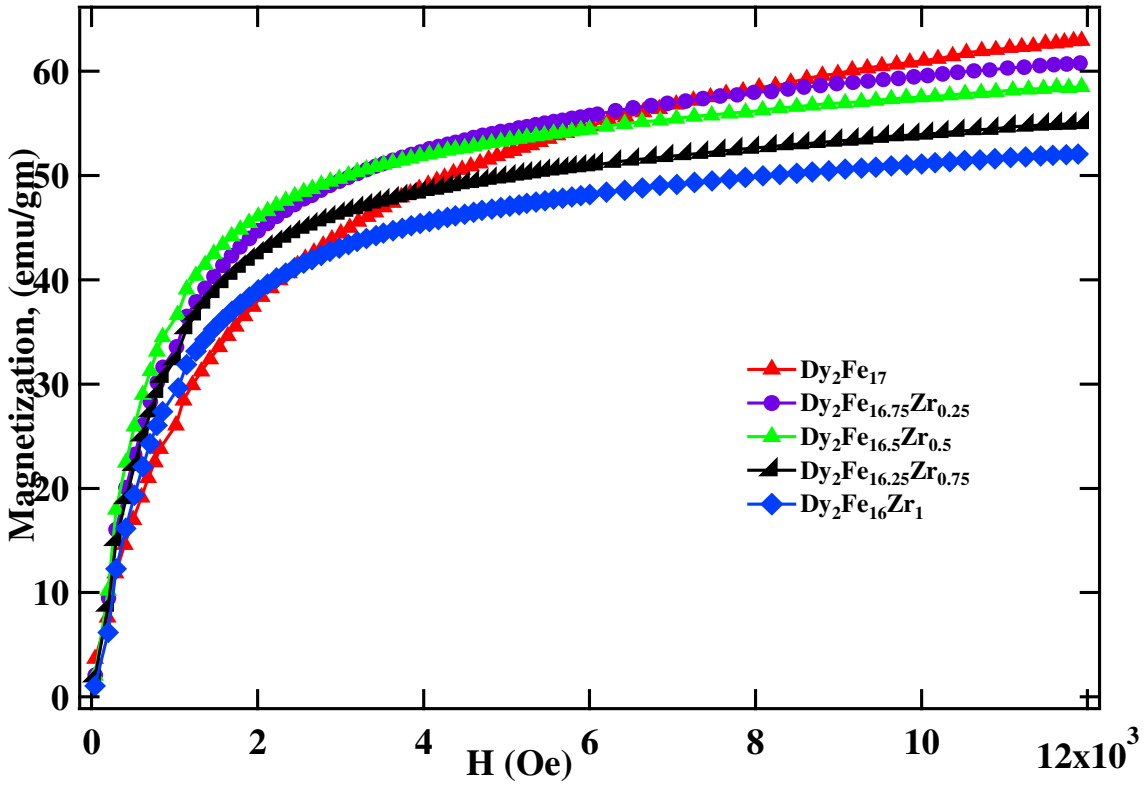

Fig. 4.11. RT M vs. H plot of $Dy_2Fe_{17-x}Zr_x$.

The saturation magnetization (Ms) of $Dy_2Fe_{16}Ga_{1-x}Zr_x$ as a function of Zr content is shown in **Fig. 4.12**, and the numerical values are listed in **Table 4.7**. From **Fig. 4.13**, it is observed that the decrease in magnetization is at the rate of 9.244 emu/gm per Zr atom. This result is interesting because the saturation magnetization is reducing with Zr addition in spite of no change in number of Fe atoms. Thus, the observed reduction in saturation magnetization may not result from the dilution effect as observed in $Dy_2Fe_{17-x}Zr_x$. This decrease in Ms of $Dy_2Fe_{16}Ga_{1-x}Zr_x$ could be due to the predomination of

positive effect on the magnetic moment caused by the optimum of bond length over negative effect caused by the magnetic dilution of non-magnetic substituents. This result is in agreement with the $Nd_2Fe_{17-x-y}Ti_xAl_y$ [53] and $Nd_2Fe_{17-x-z}Al_xSi_z$ [50].

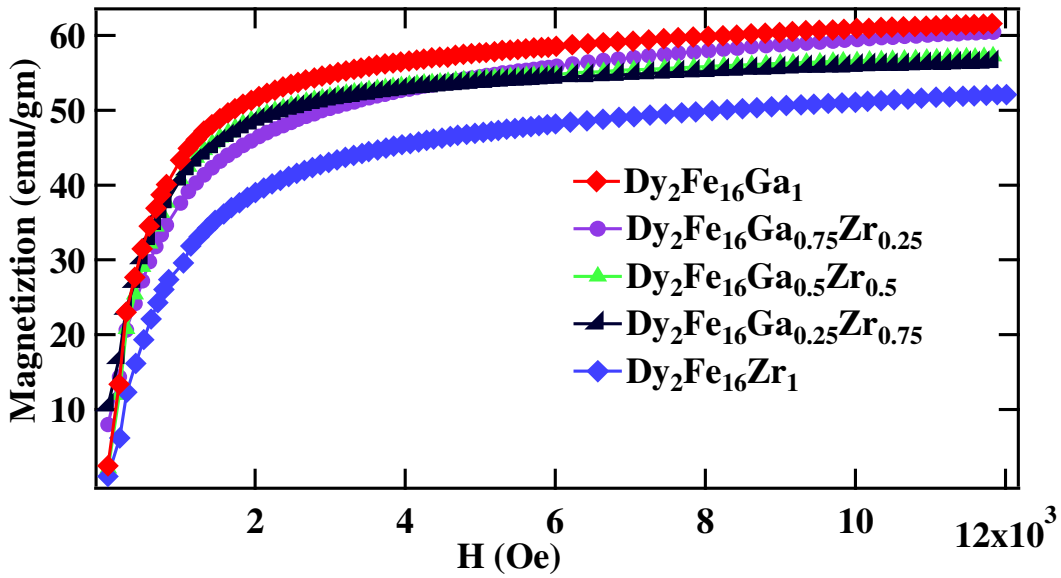

Fig. 4.12 . RT M vs. H plot of $Dy_2Fe_{16}Ga_{1-x}Zr_x$.

Table 4.7. Ms and Tc of $Dy_2Fe_{17-x}Zr_x$ and $Dy_2Fe_{16}Ga_{1-x}Zr_x$.

x	$Dy_2Fe_{17-x}Zr_x$		$Dy_2Fe_{16}Ga_{1-x}Zr_x$	
	Ms(emu/gm)	**Tc (K)**	**Ms(emu/gm)**	**Tc (K)**
0.00	62.94	408.0	61.58	488.0
0.25	60.78	456.0	60.48	500.1
0.50	58.57	503.9	57.25	505.1
0.75	55.04	510.0	56.39	502.5
1.00	52.07	425.0	52.07	425.0

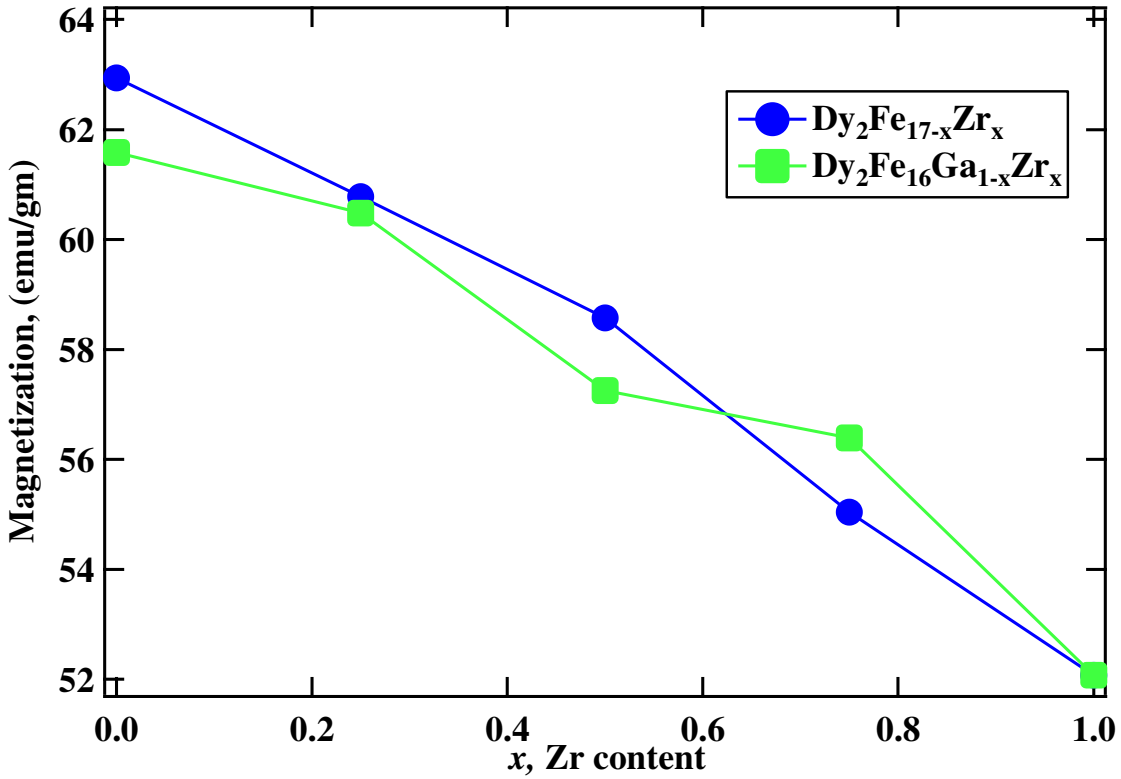

Fig. 4.13 . Ms vs. *x* plot for $Dy_2Fe_{17-x}Zr_x$ and $Dy_2Fe_{16}Ga_{1-x}Zr_x$ as a function of Zr content.

The Curie temperature Tc of $Dy_2Fe_{17-x}Zr_x$ as a function of the content of Zr content is shown in **Fig. 4.14**. It is observed that the Curie temperature in the initial Zr concentration increases rapidly from 408 K (x = 0.00) to a maximum of 510 K (x = 0.75) and then decreases to 425 K (x = 1.00). This achieved Curie temperature of $Dy_2Fe_{16.25}Zr_{0.75}$ is 102 K higher than that of $Dy_2Fe_{17.}$ As discussed in **Table 4.**3 and **Table 4.6**, the bond length increases with the increase in the Zr content. The increase in Tc is mainly due to the increase in strength of the Fe-Fe exchange coupling that occurs from the increase in Fe-Fe bond lengths as observed in **Fig. 4.5** and **Fig. 4.10** [9].

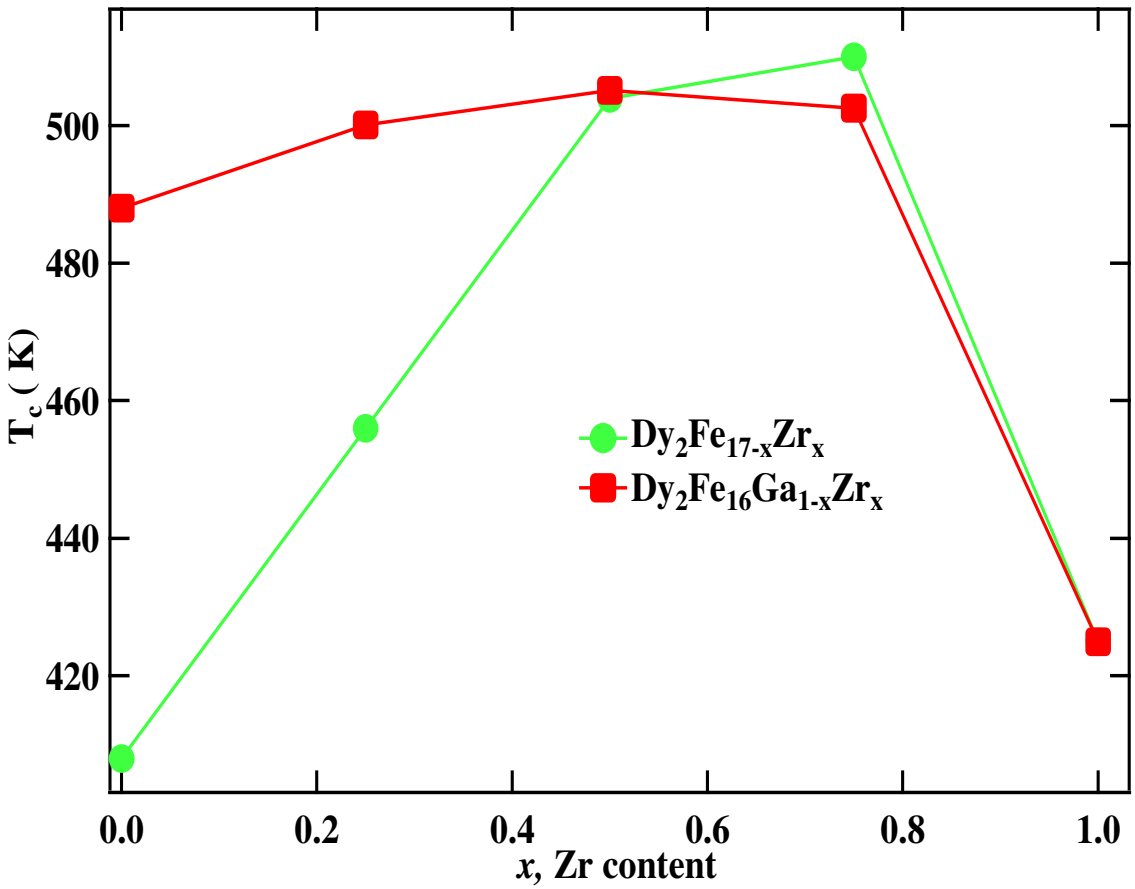

Fig. 4.14. RT Tc plot for $Dy_2Fe_{17-x}Zr_x$ and $Dy_2Fe_{16}Ga_{1-x}Zr_x$ as a function of Zr content.

The Curie temperature Tc of $Dy_2Fe_{16}Ga_{1--x}Zr_x$ as a function of Zr content is shown in the **Fig. 4.14**. It is observed that the Curie temperature increases slowly from 488 K (x = 0.00) to maximum of 505.1 K (x = 0.50) and then decreases to 425 K (x = 1.00). Thus achieved Tc of $Dy_2Fe_{16}Ga_{0.5}Zr_{0.5}$ (505.1 K) is 17.1 K greater than that of $Dy_2Fe_{16}Ga_1$ and 97 K higher than the Dy_2Fe_{17}. Thus it is observed the double substitution of Zr and Ga does slow enhancement in Tc over the single substation.

In general the Curie temperature in rare earth intermetallic is due to three kinds of exchange interactions namely the 3d-3d exchange interactions, *i.e.* between the magnetic moment of the Fe sub-lattice (J_{FeFe}), 4f-4f exchange interaction, i.e. the interaction between the magnetic moment within the R sub-lattice (J_{RR}), and the inter sub-lattice 3d-

4f exchange interaction (J_{RFe}). It is found in the literature that the Curie temperature (Tc) increases with the increase in the J_{FeFe} [10]. Thus the increase or decrease in Tc in the $Dy_2Fe_{17-x}Zr_x$ and $Dy_2Fe_{16}Ga_{1-x}Zr_x$ may be due to the increase or decrease in the interaction parameter J_{FeFe}. The interactions between the rare earth spins (4*f*-4*f*) are assumed to be weak and negligible in comparison with the other two types of interactions. The low curie temperature of R_2Fe_{17} compounds primarily due to the very short Fe-Fe interatomic distance at the dumbbell sites (4*f* or 6*g*) where the Fe atoms couple antiferomagnetically [55]. In the compounds with hexagonal structure the Fe(4*f*)-Fe(4*f*) interactions are strongly negative whereas the Fe(6*g*)- Fe(12*j*) , Fe(6*g*)-Fe(12*k*) and Fe(12*k*)-Fe(12*k*) interactions are weakly negatives.

4.4 Mössbauer Studies

Mössbauer studies of $Dy_2Fe_{17-x}Zr_x$

The Mössbauer spectra of $Dy_2Fe_{17-x}Zr_x$ (x=0.00, 0.25, 0.50, 0.75, 1.00) are plotted in **Fig. 4.16**. The resulting spectra were fitted using WMOSS program. Since the Dy_2Fe_{17} compounds have a basal magnetization, either seven or eight magnetic sextets are required to fit their Mössbauer spectra [56]. So, the fits shown in **Fig. 4.16** have been carried out with eight magnetic sextets assigned to 4*f*, 6*g*, 12*j*, and 12*k* sites in Dy_2Fe_{17}. Doublets were used for additional phases for some samples having paramagnetic phase during Mössbauer fitting. The spectra agree well with those reported by Bara et.al. [29].

The hyperfine parameters resulting from these fits at room temperature are tabled in **Table 4.8**. The hyperfine field (B_{hf}) decreases with increasing Zr concentration. The hyperfine field values of Dy_2Fe_{17} are similar to Dy_2Fe_{17} of $Dy_2Fe_{17}H_x$ [56]. This

decrease in the hyperfine fields results from the decrease in magnetic moments of iron in $Dy_2Fe_{17-x}Zr_x$. It was found that percentage area occupied by the formation of $DyFe_3$ phase is increasing and for $x = 1$ it was observed 9.23%. This observation supports the formation of additional paramagnetic phase $DyFe_3$ as seen in XRD (**Fig. 4.1**).

On an average, the isomer shifts (IS) of all sites increases with the increase in Zr content. The increase in the isomer shift (IS) could be related to the volume expansion resulting from the Zr substitution for Fe. The volume expansion lowers the *s*-electron density at the Fe nuclei which leads to an increase in isomer shift (IS). At higher Zr content ($x = 1$) decrease in isomer shift (IS) was observed. This decrease in the isomer shift may result from the combine effect of volume expansion and increase the in electron density.

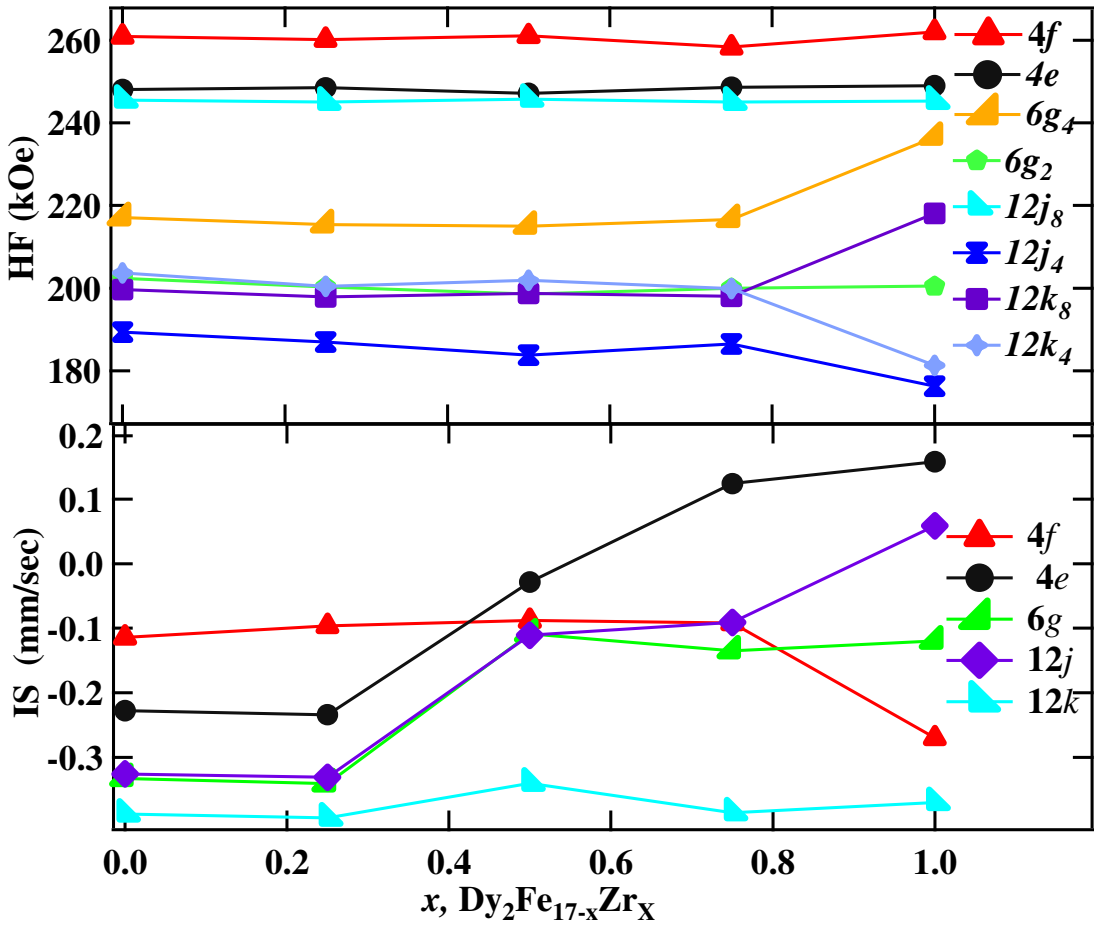

Fig. 4.15 . RT Mössbauer hyperfine parameters for $Dy_2Fe_{17-x}Zr_x$.

Table 4.8. Mössbauer spectral hyperfine parameters for $Dy_2Fe_{17-x}Zr_x$.

	x	4*f*	4*e*	6g_4	6g_2	12j_8	12j_4	12k_8	12k_4	Doublet
HF (kOe)	0.00	261.0	248.0	217.0	202.4	245.6	189.0	199.7	203.7	
	0.25	260.2	248.5	215.3	200.3	245.0	187.0	197.9	200.4	
	0.50	261.1	247.1	214.9	198.6	245.8	184.0	198.7	201.9	
	0.75	258.4	248.7	216.6	200.0	245.0	186.0	198.0	199.9	35.2
	1.00	262.1	249.0	236.5	200.5	245.3	176.0	218.1	181.3	34.0
IS (mm/sec)	0.00	-0.114	-0.228	-0.333	-0.33	-0.326	-0.33	-0.39	-0.39	
	0.25	-0.096	-0.234	-0.341	-0.34	-0.331	-0.33	-0.39	-0.39	
	0.50	-0.088	-0.028	-0.109	-0.11	-0.111	-0.11	-0.34	-0.34	
	0.75	-0.092	0.124	-0.135	-0.14	-0.091	-0.09	-0.39	-0.39	-0.035
	1.00	-0.27	0.158	-0.12	-0.12	0.059	0.06	-0.37	-0.37	0.056
QS (mm/sec)	0.00	0.152	0.191	0.152	0.303	-0.295	0.4	0.083	-0.58	
	0.25	0.152	0.16	0.128	0.296	-0.291	0.4	-0.03	-0.58	
	0.50	0.119	0.163	0.175	0.289	-0.276	0.4	0.121	-0.5	
	0.75	0.178	0.301	0.157	0.335	-0.199	0.4	-0.03	-0.58	-0.58
	1.00	0.123	0.25	-0.048	0.155	-0.25	0.35	0.042	-0.58	-0.39
Area (%)	0.00	4.0	1.9	15.3	17.5	4.3	19.5	10.9	13.1	
	0.25	5.5	8.2	17.7	17.4	6.3	16.0	10.4	13.3	
	0.50	6.2	6.7	21.9	17.3	6.0	11..7	9.60	15.1	
	0.75	5.2	4.0	18.0	19.0	7.6	10.0	14.2	13.5	9.14
	1.00	4.2	4.9	11.2	31.9	6.2	4.21	23.1	15.2	9. 23

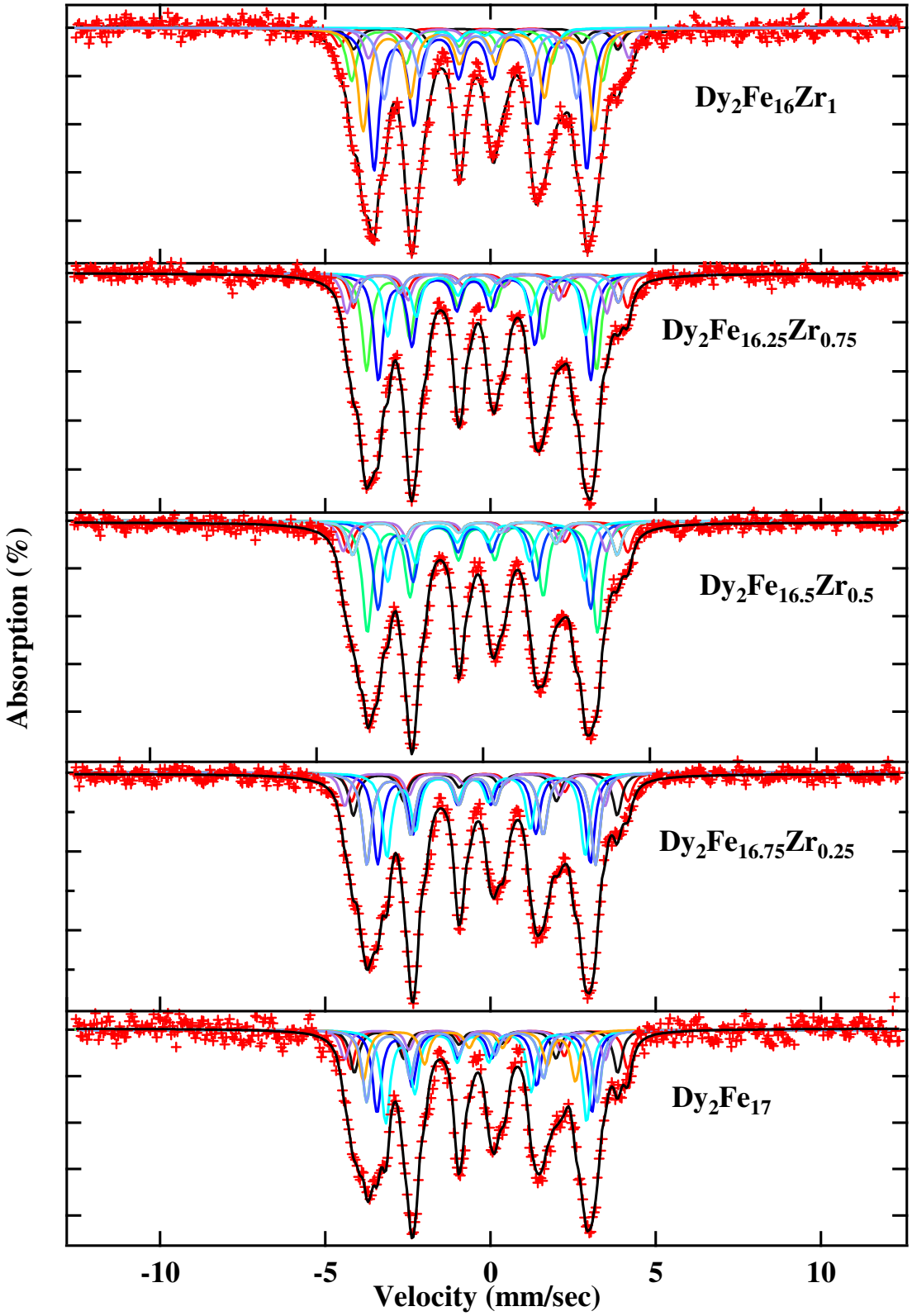

Fig. 4.16. RT fitted Mössbauer spectra of $Dy_2Fe_{17-x}Zr_x$.

Mössbauer studies of $Dy_2Fe_{16}Ga_{1-x}Zr_x$

The Mössbauer spectra of $Dy_2Fe_{16}Ga_{1-x}Zr_x$ (x = 0.00, 0.25, 0.50, 0.75, 1.00) are obtained with Cobalt-57 source and were calibrated at room temperature with α-iron foil. The resulting spectra have been fitted using WMOSS program using sextet and are shown in **Fig. 4.18** as a function of Zr content. The hyperfine parameters are obtained by fitting and are shown in **Fig. 4.17**. Eight magnetic sextets were assigned to the 4*f*, 6*g*, 12*j*, and 12*k* during fitting. Doublets are used for additional phases in some samples during Mössbauer analysis.

The hyperfine field resulting from these fit at room temperature were found to be decreasing with increasing Zr concentration. The decrease in hyperfine fields on $Dy_2Fe_{16}Ga_{1-x}Zr_x$ is attributed due to the decrease in magnetization because of the competition between positive effect on magnetic moments due to bond length and the negative effect caused by magnetic dilution of substituted non-magnetic atom.
The average isomer shift (IS) of all sites increases with increasing Zr content except 12*k* site. The increase in the isomer shift (IS) could be related to the volume expansion resulting from the Zr substitution for Ga. The volume expansion lowers the electron density at the Fe nuclei which leads to an increase in isomer shift (IS).

Table 4.9 . The RT hyperfine parameters, HF (kOe), IS (mm/sec), QS (mm/sec) and area (%) of the $Dy_2Fe_{16}Ga_{1-x}Zr_x$.

	x	4*f*	4*e*	6g_4	6g_2	12j_8	12j_4	12k_8	12k_4	Doublet
HF (kOe)	0.00	278.7	249.7	230.2	214.9	260.0	218.2	196.5	220.0	
	0.25	282.9	249.9	224.5	204.0	288.1	164.8	220.3	195.3	
	0.50	267.6	267.9	229.0	204.0	254.2	123.4	226.8	185.3	34.1
	0.75	266.7	243.7	238.1	199.4	248.6	120.7	219.2	178.3	33.4
	1.00	262.1	248.9	236.5	200.4	245.3	122.0	218.1	181.3	34.0
IS (mm/sec)	0.00	-0.126	-0.301	-0.309	-0.309	-0.422	-0.422	-0.254	-0.254	
	0.25	-0.257	-0.335	-0.356	-0.356	0.215	0.215	-0.301	-0.301	
	0.50	-0.227	-0.509	-0.367	-0.367	0.068	0.068	-0.327	-0.327	0.0023
	0.75	-0.252	0.145	-0.370	-0.370	0.041	0.041	-0.373	-0.373	0.0502
	1.00	-0.270	0.158	-0.378	-0.378	0.058	0.058	-0.370	-0.370	0.0557
QD (mm/sec)	0.00	0.158	0.0107	0.133	0.259	-0.418	-0.48	0.259	-0.58	
	0.25	0.084	-0.102	-0.093	-0.568	0.500	-0.477	0.284	0.178	
	0.50	-0.069	-0.700	-0.196	0.201	0.500	-0.134	0.249	0.118	-0.562
	0.75	-0.029	-0.600	-0.102	0.156	0.500	-0.214	0.057	0.079	-0.444
	1.00	-0.181	-0.600	-0.049	0.155	0.39	-0.142	0.042	0.136	-0.388
Area(%)	0.00	13.7	15.9	20	21.0	10.5	5.50	11.9	3.90	
	0.25	5.20	16.7	18.8	4.62	5.50	2.60	19.0	20.2	
	0.50	10.4	7.80	20.7	24.0	6.17	4.50	22.1	14.1	1.08
	0.75	6.70	3.00	28.2	4.30	3.00	26.8	12.0	14.4	1.60
	1.00	4.20	4.87	11.2	31.9	6.16	4.20	23.1	15.2	9. 23

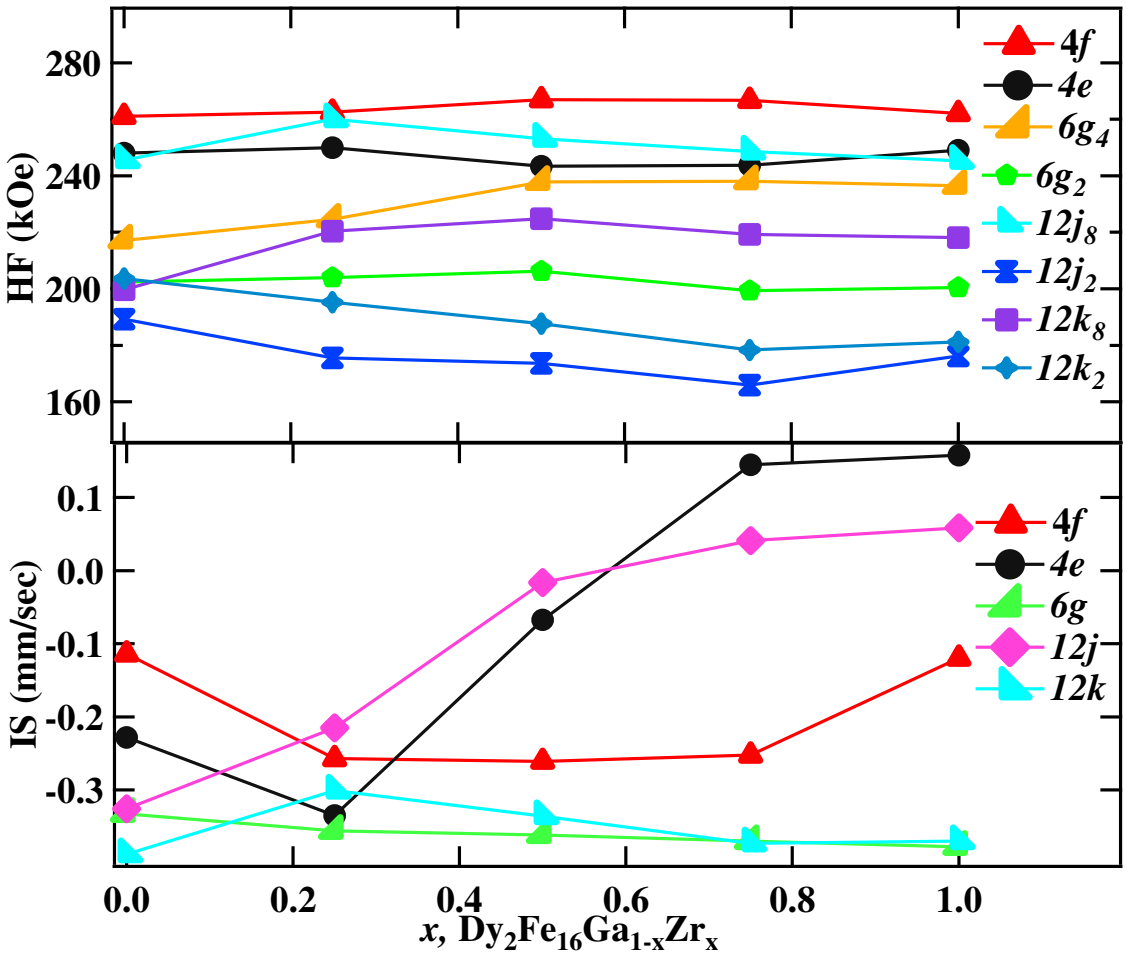

Fig. 4.17. RT Mössbauer hyperfine parameters for $Dy_2Fe_{16}Ga_{1-x}Zr_x$.

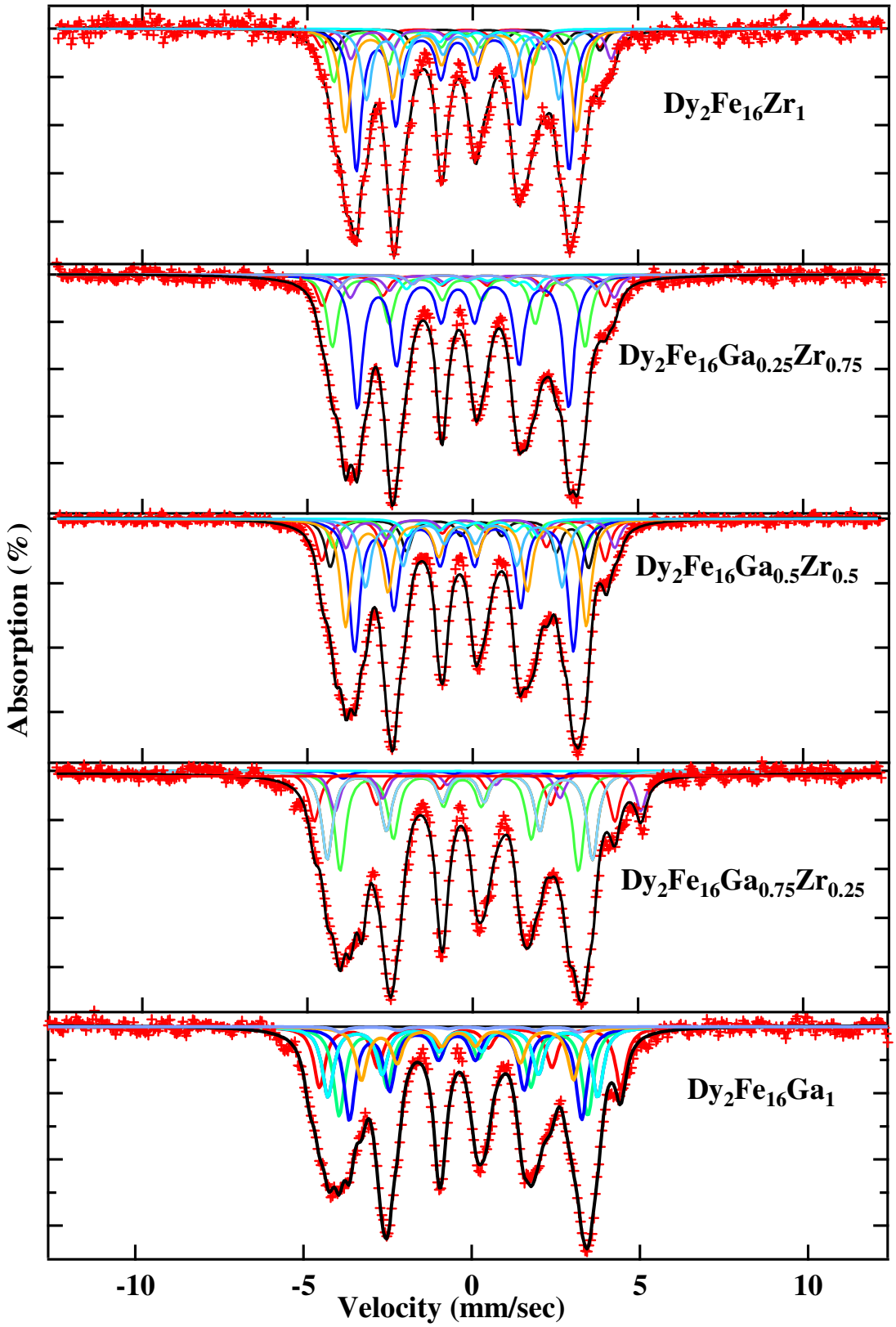

Fig. 4.18. RT fitted Mössbauer spectra of $Dy_2Fe_{16}Ga_{1-x}Zr_x$.

4.5 Comparative study of $Dy_2Fe_{17-x}Zr_x$ and $Dy_2Fe_{16}Ga_{1-x}Zr_x$

It is found from the structural analysis that both sets of intermetallic compounds are hexagonal in shape with the same space group. In the $Dy_2Fe_{17-x}Zr_x$ for higher Zr concentration beyond $x = 0.75$, the extra secondary paramagnetic phase $DyFe_3$ phase is formed but in the $Dy_2Fe_{16}Ga_{1-x}Zr_x$ the paramagnetic phase $DyFe_3$ phase appears for $x = 0.5$ and for other higher concentration. The site occupancy study of $Dy_2Fe_{17-x}Zr_x$ shows that the Zr atom occupies all the 4*f*, 6*g*, 12*j* and 12*k* Fe site. It is seen from the study of the site occupancy table that the 12*j* and 12*k* skits are mostly affected with the Zr substitution. The *c* axis parameters are found to increase slowly on $Dy_2Fe_{17-x}Zr_x$ as compared to the $Dy_2Fe_{16}Ga_{1-x}Zr_x$.

Magnetization study shows that the decrease in magnetization (Ms) is at the rate of 10.99 emu/gm per Zr atom for $Dy_2Fe_{17-x}Zr_x$ and 9.244 emu/gm per Zr atom for $Dy_2Fe_{16}Ga_{1-x}Zr_x$. The dropdown of magnetization on $Dy_2Fe_{17-x}Zr_x$ may be due to the reduction of magnetic moment of iron by Zr atoms.

The Curie temperature improvement on $Dy_2Fe_{17-x}Zr_x$ is found better on $Dy_2Fe_{16}Ga_{1-x}Zr_x$. The maximum Curie temperature observed was 510 K on $Dy_2Fe_{16.25}Zr_{0.75}$ and 505.1 K on $Dy_2Fe_{16}Ga_{0.5}Zr_{0.5}$. The rapid increase in bond length and isomer shift coming from the unit cell volume expansion helps increase in the Curie temperature of $Dy_2Fe_{17-x}Zr_x$ compared to $Dy_2Fe_{16}Ga_{1-x}Zr_x$.

4.6 Structural analysis of $Gd_2Fe_{16}Ga_{0.5}TM_{0.5}$

The substitution effect of transition metals TM = Cr, Mn, Co, Ni, Cu, Zn on the $Gd_2Fe_{16}Ga_1$ is observed and structural analysis is done using XRD with Cu-Kα radiation. **Fig. 4.19** shows that the XRD patterns of $Gd_2Fe_{16}Ga_{0.5}TM_{0.5}$ (TM = Cr, Mn, Co, Ni, Cu, Zn). The XRD result shows that the samples have Th_2Ni_{17} structure (hexagonal, space group, $P6_3/mmc$).

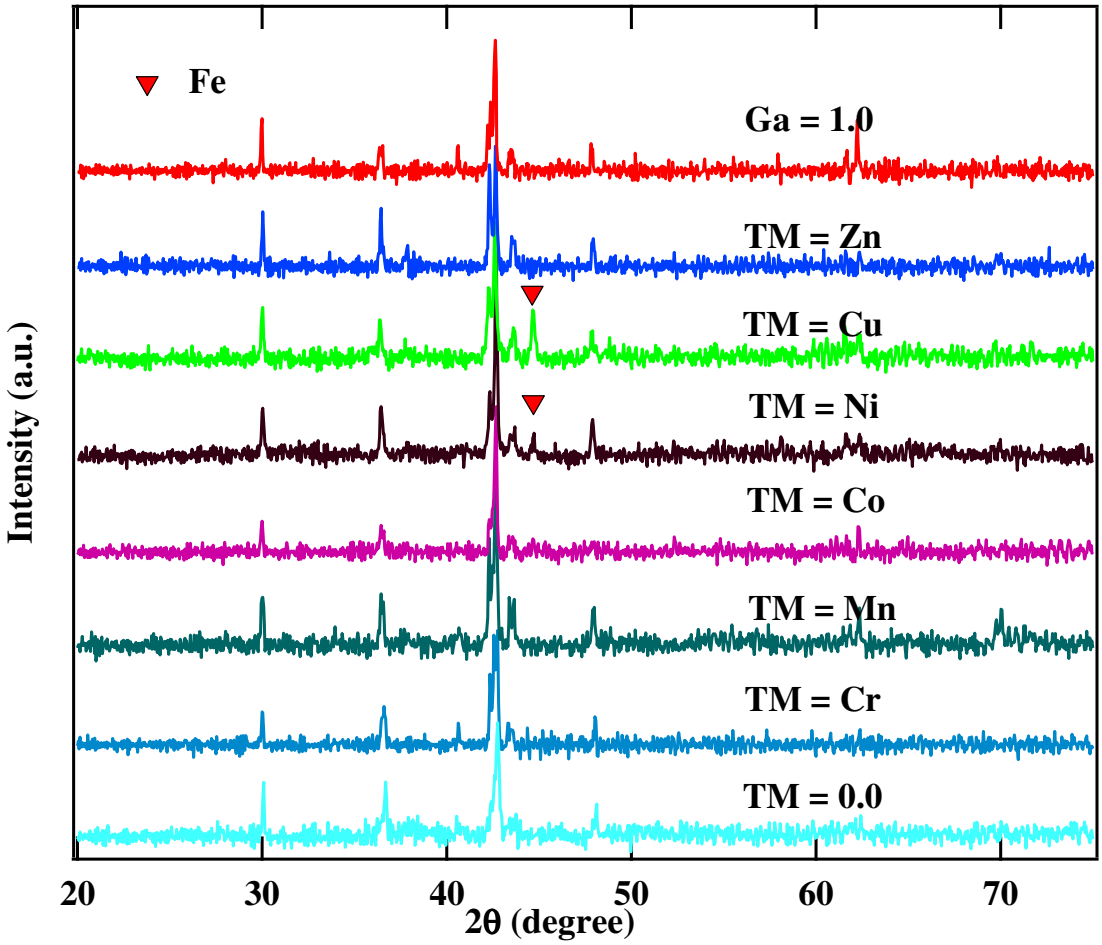

Fig. 4.19. The X-ray diffraction patterns of $Gd_2Fe_{16}Ga_{0.5}TM_{0.5}$.

The samples are in single phase for TM = Cr, Mn, Co, Zn but for TM = Ni, Cu additional iron peak was observed. This shows that the iron is not fully replaced during the formation of the intermetallic compounds with these transition metals. The lattice parameters viz. '*a*' and '*c*' of the intermetallic were calculated by using the formula

$$d_{(hkl)} = \left(\frac{4}{3} \frac{h^2 + hk + k^2}{a^2} + \frac{l^2}{c^2} \right)^{-\frac{1}{2}}$$

where, $d_{(hkl)}$ is the crystal face distance and (hkl) are the Miller indices. During the calculation for lattice parameters '*a*' and '*c*' D (300) and D (302) peaks from XRD pattern were considered.

The volume of the unit cell 'V' was obtained by using the formula,

$$V = a^2 c \sin 60^\circ$$

The calculated values of '*a*', '*c*' and unit cell volume are listed in **Table 4.10** and plotted in **Fig. 4.20**. It is observed that the metallic radius of Cr = 128 pm, Mn = 127 pm, Fe = 126 pm, Co = 125 pm, Ni = 124 pm, Cu = 128 pm, Zn = 134 pm and Ga = 135 pm. This could be the reason of fluctuation in volume with the different transition metal doped intermetallic, though they were expected to be increased in volume with the increase in their atomic number. The maximum volume was observed for $Gd_2Fe_{16}Ga_{0.5}Cu_{0.5}$ (524.289 $Å^3$) and minimum volume was observed for $Gd_2Fe_{16}Ga_{0.5}Ni_{0.5}$ (521.897 $Å^3$).

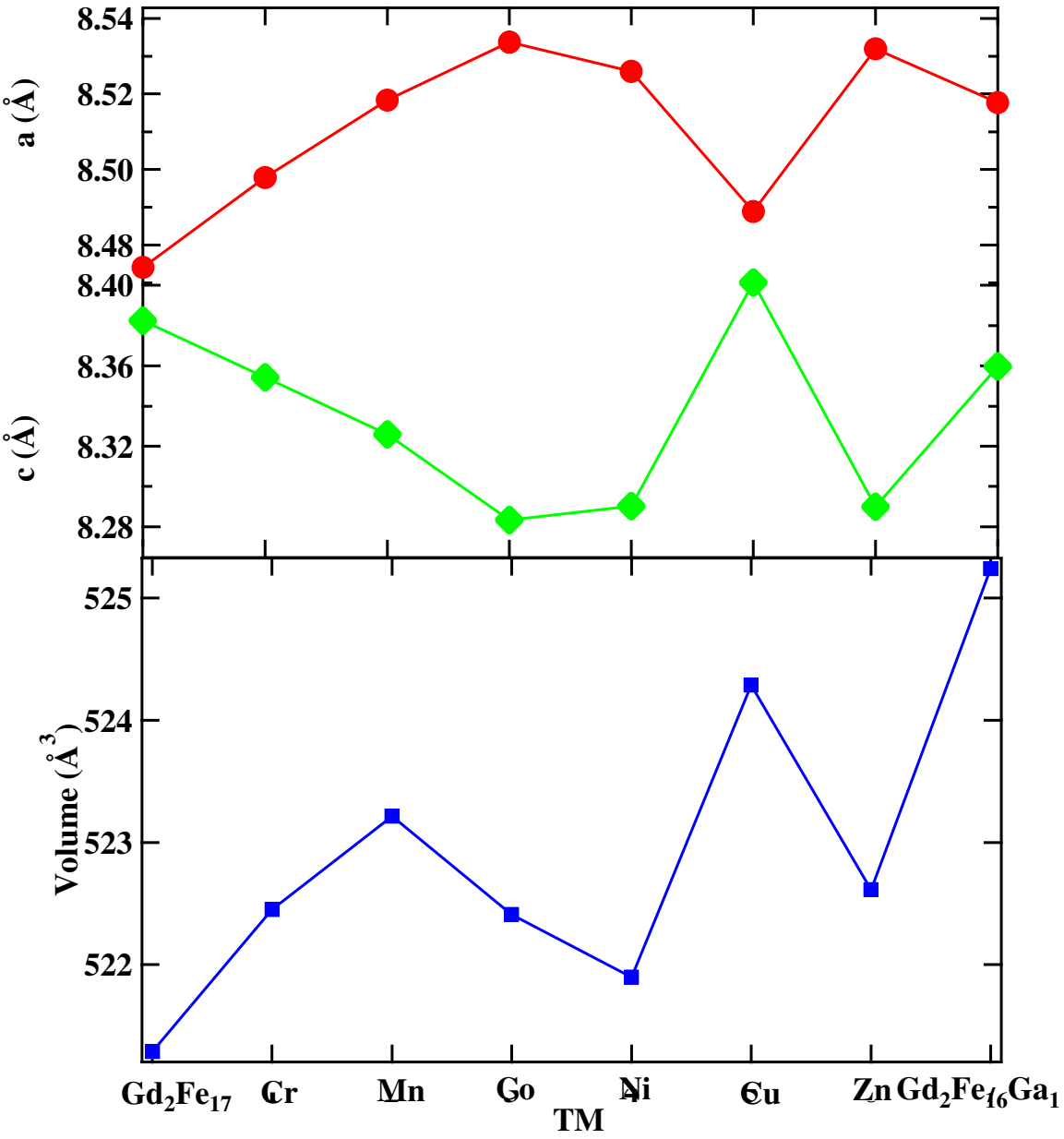

Fig. 4.20. Lattice parameters '*a*' and '*c*' with unit cell volume of $Gd_2Fe_{16}Ga_{0.5}TM_{0.5}$.

Table 4.10. Unit cell volume, Ms, Tc of $Gd_2Fe_{16}Ga_{0.5}TM_{0.5}$.

	a (Å)	*c* (Å)	Volume (Å^3)	Ms(emu/gm)	Tc (K)
Gd_2Fe_{17}	8.47402	8.38241	521.289	67.00	513
TM = Cr	8.49782	8.35411	522.451	59.78	571
TM = Mn	8.5184	8.32596	523.215	56.75	526
TM = Co	8.53375	8.28326	522.409	68.61	587
TM = Ni	8.52599	8.29021	521.897	72.61	557
TM = Cu	8.48882	8.4013	524.289	76.79	570
TM = Zn	8.53198	8.28992	522.613	59.04	537
$Gd_2Fe_{16}Ga_1$	8.51767	8.35962	525.241	67.49	559

4.7 Magnetic properties of $Gd_2Fe_{16}Ga_{0.5}TM_{0.5}$

The room temperature magnetic parameters obtained from M vs. H measurement for $Gd_2Fe_{16}Ga_{0.5}TM_{0.5}$ (TM= Cr, Mn, Co, Ni, Cu, Zn) are plotted in **Fig. 4.21** and are listed in **Table 4.10**. The variation in saturation magnetization (Ms) and Curie temperature (Tc) of $Gd_2Fe_{16}Ga_{0.5}TM_{0.5}$ were observed. As shown in **Fig. 4.22**, the observed variation in magnetization of $Gd_2Fe_{16}Ga_{0.5}TM_{0.5}$ with TM substitution may be based on 3d-3d band hybridization effect. The extent of 3d-3d hybridization raises or lowers the bands width, which eventually changes the magnetic moment of Fe atoms [Huang *et al* (1994) and Huang *et al* (1996)]. The electronic conFig.uration of Cr ($[Ar]4s^13d^5$, Mn $[Ar]4s^23d^5$, Fe $[Ar]4s^23d^6$, Co $[Ar]4s^23d^7$, Ni $[Ar]4s^23d^8$, Cu $[Ar]4s^13d^{10}$ and Zn $[Ar]4s^23d^{10}$). Thus, it is seen that 3d electrons in Cr, Mn is less than that of Fe which lowers the magnetization while 3d electrons of Co, Ni and Cu are more greater than 3d electrons of Fe which increases the magnetization of Fe upon hybridization. In the case of completely filled 3d band such as Zn reduces the magnetization. The lower

magnetization value observed for Mn doped compound may result from the tendency of Mn to couple antiferromagneticaly with Fe atoms.

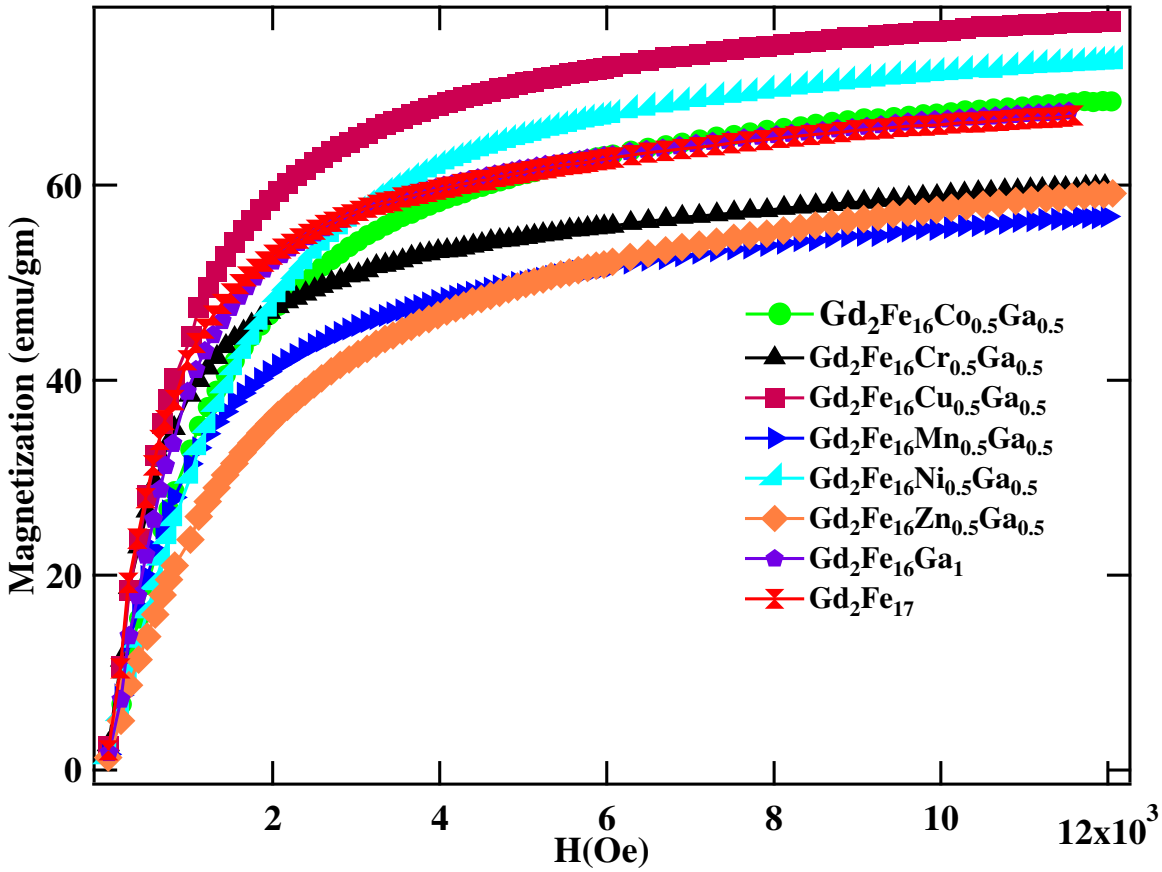

Fig. 4.21 . RT M vs. H plot of $Gd_2Fe_{16}Ga_{0.5}TM_{0.5}$.

The variation of Curie temperature with the different transition metal dopping is as reported in **Table 4.10**. It is found that the Curie temperature (Tc) is greater than the Curie temperatue for $Gd_2Fe_{16}Ga_1$for TM = Cu, Co, and Cr and less than $Gd_2Fe_{16}Ga_1$ for TM = Mn, Ni, Zn but still all samples show Tc values are greater than the Curie temperature of Gd_2Fe_{17}.The Tc and Ms plot is reported in **Fig. 4.22**. The increase in Curie temperature may be due to the lattice parameter expanssion as well as the increase in Fe-Fe exhange coupling.

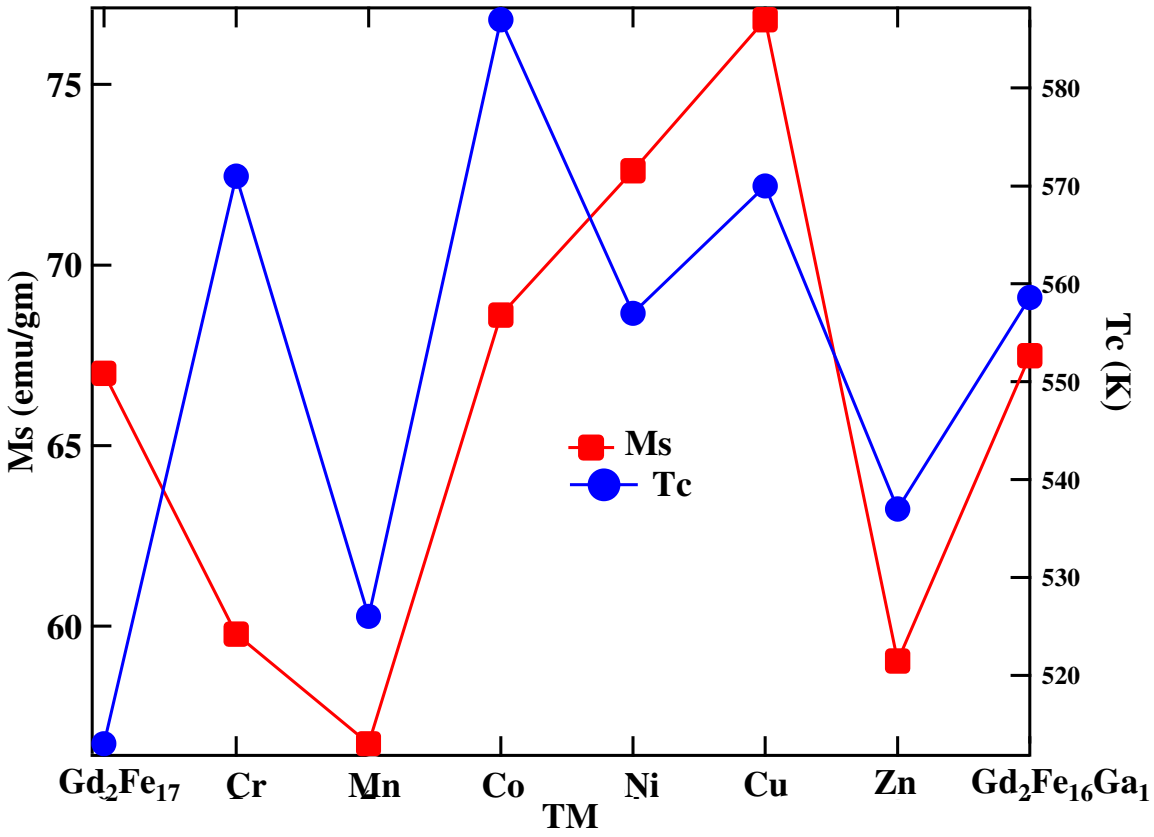

Fig. 4.22. Ms and Tc plot for $Gd_2Fe_{16}Ga_{0.5}TM_{0.5}$.

4.8 Mössbauer studies

Mössbauer spectra of $Gd_2Fe_{16}Ga_{0.5}TM_{0.5}$ (TM = Cr, Mn, Co, Ni, Cu, Zn) with Cobalt-57 source and were calibrated at room temperature with α-iron foil. The resulting spectra were fitted using WMOSS program using sextet and are shown in **Fig. 4.23** and **Fig. 4.24** as function of TM (Cr, Mn, Co, Ni, Cu, Zn). The weighted average hyperfine fields and isomer shift (IS) are plotted in **Fig. 4.25**.

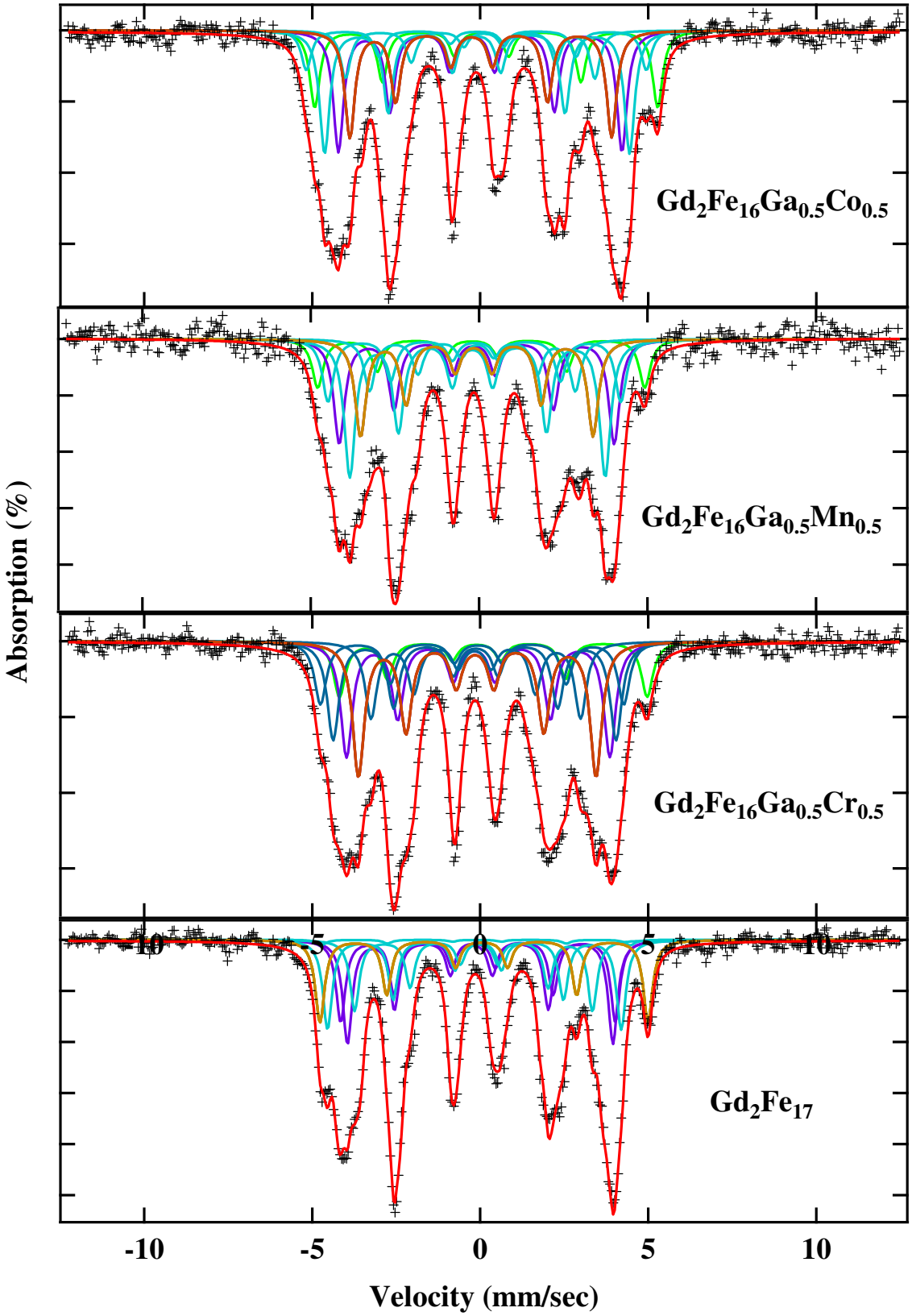

Fig. 4.23. RT fitted Mössbauer spectra of $Gd_2Fe_{16}Ga_{0.5}TM_{0.5}$ (TM = Cr, Mn, Co) and Gd_2Fe_{17}.

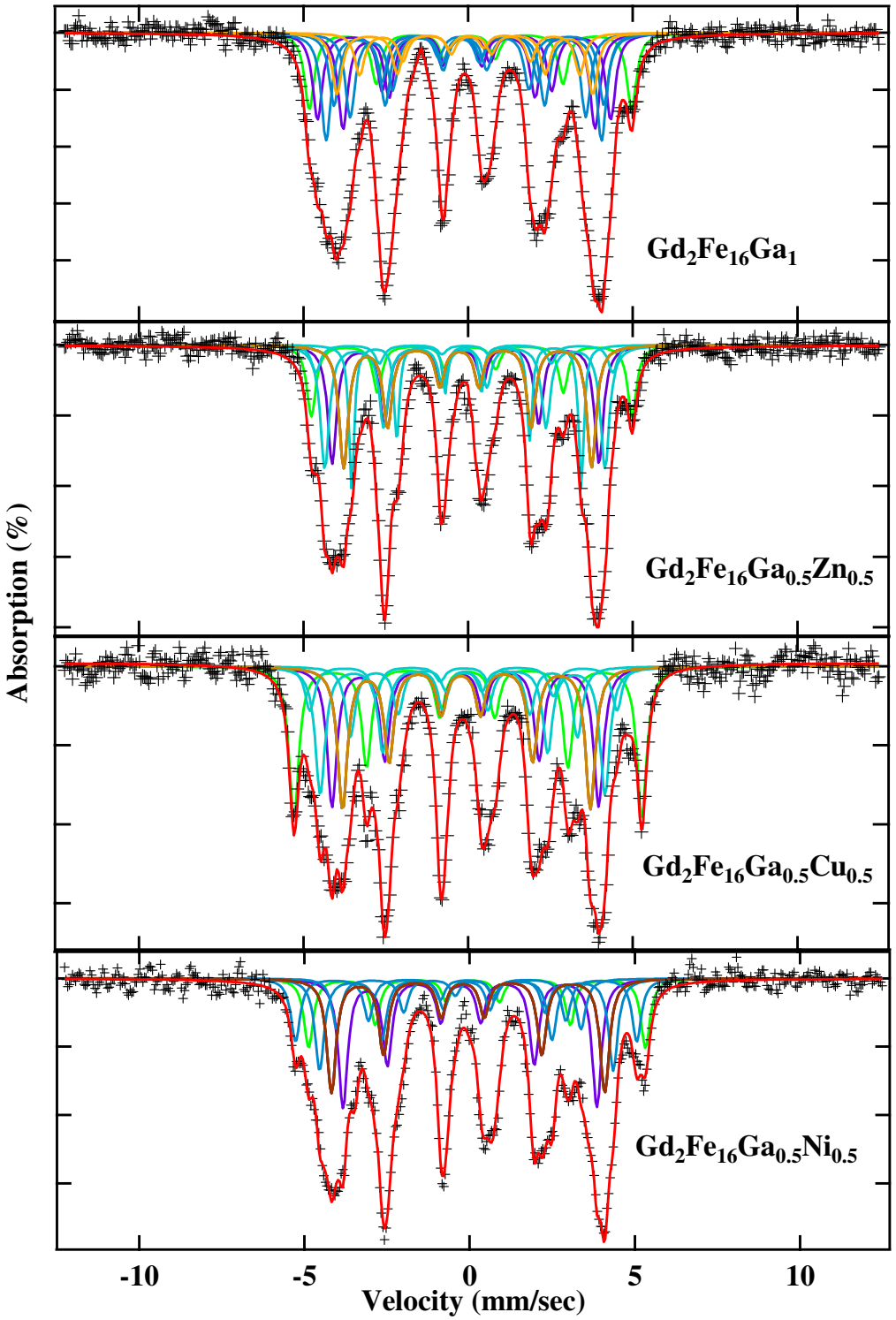

Fig. 4.24. RT fitted Mössbauer spectra of $Gd_2Fe_{16}Ga_{0.5}TM_{0.5}$ (TM= Ni, Cu, Zn) and $Gd_2Fe_{16}Ga_1$.

It was observed that the weighted hyperfine field decreases for TM = Cr and Mn. For TM = Co, and Ni the hyperfine fields increases because of the increase in magnetic moment due to doping. Similarly, the weighted average hyperfine field increases for Zn because of the decrease in magnetic moment upon substitution. The average hyperfine field decreases or increases with increase in the atomic number of transition metal doping and follow patterns 4f > 12j > 6g > 12k as stated in the literature $R_2Fe_{17-x}V_x$ (R = Y, Gd) [57].

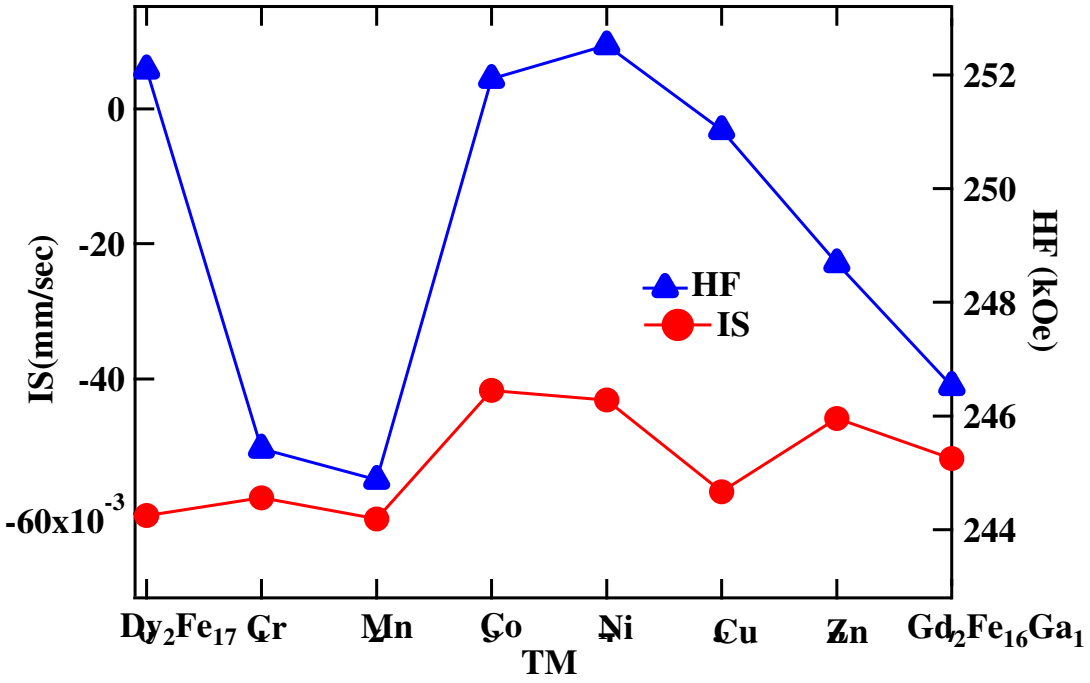

Fig. 4.25 . Weighted average HF and IS $Gd_2Fe_{16}Ga_{0.5}TM_{0.5}$.

Fig. 4.25 shows the weighted average isomer shift (IS) as a function of TM doping. The variation in isomer shift with TM doping may arise from combined effect of (i) volume change (ii) change in net electron density with TM doping (iii) screening of *s*-electron with 'd' electrons of Co $[Ar]4s^23d^7$, Ni $[Ar]4s^23d^8$, Cu $[Ar]4s^13d^{10}$ due to higher *d*-electron concentration, upon hybridization. The 3d (Fe)-(Co, Ni, Cu) hybridization with

Fe (3d) increases the screening of '*s*' electrons and hence is expected to show the increase in isomer shift.

CHAPTER 5

CONCLUSION

Single phase intermetallic compounds of $Dy_2Fe_{17-x}Zr_x$, $Dy_2Fe_{16}Ga_{1-x}Zr_x$ and $Gd_2Fe_{16}Ga_{0.5}TM_{0.5}$ (TM = Cr, Mn, Co, Ni, Cu, Zn) were successfully prepared via arc melting. The structural and magnetic properties were studied using x-ray diffractometer (XRD) and vibrating sample magnetometer (VSM), and hyperfine parameters were studied using Mössbauer spectrometer (MS).

From structural analysis, it was found that $Dy_2Fe_{17-x}Zr_x$ compounds formed single phase up to $x = 0.50$ and became diluted and formed a paramagnetic secondary phase $DyFe_3$ for $x \geq 0.75$. In the case of $Dy_2Fe_{16}Ga_{1-x}Zr_x$, the compounds formed the paramagnetic secondary phase $DyFe_3$ for $x \geq 0.50$. The presence of secondary phase was also confirmed using Mössbauer spectroscopy. About 9% of secondary phase was detected in sample with $x = 1.00$ for both set of compounds. From the Rietveld refinement of $Dy_2Fe_{17-x}Zr_x$ and $Dy_2Fe_{16}Ga_{1-x}Zr_x$, it was observed that Zr atoms preferentially occupy 12*j* and 12*k* sites of Fe. The unit cell volume of the intermetallic compounds show increase with the increase in the Zr concentration for both compounds.

The magnetic studies show that the magnetization of the both $Dy_2Fe_{17-x}Zr_x$ and $Dy_2Fe_{16}Ga_{1-x}Zr_x$ decreases with the increase in Zr concentration. The decrease in magnetization was attributed to the competition between magnetic dilution effect and Fe-Fe exchange interaction. The maximum Curie temperature was observed for $Dy_2Fe_{17-x}Zr_x$ ~510 K and for $Dy_2Fe_{16}Ga_{1-x}Zr_x$ the maximum Tc was observed 505.1 K. This increase in the Curie temperature was attributed to enhancement in Fe-Fe positive interaction.

The hyperfine field value decreased with Zr doping for both $Dy_2Fe_{17-x}Zr_x$ and $Dy_2Fe_{16}Ga_{1-x}Zr_x$ due to decrease in magnetic moment of Fe atoms upon substitution. The isomer shift (IS) showed an increase in nature due to an increase in volume expansion for both compounds.

In the case of $Gd_2Fe_{16}Ga_{0.5}TM_{0.5}$ (TM = Cr, Mn, Co, Ni, Cu, Zn) it was observed from the XRD data that the intermetallic compounds were in single phase except for TM = Ni and Cu where secondary α-Fe phase were reported. The volume of unit cell for $Gd_2Fe_{16}Ga_{0.5}TM_{0.5}$ was observed to depend on the metallic radius of doped transition metal for TM = Cr, Mn, Co, Ni, Cu, Zn. In case of $Gd_2Fe_{16}Ga_{0.5}TM_{0.5}$ (TM = Cr, Mn, Zn), the magnetization was observed to be less than that of Gd_2Fe_{17} but for TM = Co, Ni and Cu the magnetization was observed to be 2.4%, 7.5%, 13.4% greater than Gd_2Fe_{17} respectively. Likewise, the Tc of Co and Cu doped intermetallic showed 5% and 2% increment as compared to $Gd_2Fe_{16}Ga_1$. The weighted average hyperfine fields (HF) of $Gd_2Fe_{16}Ga_{0.5}TM_{0.5}$ (TM = Cr, Mn, Co, Ni, Cu, Zn) were increased or decreased depending upon the type of TM metal. The weighted average HF and IS showed the dependence of these parameters with the type of doping TM atom. These changes are attributed to the 3d (Fe)-3d (TM) hybridization which affect the magnetic moment of Fe atom and alters the *s*-electron density of Fe nucleus.

In summary, Zr doping proved beneficial in increasing Tc for $Dy_2Fe_{17-x}Zr_x$ while detrimental for $Dy_2Fe_{16}Ga_{1-x}Zr_x$. The study on TM metal doped compounds shows that the careful selection of TM dopants can bring improvement in magnetization and Tc of the $R_2Fe_{17-x}(Ga,TM)_x$ compounds.

REFERENCES

[1]. H. R. Kirchmayr, "Permanent magnets and hard mangetic materials," *J. Phys. D. Appl. Phys. ,* vol. 29, pp. 2763-2778, 1996.

[2] . K. J. Strnat, "Modern Permanent Magnets for Application in Electro-technology," vol. 78(6), p. 923, 1990.

[3] . N. I. LLC, "Permanent magnet selection and design handbook," Magcraft, Advance magnetic materials, Vienna VA, 2007.

[4] . B. Cullity and C. Graham, Introduction to Magnetic Materials, vol. 2nd edition , 2009..

[5] . S. Trout, "Rare Earth Magnet Industry in the USA Current status and future trends," XVII Rare Earth Magnet Workshop, Newark, DE, USA, 2002.

[6] . O. Gulfleisch, *J. Phys. D; Appl. Phys.,* vol. 33, p. R157, 2000.

[7] . E. N. D. C. Andrade, "The Early History of the Permanent Magnet," *Endeavour,* vol. 17, no. 65, 1958.

[8] . H. Lou, B. Rai, S. R. Mishra, V. Nguyen and J. Liu, "Physical and magnetic properties of highly aluminum doped strontium ferrite nanoparticles prepared by auto-combustion route," *J. of Magn. and Magn. Mater.,* vol. 324, pp. 2602-2608, 2012.

[9] . P. C. Dent, "Rare earth element and permanent magnets," *J. Appl. Phys.,* vol. 111, no. 7, pp. 07A721-1-6, 2012.

[10]. K. R. Rao, H. Ehrenberg, G. Markandeyulu, U. Varadaraju, M. Venkatesan, K. Suresh, V. Murthy, P. Schmidt and H. Fuess, "On the Structural and Magnetic

Properties of $R_2Fe_{17-x}(A,T)_x$ (R = Rare Earth; A = Al, Si, Ga; T = Transition Metal) Compounds," *physica status solidi (a),* vol. 189, no. 2, p. 373–388, 2002.

[11]. R. Lemaire, "Magnetic properties of the intermetallic compounds of cobalt with the rare earth metals and yitrium," *Cobalt,* vol. 33, p. 201, 1966.

[12]. K. Kumar, "$RETM_5$ and RE_2TM_{17} permanent magnets development," *J. Appl. Phys.,* vol. 63, no. 6, p. R13, 1988.

[13]. K. J. Strnat, "Chapter 2 - Rare earth-cobalt permanent magnets," in *Handbook of Ferromagnetic Materials*, vol. 4, 1988, p. 131–209.

[14]. J. X. Zhang, J.-x. Z.-h. Cheng, B.-g. Shen, B. Liang, J. v. Lier, I. Kleinschroth, W.-s. Zhan and H. Kronmuller, "Magnetic properties of $R_2Fe_{17-x}Ga_xC$ (R = Gd, Tb) compounds," *J. of Magn. and Magn. Mater.,* vol. 183, pp. 111-116, 1998.

[15]. J. Coey and H. Sun, "Improved magnetic properties by treatment of iron-based rare earth intermetallic compounds in anmonia," *J. Magn. Magn. Mater.,* vol. 87, no. 3, p. L251–L254, 1990.

[16]. P. M. Gubbens, A. A. Moolenaar, G. J. Boender, A. M. v. d. Kraan, T. H. Jacobs and K. H. J. Buschow, "^{166}Er and ^{57}Fe Mössbauer effect in $Er_2Fe_{17}N_x$," *J. Magn. Magn. Mater.,* vol. 97, no. 1-3, pp. 69-72, 1991.

[17]. T. H. Jacabs, "Crystallographic and magnetic properties of R_2Fe_{17} compounds," University of Amsterdam , 1992.

[18]. O. Isnard, S. Miraglia, J. L. Soubeyroux and D. Fruchart, "Neutron powder diffraction study of $R_2Fe_{17}H_x$ compounds with R = Pr and Nd," *Solid State Communications,* vol. 81, no. 1, pp. 13-19, 1992.

[19]. D. Hautot, G. J. Long, F. Grandjean, O. Isnard and S. Miraglia, "Hydrogen dynamics in the hydrides of Pr_2Fe_{17} as revealed by Mössbauer spectroscopy," *J. Appl. Phys.,* vol. 86, no. 4, pp. 2200-2207, 1999.

[20]. F. Grandjean, G. J. Long, S. Mishra, O. A. Pringle, O. Isnard, S. Miraglia and D. Fruchart, "A Mössbauer effect study of the interstitial hydrides and nitride of Nd_2Fe_{17}," *Hyperfine Interactions,* vol. 95, no. 1, pp. 277-289, 1995.

[21]. D. Hautot, G. J. Long, F. Grandjean, O. Isnard and D. Fruchart, "An ^{57}Fe Mössbauer spectral study of $Gd_2Fe_{17}H_x$ (for x = 0, 3, and 5) and $Sm_2Fe_{17}D_5$," *J. Magn. Magn. Mater.,* vol. 202, no. 1, pp. 107-118, 1999.

[22]. I. Betancourt and H. Davies, "Influence of Zr and Nb dopant additions on the microstructure and magnetic properties of nanocomposite $RE_2(Fe,Co)_{14}B/\alpha(Fe,Co)$ (RE = Nd–Pr) alloys," *J. Mag. Magn. Mater.,* vol. 261, no. 3, p. 328–336, 2003.

[23]. Z. Chen, H. Okumura, G. C. Hadjipanayis and Q. Chen, "Enhancement of magnetic properties of nanocomposite $Pr_2Fe_{14}B$Õa-Fe magnets by small substitution of Dy for Pr," *J. of App. Phys.,* vol. 89, no. 4, pp. 2299-2303, 2001.

[24]. Z. Chen, H. Okumura, G. C. Hadjipanayis and Q. Chen, "Microstructure refinement and magnetic property enhancement of nanocomposite Pr Fe B/a-Fe magnets by small substitution of M for Fe (M = Cr, Nb, Ti and Zr)," *Journal of Alloys and Compounds,* vol. 327, p. 201–205, 2001.

[25]. G. J. Long, G. K. Marasinghe, S. Mishra, O. A. Pringle, Z. Hu, W. B. Yelon, D. P. Middleton, K. H. J. Buschow and F. Grandjean, "A Magnetic, Neutron Diffraction, and Mössbauer Spectral Study of the $Nd_2Fe_{17-x}Al_x$ Solid Solutions," *J. Appl. Phys.,*

vol. 76, no. 9, pp. 5383-5384, 1994.

[26]. E. Kokorina, M. V. Medvedev and I. Nekrasov, "Ab Initio Exchange Interactions and Magnetic Properties of Intermetallic Compound $Gd_2Fe_{17-x}Ga_x$," *Solid State Phenomena,* Vols. 168-169, pp. 196-199, 2011.

[27]. B.-g. Shen, Z.-h. Cheng, H.-y. Gong, B. Liang, Q.-w. Yan and W.-s. Zhan, "Magnetic anisotropy of $Dy_2Fe_{17-x}Ga_x$ compounds," *Solid State Communications,* vol. 95, no. 11, pp. 813-816, 1995.

[28]. O. Isnard and M. Guillot, "Investigation of magnetic properties of Nd_2Fe_{17} and $Nd_2Fe_{17}H_x$ in high magnetic field," *J. of appl. phys.,* vol. 86, no. 9, pp. 5326 - 5328, 2000.

[29]. F. Grandjean, O. Isnard, D. Hautot and G. J. Long, "A structural, magnetic, and Mössbauer spectral study of Er_2Fe_{17} and hydrides," *Physical Review B,* vol. 63, no. 5, 2000.

[30]. Y. Hao, X. Zhang, B. Wang, Y. Yuang and F. Wang, "Anomalous thermal expansion and magnetic properties of $Tm_2Fe_{17-x}Cr_x$ compounds," *J. of appl. phys.,* vol. 108, p. 023915, 2010.

[31]. A. Kunchin and W. Iwasieczko, "Enhancement of the magnetocaloric effect in the $Lu_2Fe_{17-x}Mn_x$ system," *Solid state communication,* vol. 150, pp. 1580-1583, 2010.

[32]. Z. Arnold, A. Kunchin and J. Kamarad, "Instability of the ferromagnetic ground state in $Lu_2Fe_{17-x}Mn_x$ [$x = 0.5, 0.7$]," *J. of Appl. Phys.,* vol. 111, no. 7, pp. 07E310-07E310-3, 2012.

[33]. F. Wang, B.-g. Shen, P. Zhang, Z.-h. Cheng, J. Zhang, H. Gong, B. Liang, X. Sun

and Q. Yan, "Effect of Ga substitution on the structure and magnetic properties of $Ho_2Fe_{17-x}Ga_x$ (x = 0-8) compounds," *J. Appl. Phys.,* vol. 83, no. 6, pp. 3250-3255, 1998.

[34]. Y. Zhang, J. I. Budnick, W. A. Hines, B. G. Shen and Z. Cheng, "Effect of Ga substitution on the Sm sublattice anisotropy in $Sm_2Fe_{17-x}Ga_x$ ($0 < x < 8$)," *J. of App. Phys.,* vol. 85, no. 8, pp. 4663-4665, 1999.

[35]. H. Luo, Z. Hu, M. Chen, W. B. Yelon, G. K. Marasinghe, P. C. Ezekwenna, W. J. James, W. C. Chang and S. H. Tsai, "Studies of V, Nb, Cr, and Zr substituted 2.17 compounds and their carbides using neutron diffraction," *J. Appl. Phys. 81, 4542 (1997),* vol. 81, no. 8, pp. 4542-4544, 1997.

[36]. S. R. Mishra, G. J. Long, O. A. Pringle, D. P. Middleton, Z. Hu, W. B. Yelon, F. Grandjean and K. H. J. Buschow, "A magnetic, neutron diffraction, and Mössbauer spectral study of the $Ce_2Fe_{17-x}Al_x$ solid solutions," *J. Appl. Phys. 79, 3145 (1996),* vol. 79, no. 6, p. 3145, 1996.

[37]. G. J. Long, S. R. Mishra, O. A. Pringle, W. B. Y. Z. Hu, F. Grandjean, D. P. Middleton and K. H. J. Buschow, *J. Magn. Magn. Mater.,* vol. 176, 1997.

[38]. Z. Zhang and Q. Yan, "Structure and magnetic properties of $Ho_2Fe_{17-x}Ga_x$ and $Ho_2Fe_{17-x}Ga_xC_2$ compounds," *Solid State Communications,* vol. 94, no. 11, p. 931–934, 1995.

[39]. R. Xu, L. Zhen, D. Yang, J. Wu, X. Wang, Q. Wang, C. Chen and L. Dai, "Effect of Ga on the structural stablity of $Sm_2(FeGa)_{17}$ compounds," *Materials letters,* vol. 57, pp. 146-150, 2002.

[40]. J. Hu, "Volume expansion and Curie temperature enhancement in $R_2Fe_{17}C_2$ compounds," *Journal of alloy and compounds,* vol. 285, pp. 51-55, 1999.

[41]. E. A. Nesbitt and J. H. Wernick, Rare-earth Intermetallics, New York. Academic, 1973.

[42]. P. Campbell, Permanent magnet materials and applications, Cambridge University Press, 1994.

[43]. H. Yan-ming, Y. Qi-wei, Z. Pan-lin, S. Xiang-dong, W. Fang-wei and S. Bao-gen, "Magnetic properties of $Dy_2Fe_{17-x}Cr_x$ and $Er_2Fe_{17-x}Cr_x$ (x = 0-3) compounds," *Acta Phys. Sin. ,* vol. 6, no. 6, 1997.

[44]. T. Monecke, S. Köhler, R. Kleeberg, P. M. Herzig and J. B. Gemmell, "QuantitativePhase-Analysis by the Rietveld Method Using X-Ray Powder-Diffraction Data. Application to the Study of Alteration Halos Associated With Volcanic-Rock-HostedMassive Sulfide Deposits," *The Canadian Mineralogist,* vol. 39, pp. 1617-1633, 2001.

[45]. R. H. Herber, "Mössbauer Spectroscopy," *Sci. Amer.,* vol. 255, no. 4, p. 86–95, 1971.

[46]. B. Fultz, "'Mössbauer Spectrometry' in Characterization of Materials," *Elton Kaufmann, Editor(John Wiley, New York, 2011).*

[47]. M. Zinkevich, N. Mattern, I. Bacher and S. Puerta, "Formation, crystal structure and magnetic properties of (1.12) compounds in the Fe-Gd-Mo-Zr system," *J. Alloys and compounds,* vol. 336, pp. 320-328, 2002.

[48]. F. M. Yang, N. Tang, J. L. Wang, X. P. Zhong, R. W. Zhao and W. G. Lin,

"Magnetic properties of $Er_2Fe_{17-x}Al_xN_y$ compounds," *J. Appl. Phys.,* vol. 75, no. 10, 1994.

[49]. J. A. Chelvane, M. Palit, S. Pandian, M. M. Raja and V. Chandrasekaran, "Microstructure and Mössbauer studies on magnetostrictive $Tb_{0.3}Dy_{0.7}Fe_{1.95-x}Nb_x$ (x = 0, 0.025, 0.05 and 0.075)," *Hyperfine Interactions,* vol. 187, no. 1-3, pp. 87-91, 2008.

[50]. Z. Hu and W. B. Yelon, "Neutron diffraction and magnetic studies of $Nd_2Fe_{17-x-z}Al_xSi_z$," *J. of Appl. Phys.,* vol. 76, no. 10, pp. 6162-6164, 1994.

[51]. Z. Hu, W. Yelon, S. Mishra and G. J. Long, *J. Appl. Phys.,* vol. 76, no. 1, 1994.

[52]. W. C. Chang, S. H. Tsai, L. J. Chao, H. L. Z.B. Hu and W. Yelon, "Magnetic and neutron diffraction studies of $R_2Fe_{17-x}Al_xC$ intermetallic compounds with Th_2Zn_{17} type crystal structure," *J. of Magn. and Magn. Mater.,* vol. 172, pp. 227-284, 1997.

[53]. X. F. Liu, J. Y. Lv, S. B. Han, J. Peng, H. Wang, Z. B. Hu, D. F. Chen, Y. J. Xue and J. H. Li, "Effects of double substitution on the magnetic properties of $Nd_2Fe_{17-x-y}Ti_xAl_y$. A combined investigation of x-ray diffraction, neutron diffraction, and magnetic measurement," *J. Appl. Phys.,* vol. 98, no. 1, p. 013537 , 2005.

[54]. I. Nehdi, L. Bessais, C. Djega-Mariadssou, M. Abdellaoui and H. Zarrouk, "X -ray and Mo¨ssbauer studies of $Sm_2Fe_{17-x}Cr_x$ materials synthesized by mechanical alloying followed by an appropriate short annealing," *J. of Alloys and compounds,* vol. 351, pp. 24-30, 2003.

[55]. J. J. Bara, A. T. Pedziwiatr and W. Zarek, "Investigations of crystal and magnetic

properties of Dy-Fe intermetallic compounds," *J. Magn. Magn. Mater.,* vol. 27, no. 2, p. 168–174, 1982.

[56]. O. Isnard, D. Hautot, G. J. Long and F. Grandjean, "A structural, magnetic and Mössbauer spectral study of Dy_2Fe_{17} and hydrides," *J. of App. Phys.,* vol. 88, no. 5, pp. 2750-2759, 2000.

[57]. M. Sorescu and M. Valeanu, "Structural and magnetic characterization of $R_2 Fe_{17-x}V_x$ compounds and their carbides," *International Journal of Inorganic Materials,* vol. 1, pp. 303-309, 1999.